Sources and Geochemical Controls on Hydrocarbons in Arctic Sediments, Kivalliq Region, Nunavut

by

Wilhelmina Asihene

A Thesis submitted to the Faculty of Graduate Studies of

The University of Manitoba

in partial fulfilment of the requirements of the degree of

MASTER OF SCIENCE

Department of Geological Sciences

University of Manitoba

Winnipeg

ABSTRACT

Expectations that increases in shipping and human activities may impact concentrations of hydrocarbon contaminants in northern areas have prompted study of existing baseline distributions and variability in marine sediments from Chesterfield Inlet and Wager Bay, Nunavut. Pyrogenic and petrogenic compounds likely supplied by local sources subtly influence the composition of PAHs in sections of core CI-08, retrieved close to the community of Chesterfield Inlet. However, pyrogenic PAHs indicative of long-distance atmospheric transport are the main compounds in all the cores. These concentrations are low compared to other northern areas influenced by industrial activities. n-alkanes are likely derived from both terrigenous and marine organic matter sources in both areas. The two embayments contrast in terms of physical and geochemical factors that affect the baseline hydrocarbon concentration and accumulation rates. Good correlation between post-1900 210Pb and parent PAH inventories is consistent with focusing into deeper sites in Wager Bay versus direct settling in Chesterfield Inlet. No significant degradational pattern was observed in the core profiles.

ACKNOWLEDGEMENT

My sincere thanks to my advisors Dr. Zou Zou Kuzyk and co-advisor Dr. Gary Stern who helped me see the bigger picture of my research. With their help I have upgraded my analytical thinking, problem-solving, statistical and writing skills. I also appreciate the opportunities they gave me to travel, learn, and share my research at ArcticNet conferences and with others and most especially to earn a Master's Degree.

I appreciate the efforts and time of the following people which helped me to successfully complete my master's project. Michelle Kamula and Samantha Huyghe, who collected the sediment samples. Jake Richie who assisted me during the hydrocarbon laboratory analyses and reading of chromatograms. Eva Slavicek who performed the radioisotope analyses at the soil science department, University of Manitoba and Misuk Yun who assisted me to analyse the samples for Total Carbon and Inorganic Carbon at the Department of Geological Sciences, University of Manitoba and Diana Saltimakova, for supporting and pointing me in the right direction.

I also thank each and every one who supported and encouraged me throughout this project, especially to my dear husband who supported me throughout the years of my studies and research.

TABLE OF CONTENTS

LIST OF TABLES

LIST OF FIGURES

LIST OF EQUATIONS

CHAPTER 1: INTRODUCTION

1.1 Foreword Notes

Hydrocarbons (HC) are organic chemical compounds contained in fossil fuels and related products (petrogenic), produced by early diagenesis of organic matter (biogenic), and combustion of organic substances (pyrogenic) (Duran and Cravo-Laureau 2016; Stogiannidis and Laane 2015). Tens of thousands of HC compounds exist and they range from small, volatile compounds to large non-volatile ones, giving rise to crude oils with different chemical and physical properties (Wigger and Torkelson 1997). They can be classified into three groups: aliphatics or saturates, Polycyclic Aromatic Hydrocarbons (PAHs) and hetero-compounds (resins) (Tissot and Welte 1984). Aliphatic hydrocarbons make up the largest weight percentage of crude oils and include straight chain alkanes (n-alkanes) and iso-paraffins among others. n-alkanes with less than less than or equal 22 carbon number ($\leq$ n-C_{22}) are highly volatile and easily degraded (Stout and Wang 2016). The PAH fraction includes alkylated and unsubstituted parent PAHs which are relatively stable and toxic to marine organisms (Harvey et al. 2014). The hetero-compounds are hydrocarbons containing one or more nitrogen, sulphur and oxygen atoms in their structure; examples include resins and asphaltenes (Stout and Wang 2016). They are generally present in most crude oils at very low concentrations; however, when present in higher concentrations they can be toxic, carcinogenic and have mutagenic effects on terrestrial and marine organisms (Yunker and Macdonald 1995; Larsen and Baker 2003). Once introduced into a marine environment via spills, fluvial transport, atmospheric transport or early diagenesis, sediments are the ultimate repository for hydrophobic HCs (Rajesh, Mackay, and Muncke 1999).

In recent years, the Canadian Arctic, including regions such as northwestern Hudson Bay, is experiencing increasing seasonal ice-free periods and a corresponding increase in resource

development (mining and petroleum exploration/exploitation) and shipping activities (Dufresne, Sim, and Davis 2013; Barber, Babb, and Andrews 2015). With this increase in regional economic activity comes a greater risk of accidental spills of fuel and other HC related contaminants. Studies in other parts of the Canadian Arctic such as the Beaufort Sea and Baffin Bay show that petrogenic sources of PAHs are predominant in marine sediments due to increasing petroleum exploration and exploitation within these areas as well as natural seeps (Yunker et al. 1996; Foster et al. 2015). Additionally, atmospherically transported aerosols as well as fluvially transported particle-bound HCs from watersheds have been found to be important sources of HCs throughout studied Canadian coastal ocean areas (Welch et al. 1991; Yunker and Macdonald 1995; Foster et al. 2015; Ma et al. 2017). Air samples collected in the Canadian High Arctic region of Alert confirmed the presence of these chemicals both in the particulate and gas phase (Wang et al. 2010). Welch et al. (1991) also observed and analysed surface layers of brown coloured snow in the then Keewatin District of the central Canadian Arctic (now Kivalliq, Nunavut) and confirmed their inputs to be atmospheric.

The communities and industries in the Canadian Arctic rely almost exclusively on diesel fuel to meet their energy needs, and as a result import millions of liters of fuel annually (http://www.canadianfuels.ca/ASR-Fuels-en/Northern-power/, accessed 3 April, 2017). Each year over the past five decades many petroleum spills have been reported in Nunavut constituting from thousands to hundreds of thousands of liters annually (Figure 1.1). Nonetheless, hydrocarbon characterisation in large portions of Nunavut including the Kivalliq region in Northwestern Hudson Bay has not received much attention.

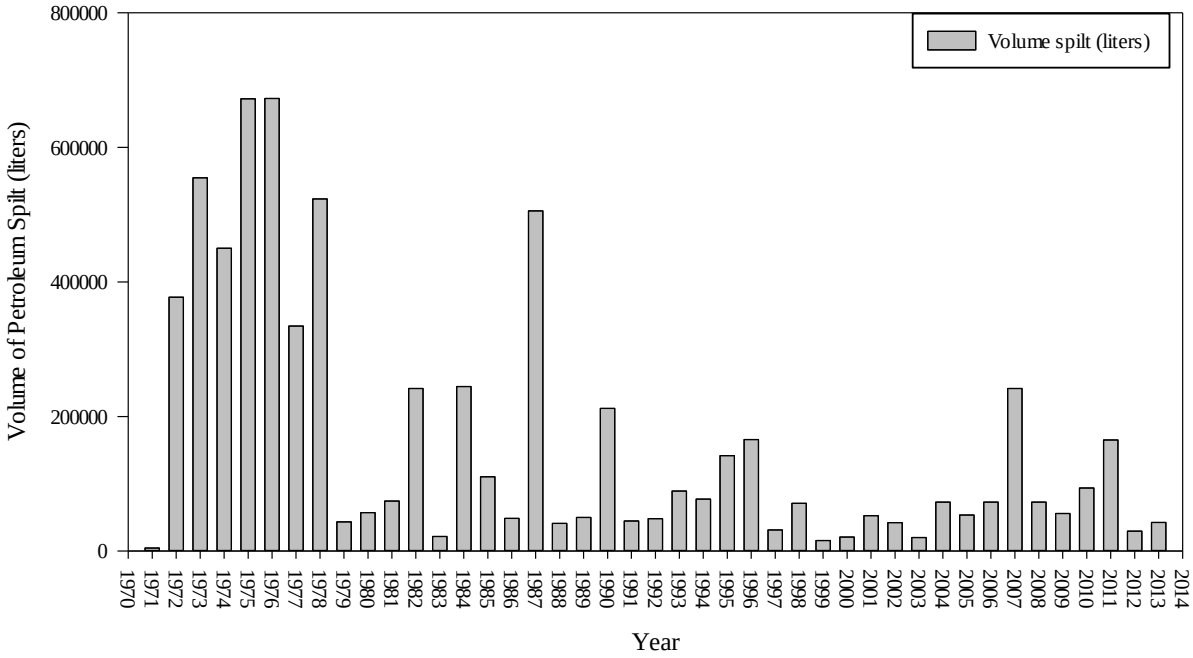

Figure 1.1: Volume of petroleum spills (liters) recorded in Nunavut from 1971-2014 (https://www.cbc.ca/news/canada/north/nunavut-fuel-spills-are-down-but-accidents-still-happen-1.2612118, accessed 3 January, 2017).

In this project, concentrations of n-alkanes and PAHs, (both parent and unsubstituted PAHs) are measured in marine sediments from two adjacent coastal areas (Wager Bay and Chesterfield Inlet in the Kivalliq region of Nunavut) differing in their population density and industrialisation as well as natural features (river influences, circulation and geomorphology). It is anticipated that the risk of accidental oil spills will rise in Hudson Bay, due to the increase in marine shipping activities (Barber, Babb, and Andrews 2015) (see the Arctic corridor in Figure 1.2). With several reported spills over the years (Figure 1.1), it is also expected that the existing HC concentrations and composition in sediments will most likely reflect anthropogenic inputs (e.g. pyrogenic and petrogenic sources). The data from this study will provide baselines for detecting possible future contamination that may occur and planning remediation actions if any spills or higher concentrations have already occurred.

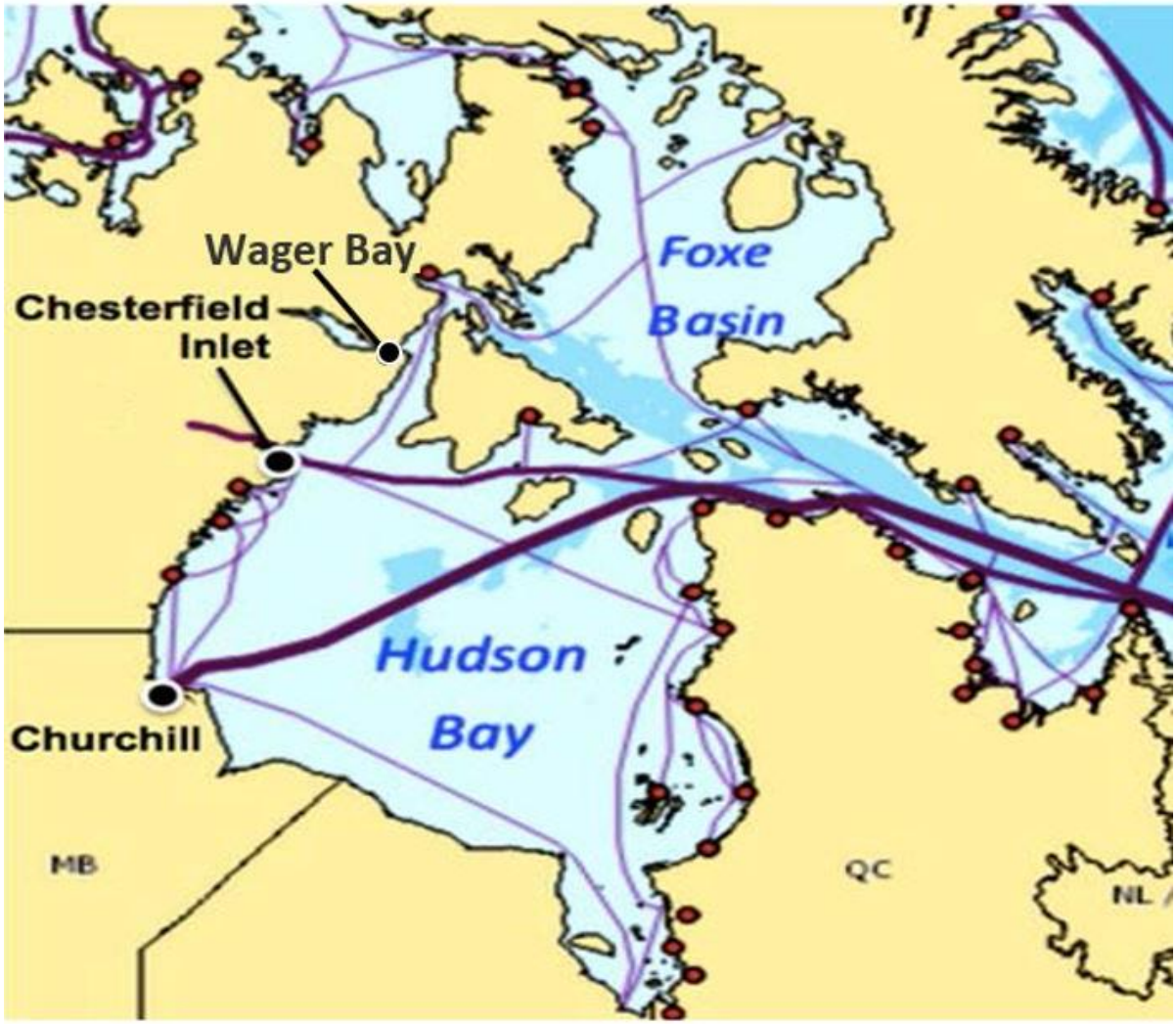

Figure 1.2: Shipping routes through Hudson Bay with selected coastal communities (Churchill, Chesterfield Inlet, and Wager Bay) indicated in black dots. Routes reflect 2010 vessel traffic, line thickness corresponds to volume of traffic (Andrews et al. 2016).

Molecular diagnostic ratios (MDR) have been used as an inexpensive and quick preliminary method to infer HC sources (Yunker et al. 2002; Ma et al. 2017; Kanzari et al. 2014). The method utilises ratios of the concentration of source-specific HC compounds to distinguish pyrogenic and petrogenic sources. Alternatively, a multivariate statistical technique, Principal Component Analysis (PCA), has been employed to infer contributions of different sources using the entire suite of measured compounds (rather than just two variables). PCA provides an unbiased means to differentiate among PAH sources. Ma et al. (2017) used these methods to establish that in the Chukchi Sea shelf and slope of the Canada Basin,

alkylated petrogenic PAHs contribute most strongly (42%) to the PAHs found in surface sediments whereas parent PAHs from combustion sources contributed a high percentage of the total PAH in surface sediments from the Central Arctic Ocean. Here also, PCA and MDR are both used to identify hydrocarbon sources for the first time within the study areas.

In addition to contributions from the various HC sources, sedimentation and geochemical processes operating both before and after deposition affect hydrocarbon contaminant fluxes and profiles in sediments (NRC 2003; Bridges and Gustavson 2014). Once released into the marine environment, the different hydrocarbon compounds in petroleum products separate or part distinctively and float on seawater due to their hydrophobicity (Brandvik and Leirvik 2008). Temperature-dependent oil properties such as solubility and viscosity are also important in the partitioning of compounds in cold regions (Stern and Evans 2003). The more stable (high molecular weight) compounds remain longer in marine environments while less stable (low molecular weight) compounds undergo weathering processes and are eventually removed. Weathering of HCs occurs according to the following sequence of increasing molecular weight: Aliphatics > aromatics > resins > asphaltenes (Maletic et al 2013).

Stable HCs are eventually transferred from the surface and water column to the sea floor by sorbing onto sediment particles, particularly fine-grained sediments and/or organic matter (OM) (Loring and Asmund 1996; Brandvik and Leirvik 2008; Kuzyk, Macdonald, and Johannessen 2015). Particles settling out of the water column or being deposited on the seafloor may occur as a result of scavenging (vertical flux), and in some cases they may be redistributed, winnowed and focused onto deeper depths. Focusing within sediment profiles may be estimated from the degree to which ^{210}Pb inventory exceeds the expected ^{210}Pb inventory from direct atmospheric deposition (cf., Muir et al. 2009). It is plausible that geochemical processes involved in early diagenesis such as biomixing, high sedimentation, and redox reactions can affect profiles of sediment content (OM content hydrocarbons, ^{210}Pb, ^{137}Cs and trace and major

elements concentrations) (Nam et al. 2008). The geochemical context of sediments as revealed by vertical profiles and inventories of organic carbon, redox elements and particle-reactive radioisotopes may be used to elucidate particle-mediated contaminant dynamics such as particle-scavenging, focusing, degradation and biomixing in marine systems (Baskaran et al. 2014; Kuzyk, Macdonald, and Johannessen 2015). A conceptual sketch of geochemical processes that occur as HCs interact with particles in the water column and are transferred with sediments to undergo deposition and subsequent burial on the sea floor is shown in Figure 1.3.

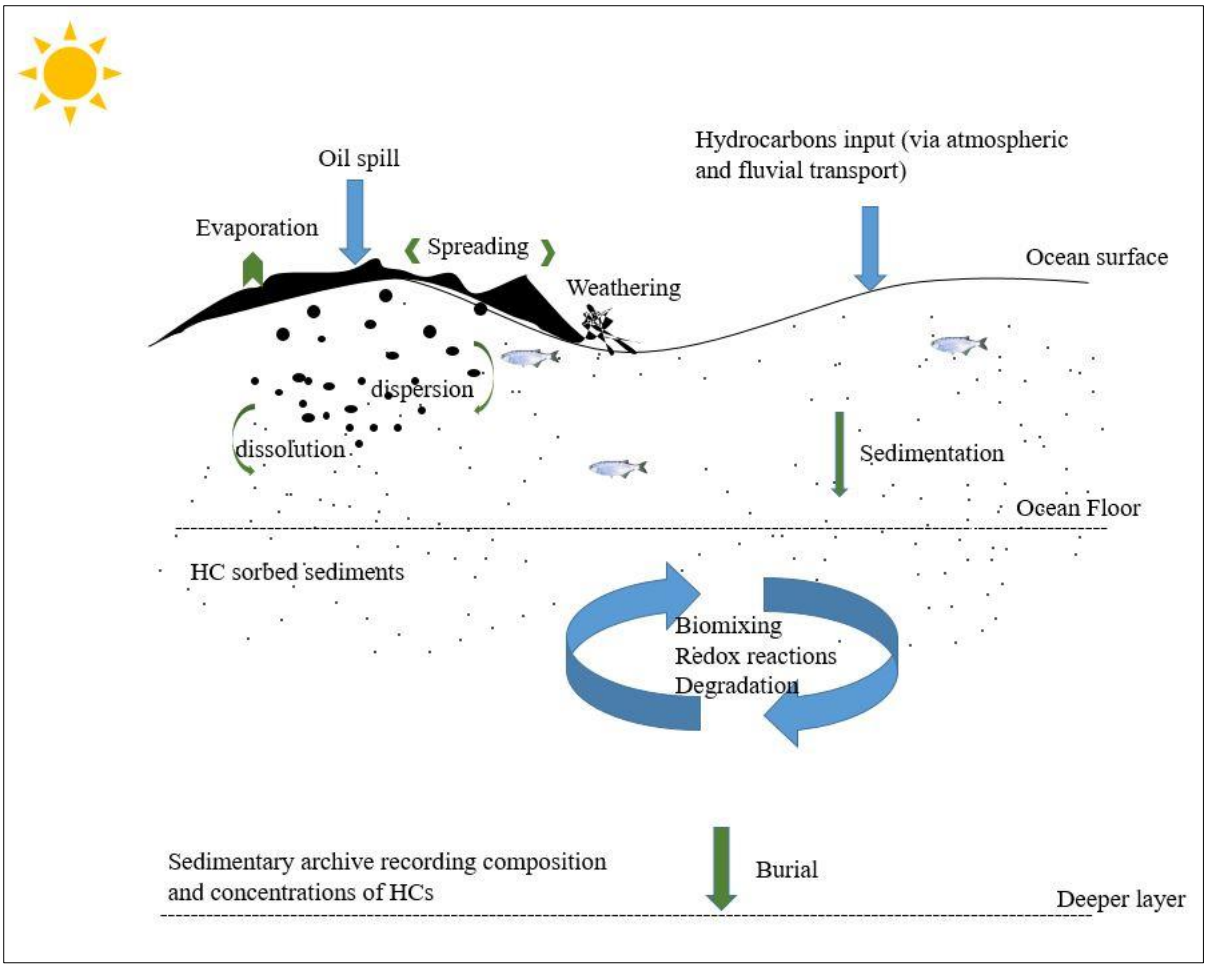

Figure 1.3: Conceptual schematic of the geochemical processes that bring about changes in sediment and hydrocarbon composition.

1.2 Objectives and Significance of Research

The above paragraphs highlight the persistence of HCs and the geochemical processes that affect their composition and inventories within marine sediments. The aims of this study are to 1) Determine the sources and inventories of PAHs and n-alkanes to marine sediments in two coastal Canadian Arctic sites; 2) Assess evidence of changes in sources and inventories over time; 3) Identify the pre-and post-deposition processes that affect the HC accumulation patterns and may drive changes independent of changes in source over time.

1.3 Study Area

Hudson Bay is a relatively shallow body of sea-water (average depth of 130 m) that covers an area of ~970,000 square kilometres (Stern and Evans 2003). Southward-flowing cyclonic currents bring Arctic waters into the northern end of the Bay (Johnson et al. 1986; Stewart and Lockhart 2005). The modern basin is believed to have formed from the heavy impact of the ice sheet that existed during the last ice age (> 20,000 years ago) and marine water invading the depression immediately after deglaciation (Stewart and Lockhart 2005). Complete deglaciation in Hudson Bay, which occurred ~8000 years ago, has led to isostatic rebound in Hudson Bay and this process continues to this present time (Stewart and Lockhart 2005; Sella et al. 2007). Currently, the Canadian sub-Arctic Inland Sea occupies about a quarter of Canada's land mass (Nicolas and Lavoie 2009). It is underlain by Paleozoic-Mesozoic sedimentary rocks of the Hudson Bay Platform (Lavoie et al. 2011). Elsewhere in the basin, the Hudson platform is underlain by the Churchill Province (Precambrian rocks) which, in turn, overlies the Superior Province (Archean rocks) (Stewart and Lockhart 2005). The sediment at the bottom of the bay consists of till, fine-grained glacio-marine deposits, and postglacial mud (Stewart and Lockhart 2005).

The climate of Hudson Bay is best described as continental-Arctic with short cool summers and long cold winters with minimal precipitation (Stewart and Lockhart 2005; Dufresne, Sim, and Davis 2013). It is characterised in most areas by average summer temperatures reaching up to 20ºC and average winter temperatures ranging from -30ºC to -35ºC. Sea ice forms by December and breaks up by mid-June (Dufresne et al. 2013). These alternating climatic conditions promote thawing of permafrost and erosion of river banks from adjacent rivers and streams during warmer temperatures (Macdonald et al. 2003), which then has the potential to release significant amounts of organic carbon from terrestrial soils (Vonk et al. 2012).

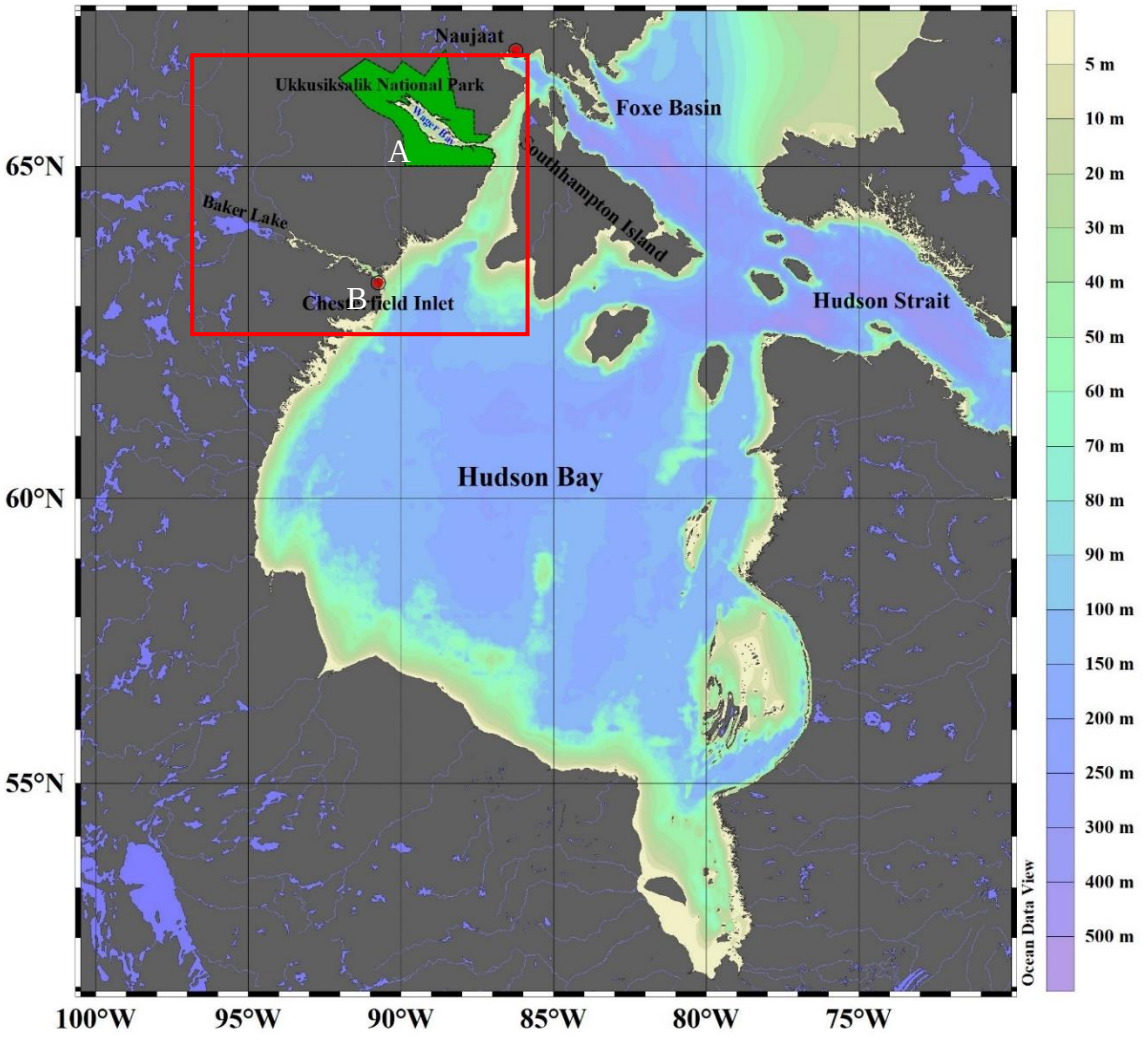

Figure 1.4: Bathymetric map of Hudson Bay showing Wager Bay (A) and Chesterfield Inlet (B).

Chesterfield Inlet and Wager Bay are two adjacent Inlets located at the northwestern part of Hudson Bay (Figure 1.4). They contrast each other in terms of water depth, tidal currents, riverine inputs, drainage area, shipping and other human activities. Chesterfield Inlet is a long narrow, exposed bay that extends approximately 200 km in a north-west direction (Figure 1.5), where it shares a boundary with the Baker Lake Watersheds at 63°39'50"N, 94°56'50"W (Roff et al. 1980) (i.e., Chesterfield Inlet connects Baker Lake to Hudson Bay). The inlet is relatively shallow (average depth 50 m) and has strong tidal currents (Roff et al. 1980). The bottom of the inlet is made up of Precambrian rocks with shell hash, silt and clay deposits near the mouth (Budgell and Flemming 1982). The Inlet receives freshwater from a number of large rivers and lakes (Baker Lake, Schultz Lake, Aberdeen Lake) draining an area of about 290,000 km^2 with mostly continuous permafrost (Budgell and Flemming 1982). A small community dating back to about mid 1800's (population ~400), which goes by the name Chesterfield Inlet, is located at the mouth of the inlet (http://chesterfield-inlet.ca accessed 3 January, 2019). This community and the Inlet receive ship traffic and mining supplies en-route to Baker Lake.

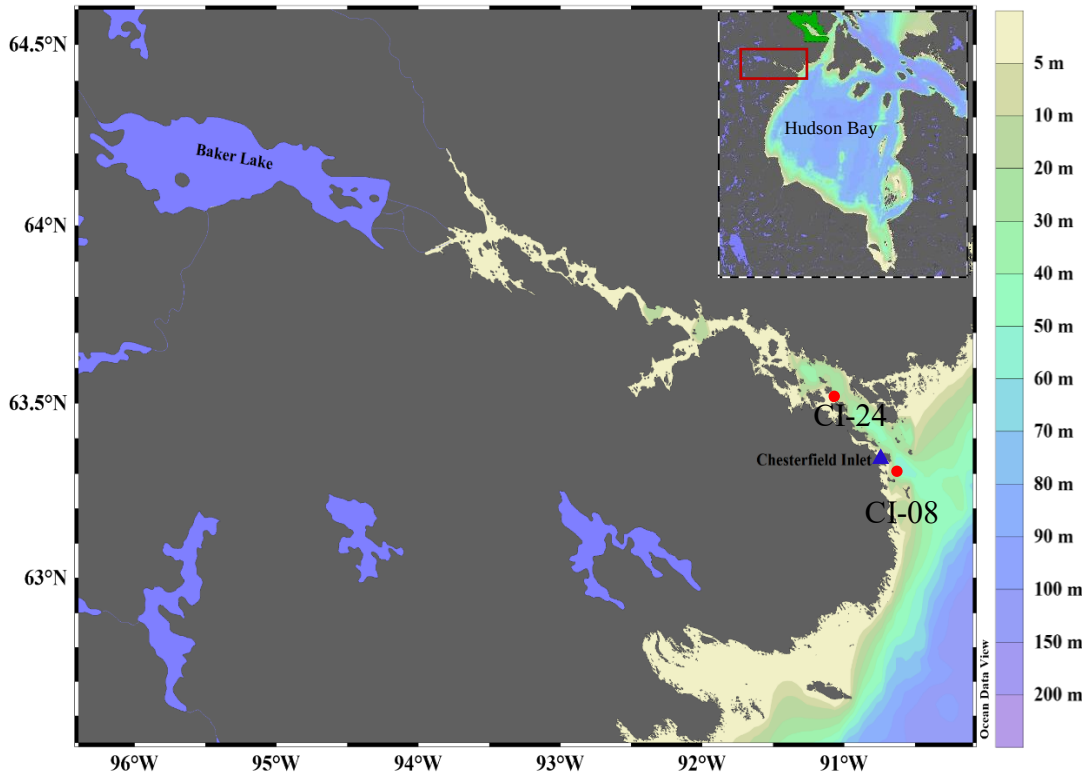

Figure 1.5: Bathymetric map of Chesterfield Inlet showing sampling stations IDs (red dots) and Chesterfield Inlet community (blue triangle).

Wager Bay is an embayment located north of CI along Roes Welcome Sound (Figure 1.6). It is about 150 km long, up to 36 km wide and much deeper than CI (>300 m in places) (Parks Canada, 1977). Wager Bay is connected to Roes Welcome Sound by a narrow and shallow passageway of minimum depth 30 m called "The Narrows" (Figure 1.6), which restricts the exchange of water between Hudson Bay and Wager Bay. According to a Parks Canada report (1977), Wager Bay was formed from a submerged rift valley. The rocks within the area are characterised by high upland and extensive granitic outcrops which are, for the most part, remnants of past surface erosion (Parks Canada 1977). Wager Bay receives very little freshwater discharge from smaller rivers such as Ford Lake and Brown Lake. These small rivers drain a total area of only about ~28,551 km^2. While there are no permanent settlements in Wager Bay, it has been an important hunting and fishing area for Inuit for millennia. Wager Bay is part of the Ukkusiksalik National Park that was established in 2003.

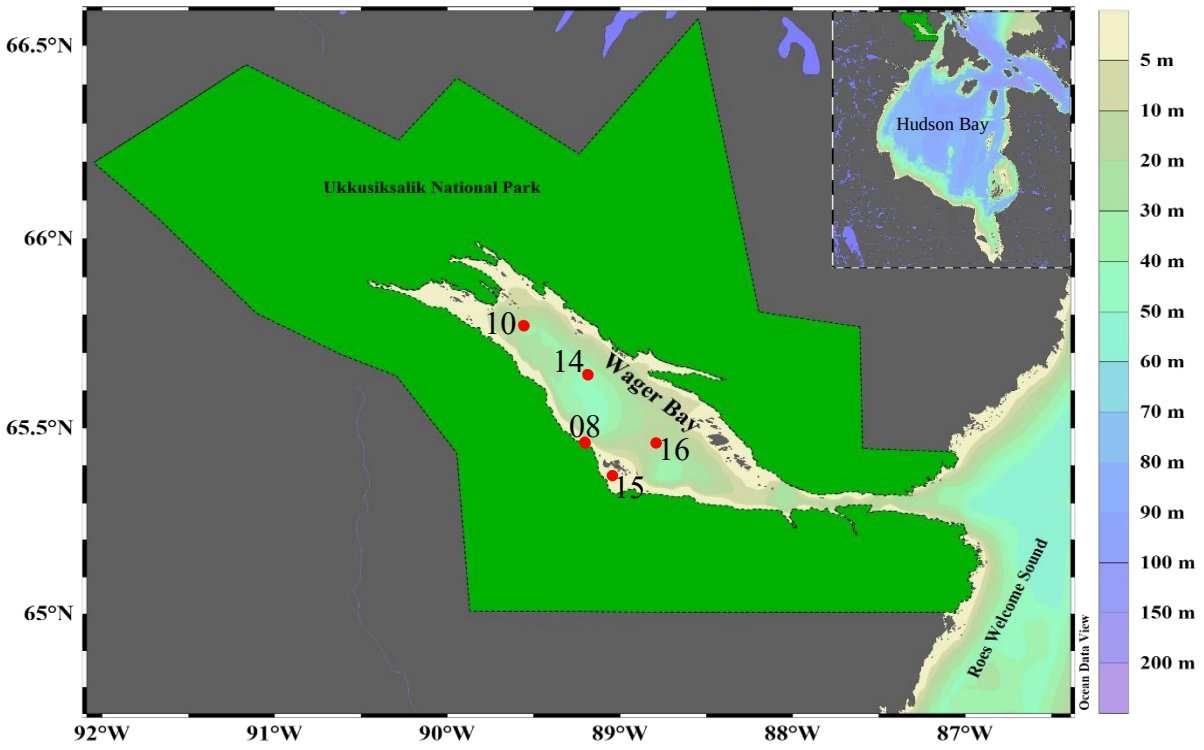

Figure 1.6: Bathymetric map of Wager Bay showing sampling stations (red dots) and Ukkusiksalik National Park.

1.4 Thesis Structure

The remainder of this thesis consists of six chapters. Chapter 2 is a literature review on hydrocarbon sources, the application of radioisotopes (^{210}Pb and ^{137}Cs) for establishing modern sedimentation rates, and geochemical proxies that provide information on early diagenesis, including organic carbon and redox-sensitive elements. Chapter 3 describes the methods used for sample analyses and data analyses. In Chapter 4, the results and findings of the study are presented while in Chapter 5, the discussion of major findings and results is provided. Chapter 6 outlines the conclusions drawn from this work and a list of references is presented in Chapter 7. The entire report ends with a list of appendices.

CHAPTER 2: LITERATURE REVIEW

2.1 Physical and Geochemical Controls on Hydrocarbons in Marine Sediments

2.1.1 Sorption and Deposition of Hydrocarbons to Seafloor

In the event of HC release in the ocean via oil spills or atmospheric transport of aerosols, it is the less volatile fractions of HC that end up in the bottom seafloor. These stable hydrophobic compounds tend to sorb onto settling sediments in aqueous media (Rajesh, Mackay, and Muncke 1999). The hydrocarbon-laden sediments are transported by currents and deposit as they reach lower energy environments (AMAP 2010; Wang et al. 2014). Since the adsorption-settling process is a continuous process, the study of sediment records provides information on history and trends of contaminants in aquatic environments (Kuzyk et al. 2015; Giuliani et al. 2008). Thus several studies have proposed that the distribution and concentrations of hydrophobic organic compounds, including HCs, at the sea bottom are controlled by sediment properties such as OM and grain size (particularly fine grained sediments) (Rajesh et al. 1999; Wang et al. 2014) and that their depositional records can be determined using radioisotopes (^{137}Cs and ^{210}Pb) (Jeter 1999; Kuzyk, Macdonald, and Johannessen 2015). Concentrations of hydrophobic compounds and total organic carbon (TOC) are often strongly correlated (Boitsov, Jensen, and Klungsøyr 2009); however, Mostafa et al. (2009) and several references therein suggest that PAH distribution and concentration in sediments are more likely associated with source inputs as they observed no significant correlation between PAHs and sediment geochemistry.

2.5.1 Sedimentation and Accumulation of Hydrocarbons

High sedimentation rates enhance rapid burial of HCs leading to increased preservation (Schulz and Zabel 2006; Hedges and Keil 1995). According to Müller and Suess (1979), a tenfold increase in sedimentation rate results in doubling of marine sediment organic carbon

burial and preservation. This signifies that there is a general positive relationship between preservation of organic carbon and sedimentation rate (Stein 1990). Consequently, we expect a positive relationship between accumulation of compounds that adhere to organic carbon (e.g. PAHs and n-alkanes) and sedimentation rate. Geochemical processes that affect contaminant fluxes can then be interpreted when contaminant concentrations are integrated with time records (Van Cappellen and Wang 1996). These sedimentary records are also useful tools for analysing the geochemical changes within sediments and chronology of deposition and contaminant flux (Karbassi and Amirnezhad 2013).

2.1.3 Application of Radioisotopes to determine Sedimentation Rates

Radioisotopes such as ^{210}Pb and ^{137}Cs can be used to record particle sedimentation rates over the past ~ 150 to 200 years (Sanchez-Cabeza et al. 1999; Jeter 1999; Van Cappellen and Wang 1996). ^{210}Pb is a decay product of radon (^{222}Rn), which is a gaseous product of radium (^{226}Ra) from the primordial uranium decay series. A portion of gaseous ^{222}Rn diffuses into the atmosphere and decays with a half-life of approximately 3.8 days to form ^{210}Pb, which can then be adsorbed on particles and brought back to the earth surface by rain and dry fallout as excess ^{210}Pb ($^{210}Pb_{ex}$) (Corcoran and Kelley 2006; Tsabaris et al. 2012). Additional sources of ($^{210}Pb_{ex}$) to marine sediments can be produced by decay of dissolved ^{226}Ra in seawater which is scavenged on settling particles (Kuzyk, et al. 2015). The ^{226}Ra, which is naturally present in rocks (the part that did not evaporate), undergoes a series of decay processes to produce supported ^{210}Pb ($^{210}Pb_{sp}$) within sediments (Kuzyk, et al. 2015). $^{210}Pb_{sp}$ is often identified in core profiles as the low, constant activities deep in the cores. With the assumption that the rate of supply is constant, a sedimentation rate can be calculated from the slope of the linear regression of the natural logarithm of the $^{210}Pb_{ex}$ activity, where no mixing is found (Kuzyk, Gobeil, and Macdonald 2013).

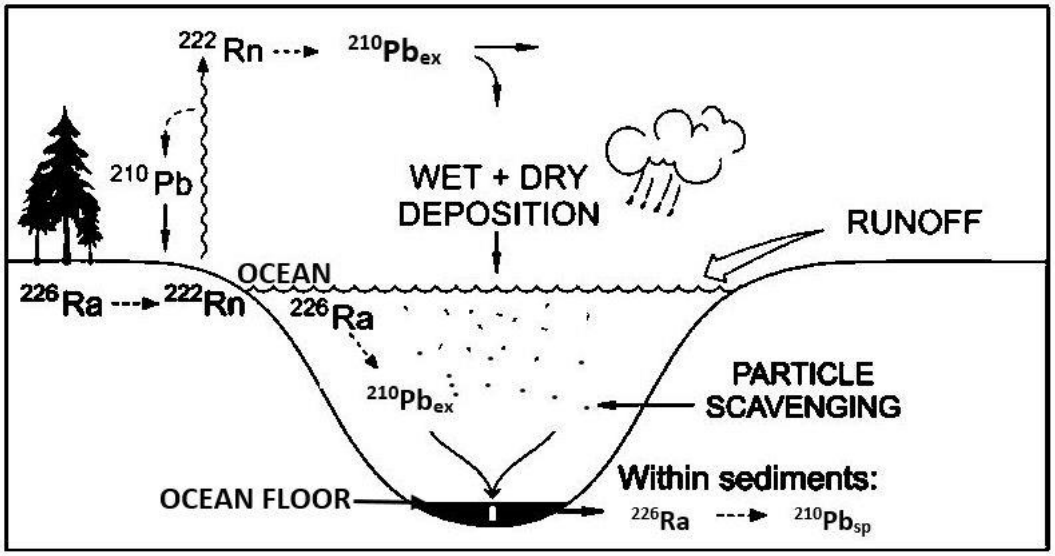

Figure 2.1: Sources and cycling of ^{210}Pb in the environment (modified from Kuzyk et al. 2015).

Sedimentation rates obtained from $^{210}Pb_{ex}$ profiles are often confirmed using other tracers that are independent of ^{210}Pb. The independent transient tracer (^{137}Cs) and ^{210}Pb (steady-state) complement one other providing for more robust and reliable calculated sedimentation rates and geochronologies in sediment cores (Johannessen and Macdonald 2012). With ^{210}Pb and ^{137}Cs each having ~ 8 half-lives = 150-200 years, they record processes on almost the same time scale and hence yield similar results for verifying sedimentation rates within sediments (Tsabaris et al. 2012).

The artificial radionuclide, ^{137}Cs, with a half-life of 30.2 years, was initially introduced into the atmosphere in measurable quantities in 1954 following atmospheric nuclear tests, which maximised in 1963 and decreased thereafter due to a ban on atmospheric weapon testing (Kuzyk et al. 2015). In 1986, peaks were measured at some regions in northern Europe due to the Chernobyl reactor fire incident (Tsabaris et al. 2012); however, the ^{137}Cs deposition in North America was low at that time (J. Wang, Baskaran, and Niedermiller 2017; Drexler, Fuller, and Archfield 2018). The fallout and deposition patterns of ^{137}Cs have been observed to be influenced primarily by the proximity to major nuclear testing areas, global air circulation patterns, rainfall intensity and frequency (NCRP 2007). In undisturbed profiles, ^{137}Cs fallout

from the atmosphere, will be buried in terrestrial and freshwater aquatic sediments (Corcoran and Kelley 2006), and their concentrations will be intact with a peak depth corresponding to the 1963 peak in atmospheric testing (Johannessen and Macdonald 2012).

2.1.4 Biomixing of Sediments

Top sections of marine sediments are most often bio-mixed (Johannessen and Macdonald 2012). Bioturbtion and other post-depositional processes result in the upper layers of marine sediment profile being disturbed. Surface mixed layers (SML) can extend to more than 20 cm in sub-oxic marine sediments and profoundly alter the depth distributions of both geochronological tracers (e.g., ^{210}Pb, ^{137}Cs) and contaminants (Kuzyk, et al. 2015). Within the SML, the net effect of mixing is that $^{210}Pb_{ex}$ activity does not decrease exponentially with depth. The mixing process tends to alter the distribution of geochemicals within the SML and thus interfere with the accuracy of radioisotope profile interpretations leading to overestimation of actual sedimentation rates (Johannessen and Macdonald 2012). Therefore, to estimate sedimentation rate from ^{210}Pb, it is necessary to treat the SML separately from the underlying sediment of low mixing and constant sedimentation rate (Kuzyk et al. 2015). As the SML depth increases, separation of mixed and unmixed (deep layer) sediments becomes difficult (Kuzyk, et al. 2013). Two layer advective-diffusive models; however, can and have been used to account for both mixing and compaction effects (Kuzyk, Gobeil, and Macdonald 2013; Bailey et al. 2013; Kamula et al. 2017). In this thesis, the activities that result in mixing of top sections of marine sediment cores will be referred to as biomixing (Johannessen and Macdonald 2012).

2.2 Organic Carbon Degradation

Early diagenesis refers to degradational processes and changes that occur during burial up to a few hundred meters where extreme temperatures are not encountered. In this thesis,

early diagenesis and degradation are used interchangeably. During organic matter and HC degradation, oxygen, if present in surface waters, is the first to be consumed (Canfield, Kristensen, and Thamdrup 2005). microbes quickly oxidise labile OM (protein, lipids, carbohydrates) and low molecular weight HC such as short chain n-alkanes and simple cyclic HCs to produce CO_2 and H_2O during aerobic degradation (Rabalais 2003; Emerson and Hedges 2003). Complex HCs, such as branched alkanes and PAHs, require multiple metabolic pathways and probably a consortia of bacteria for degradation (Tissot and Welte 1984). Although oxic degradation is thought to be a more effective OM degradation process (Lee et al. 2011), the thickness of the aerobic layer in Arctic sediments oftentimes may be a few mm or less (Kuzyk et al. 2017). In zones where oxygen is limited, microbes degrade hydrocarbon-based materials using a series of electron acceptors such as Mn(IV), NO_3^-, Fe((III) and SO_4^{2-} (Hedges and Keil 1995; Emerson and Hedges 2003).

Sediment redox conditions reflect the balance between downward diffusion of O_2 from the bottom water into sediments and the demand for O_2 associated with metabolism of labile OC (Kuzyk et al. 2017). An anoxic environment succeeds oxic and suboxic environments vertically in the sediment column as O_2 is replaced as oxidant by Mn(IV), NO_3^-, Fe((III) and SO_4^{2-} in succession, such that in the absence of one electron acceptors, microbes are forced to unitise an alternative electron acceptors (Emerson and Hedges 2003). The distribution of elements sensitive to redox concentrations (Fe, Mn, S and others including Mo) can be used to establish depth of O_2 penetration below which the oxides and oxyhydroxides are converted to reduced forms and sulphide minerals are formed (Macdonald et al. 2008; Kuzyk et al. 2010). In this thesis, the vertical distribution of RSE were used to infer labile OC flux, with the profiles of OC in sediments reflecting loss of labile OC component (degradation) when the profiles show a general decrease with depth (Kuzyk et al. 2010). Strong correlation between TOC and HC concentrations served as bases for interpreting HC degradation. Where a degradation

process is established in the sediment RSE profile, and HC concentrations decrease with depth, subsequent interpretation of HC degradation were inferred from.

2.3 Biogenic Sources of Hydrocarbons

In addition to contributing the largest fraction of crude oil, n-alkanes are also biogenic indicators and are used to identify HCs originating either from decomposition of plant waxes or marine biota (Zhendi Wang and Fingas 2003; Parinos et al. 2013). These groups of compounds consist of straight carbon chains with the general formula C_nH_{2n+2}. Like PAHs, n-alkanes are reported to be widespread in the Arctic marine sediment (Lee et al. 2011) and have potential harmful effects when present at significant concentrations (Nemr et al. 2016).

Such high concentrations in the Arctic marine sediments are influenced by decomposition of marine organic matter (Goñi et al. 2000) as well as thawing and erosion of northern circumpolar permafrost soils and associated organic carbon deposits (Curtosi et al. 2007). Deposits of frozen unlithified and highly susceptible erosional materials erode at a rate of 0.5 m/yr on average for the Arctic coast, with higher rates recorded in the Beaufort, Laptev and East Siberian seas (Bischoff et al. 2016). River discharge delivers sediment and terrestrial organic carbon (OC) including vascular plant debris containing long chain n-alkanes (< n-C_{23}), into the oceanic environment during the summer. (Bischoff et al. 2016; R. Stein et al. 2004; Goñi et al. 2005). Harvey et al. (2014), Short et al. (2007), Foster et al. (2015) have revealed significant concentrations of C_{27} and C_{29} n-alkanes in Arctic marine sediments compared to PAHs.

Since n-alkanes in marine sediments are obtained from a large number allochthonous and autochthonous sources, their composition in marine sediments is often complex (Tran et al. 1994). Nonetheless, they have good preservation characteristics (Gonzalez-Vila 1995) which can provide relevant information to ascertain the source of HCs (Tran et al. 1994). Long-chain

n-alkanes (n-C_{27}, n-C_{29}, n-C_{31}…) are often used to confirm terrigenous sources while short-chain n-alkanes (nC_{15}, n-C_{17}, n-C_{19}) indicate marine sources of HCs. The terrestrial aquatic ratio (TAR) defined as the quotient of the concentrations of selected odd carbon numbered long chain n-alkanes over odd carbon numbered short chain n-alkanes exploits these characteristics in Equation 1.

$$TAR = \frac{C_{27}+C_{29}+C_{31}}{C_{15}+C_{17}+C_{19}} \qquad \text{Equation (1)}$$

Higher TAR values generally indicate terrestrial sources and lower values aquatic sources (Ines et al. 2013; Bourbonniere and Meyers 1996). The Carbon Preference Index (CPI) is the ratio of concentrations of odd numbered to even numbered higher molecular weight n-alkanes (Harvey et al. 2014). The index is also used to distinguish between allochthonous vascular land plants from bacteria and petroleum signatures (Nemr et al. 2016). Basically vascular plants which are dominated by odd carbon numbered long chain n-alkanes have high CPI (>5) compared bacteria and petroleum which contain even carbon numbered long chain n-alkanes (Nemr et al. 2016). According to Harvey et al. (2014) CPI is given by the formula in Equation (2). From this Harvey et al. (2014) determined that terrestial sources were dominant in Chuckchi Sea surface sediments.

$$CPI=0.5\left(\frac{C_{25}+C_{27}+C_{29}+C_{31}+C_{33}}{C_{26}+C_{28}+C_{30}+C_{32}+C_{34}}+\frac{C_{25}+C_{27}+C_{29}+C_{31}+C_{33}}{C_{24}+C_{26}+C_{28}+C_{30}+C_{32}}\right) \qquad \text{Equation (2)}$$

2.4 Discriminating Sources of PAHs

PAHs are hydrocarbons made up of two or more benzene rings. There are several sources of natural and anthropogenic sources PAHs, producing a complex mixture of compounds in marine sediments, which complicates source discrimination and apportionment (Van Kooten,

Short, and Kolak 2002; Zeng and Vista 1997) Also, the exact source may be difficult to trace, due to early diagenesis and physical processes (weathering and evaporation) that affect concentration and composition of PAHs in sediments (Yunker et al. 2002). Therefore to effectively discriminate PAH sources, one approach is to classify them into biogenic, pyrogenic and petrogenic sources based on the abundance of certain source-specific thermodynamically stable compounds as defined by Stogiannidis and Laane (2015), Yunker et al. (2002), Ma et al. (2017), Larsen and Baker (2003) and references herein. To effectively use these compounds to identify PAH sources, oil characteristics such as volatility, water solubility, molecular weight of the compounds, resistance to weathering must be taken into consideration (Yunker et al. 2002). This is because loss or degradation of compounds occurs with time during transportation of components between source and sink. During long range transportation, low molecular weight (LMW) PAHs can react with OH^-, undergo photolytic oxidation, volatilisation and even sorption to other phases (e.g., aerosols and precipitation) leading loss or depletion of susceptible LMW compounds and leaving behind stable HMW compounds (Readman, Mantoura, and Rhead 1987; Welch et al. 1991; Hung et al. 2005). These processes act to change the composition of the suite of compounds that end up in marine sediments. Compounds for source analyses are therefore restricted to compound groups within a given molecular mass of proven thermodynamic stability (Budzinski et al. 1997; Yunker et al. 2002).

2.4.1 Biogenic PAHs

The PAH compound perylene (Per) while being produced by combustion, is also found in sediments as a result of post-deposition transformation (during early diagenetic processes and biosynthesis) of terrestrial organic matter under anaerobic conditions (Stogiannidis and Laane 2015; Budzinski et al. 1997; Venkatesan 1988; Wang and Fingas 2003). According to previous workers, Venkatesan (1988) and Bakhtiari et al. (2009) only trace amounts of perylene

present in marine sediments are actually produced from the pyrolysis of organic material. Furthermore, a general increase in concentration of perylene with depth in marine sediments, is an indication that perylene was formed after deposition under anoxic conditions rather than transported to and deposited in the marine sediments (Bakhtiari et al. 2009).

2.4.2 Pyrogenic PAHs

Pyrogenic PAHs are formed when organic materials are burnt under low oxygen, resulting in incomplete combustion (Abdel-Shafy and Mansour 2016). Growing industrialisation and crude oil demand for energy production and transportation consequently increases the release of pyrogenic PAHs into the marine environment. PAHs can also be introduced into the aquatic environment *via* direct atmosphere deposition (Budzinski et al. 1997). Exhaust fumes associated with diesel generators and cruise vessels are also known contributors of pyrogenic PAHs to the marine environment (Foster et al. 2015; Larsen and Baker 2003). Another important pathway for transporting pyrogenic PAHs to the Canadian Arctic is long-range atmospheric transport which may occur either in the vapour phase or on aerosols (Yunker and Macdonald 1995). Atmospheric concentrations of PAHs have been monitored at several Arctic stations since the early 1990s (Hung et al. 2005; Halsall et al. 1997; Becker et al. 2006). Halsall et al. (1997) reported that parts of the Canadian Arctic such as Alert and Tagish were strongly influenced by air pollutants originating from Eurasian and Pacific regions. In some areas, such as the Mackenzie Basin and Baffin Bay, atmospheric sources are only minor contributors of PAH concentrations while petroleum inputs, possibly from reservoir seeps and petroleum exploration/exploitation are recorded as the principal HC source in Arctic marine sediments (Foster et al. 2015; Yunker and Macdonald 1995).

Other sources include forest fires, the burning of biofuels and commonly vehicular and domestic diesel generator emissions (Ravindra et al. 2008). In Canada, large forest fires have

been recorded from 1980s to 2000s (Hanes et al. 2010; Stocks et al. 2002). Although pre 1980s data have been reported, they are deemed less reliable due to the poor monitoring methods and data loss (Stocks et al. 2002). The total forest area burnt by large fires between 1980 and 2010 is estimated to be between 175,000 and 255,000 km^2 per decade (Hanes et al. 2010). The greatest percentage of these fires were recorded within the Boreal Shield, Taiga Shield and Plains (Stocks et al. 2002; Hanes et al. 2010). Atmospheric circulation data reported over this time period indicate that the prevailing winds into the Hudson Bay system, particularly in the winter, emanate from these ecozones (Vickers et al. 2000). Forest fires in the Nunavut occur on an almost annual basis with the fire in 2014 reported to be the worst in the past 3 decades (www.nunatsiaqonline.ca/stories/article/65674forest_fires_heat_wave_colour_otherwise_normal_arctic_summer/, accessed 21 October, 2017).

Organic matter combustion generally results in an increase of unsubstituted parent PAH concentrations relative to the alkylated PAHs (Pampanin and Sydnes 2013). A higher ratio of parent versus alkylated PAH concentrations is indicative of combustion activities and sources (Baumard et al. 1998; Yunker et al. 2002; Yunker et al. 1996).

2.4.3 Petrogenic PAHs

Petrogenic hydrocarbons are derived from petroleum, and related products such as crude oil, lubricants, and other petroleum derivatives (Stogiannidis and Laane 2015). Such HCs are deposited into the marine environment *via* accidental oil spills, discharge from routine tanker operations, ruptured pipelines, discharge during oil exploration and exploitation, municipal and urban runoff and natural petroleum reservoir seeps (Foster et al. 2015; AMAP 2010). At present, shipping in Arctic waters is primarily associated with fishing, research vessels, delivering goods to isolated communities, transport of products to and from mining sites, ice-breaker support for sealift traffic, supply ships for offshore drilling operations, tourist ships and

the transportation of crude oil by tankers from oil fields (AMAP 1998; Martinsen, Hustad, and Sverud 2013). Intentional and unintentional oil spills have been recorded in the marine environment. The best records are available for industrial activities. For example, from 1980 to 2005, an estimated 1,048 individual accidental spills occurred in the South Coast of Newfoundland, Canada (Li et al. 2016). In 2004, two large oil spills occurred offshore from Sable Island, Nova Scotia, which released 4,000 L of diesel and the 354,000 L of drilling mud respectively, at an exploratory well. (Li et al. 2016). There are also records of oil spills in Nunavut region as the area relies extensively on imported fossil fuel for its energy needs (Figure 1.1). The region imports millions of liters of fuel annually and has done so for several decades (http://www.canadianfuels.ca/ASR-Fuels-en/Northern-power/, accessed 3 April 2017). According to an article posted by Government of Nunavut in 2016 (https://climatechangenunavut.ca/en/energy/energy-nunavut, accessed 4 January 2019), it was estimated that in 2012-2013 alone, the territory imported $195 million worth of fossil fuel of which more than 50 % was used for electricity and heating purposes. More than 200 million liters of fuel was imported into the territory in 2016-2017 (https://climatechangenunavut.ca/en/energy/energy-nunavut, accessed 4 January 2019). All of these purchased fuels are shipped in bulk during the short summer season and stored in tank facilities in each community (https://www.gov.nu.ca/petroleum-products-division, accessed 10 June 2018). With accidental spills and intentional discharges of fuel oils being recorded as the most frequent occurrences in water bodies (Stout and Wang 2016), shipping and industrial activities in the Arctic are collectively a significant source of petrogenic pollution to Arctic marine waters (Barber, Babb, and Andrews 2015).

Natural reservoir leaks, which have existed since primeval times, also contribute significant quantities of petrogenic HCs into the marine environment (Stout and Wang 2016). In the Canadian Arctic, both known and unknown natural reservoir petroleum leaks have been

reported to occur (Li et al. 2016). In Baffin Bay, for instance, seeps have been recorded in Scott Inlet, and in west Lancaster Sound (Bennett, Campbell, and Furze 2013). Of the different sources of HC entering the marine environment every year, it is estimated that at least 15% comes from natural oil seeps (AMAP 1998). Though no annual budgets are yet available for the Arctic region, the rate of percolation is believed to be higher than the global average (AMAP 1998). These seeps have led to the finding of commercially recoverable petroleum reserves (AMAP 1998); however, they are inevitable sources of HC contamination to the Arctic environment. Recoverable petroleum reserves have been discovered in several parts of the northern Canadian Arctic such as Baffin Bay, the Arctic Islands, the Mainland Territories, and the Beaufort Mackenzie Basin (Yunker and Macdonald 1995; Lee et al. 2011; Foster et al. 2015) and notable HC exploration is taking place in other parts of the Canadian Arctic. Given the scarce data available for large parts of the Canadian Arctic, there is no doubt that contamination can extend even to unassessed areas such as Wager Bay and Chesterfield Inlet.

2.4.4 Source-specific PAH Compounds

Certain PAH compounds have source discrimination abilities by their absence or presence in oil contaminated samples (e.g., sediments, biological tissues or shorelines). The abundance of selected unsubstituted parent PAHs over their alkylated counterparts and vice versa can be used to distinguish pyrogenic and petrogenic sources. According to Larsen and Baker (2003) and Stogiannidis and Laane (2015) and references therein, indeno [1,2,3-c,d] pyrene (IP), pyrene (Py), benzo[e]Pyrene (BePy), benzo[g,h,i]Perylene (Bghi), fluoranthene (Fl), benzo[b,j,k]fluoranthene (BF), chrysene (Ch) and phenanthrene (Pn) are PAHs associated with combustion processes. Bghi in samples are identified as tracers of vehicular emissions. Higher levels of BF is suggested to indicate diesel vehicles and IP is found in both diesel and gas engine emissions (Larsen and Baker 2003). Low molecular weight (LMW) pyrogenic

compounds such as Pn, Fl and Py are considered to be pyrogenic components of short-range atmospheric transportation (Welch et al. 1991; Hung et al. 2005). Substantial amounts of alkylated naphthalenes (Na), and Pn are derived from petrogenic sources as recorded in Beaufort sea sediments (Yunker and Macdonald 1995). Other alkylated PAH homologues of fluorine (F), and Ch are found and have also been attributed to petrogenic sources (Yunker et al. 2002).

CHAPTER 3: SAMPLE COLLECTION AND ANALYSES

3.1 Sampling

During an August 2016 expedition as part of a marine baseline assessment initiated and funded by Parks Canada and the Government of Nunavut's Department of Environment Fisheries and Sealing Division, sediment cores were collected from seven locations across Chesterfield Inlet and Wager Bay, Nunavut, (Figure 1.3). The cores were collected aboard the Research Vessel Nuliajuk using a Gomex box corer (dimensions; 40 x 45 and 55 cm high). The sampling covered a wide range of water depths ranging from 41 m in Chesterfield Inlet to between 131 and 332 m in Wager Bay (Table 3.1). The box corer was deployed at ~1 m/s until it contacted the seafloor to collect the samples. Once the box corer was lifted onto the deck, a core tube (10 cm diameter) was carefully pushed into the undisturbed sediments, away from the side walls of the box, being sure to minimize compression, then sealed at the bottom and removed from the box. The sediment cores, ranging in depth from 6 to 27 cm were extruded and sub-sectioned at 1 cm intervals for the first 10 cm and at 2 cm intervals thereafter (Table 3.1). Samples were kept in certified clean glass jars and stored in a chest freezer at approximately – 20°C until they were shipped to the University of Manitoba in Winnipeg. Upon arrival, wet sediment samples were weighed and freeze-dried in a Labconco FreeZone 2.5 Liter Benchtop Freeze Dry System at -45ºC and 0.03 mbar for ~96 hours. The dried sediments were then ground up with a mortar and pestle into a fine powder prior to analyses.

Table 3.1: Station IDs, coordinates, distance to sea bottom and recovered core length

Station IDs	Core IDs	Latitude (N)	Longitude (W)	Sea Bottom Depth (m)	Core Length (cm)
CI-08	CI-08	63.307	-90.625	42	21.5
CI-24	CI-24	63.518	-91.079	41	11.5
08	NU-WAB-08	65.466	-89.207	332	27
10	NU-WAB-10	65.775	-89.563	221	13
14	NU-WAB-14	65.646	-89.192	197	13
16	NU-WAB-16	65.46	-88.789	202	6
15	PLK-NU-15	65.373	-89.048	131	18

3.2 Total ^{210}Pb and ^{137}Cs Analyses

3.2.1 Total ^{210}Pb Analyses

About 1 g of dried ground sediments samples were analysed for total ^{210}Pb from the alpha energy spectrum recorded on an alpha spectroscopy system consisting of Ortec model 576 dual alpha spectrometers with surface barrier detectors, mixer router, multichannel analyzer and vacuum pump. Total ^{210}Pb ($^{210}Pb_{sp}$+$^{210}Pb_{ex}$) was determined *via* the ^{210}Po daughter isotope using alpha spectroscopy, with the assumption that ^{210}Po and total ^{210}Pb ($^{210}Pb_t$) are in equilibrium (Baskaran et al. 2014). The procedure employs a ^{209}Po tracer for quantitation. ^{209}Po tracer was calibrated against a ^{210}Po standard solution that is NIST traceable (Isotope Product Laboratories, product # 6310, Source No.: 1130-1). ^{209}Po tracers are used to determine the absolute activities of the $^{210}Pb_t$ and are standardized by weight rather than volume (i.e. Bq/g) to allow for more precise additions using Eppendorf pipettes which can be calibrated to deliver a known weight of each tracer solution.

Details of this method are outlined by Slavicek (2011). Briefly, for this method, about 1.0 g sample is weighed into a 100 mL beaker. Measured amounts of mixed ^{209}Po tracer and ^{210}Po standard and 30 mL 6N HCl are added and the beaker is covered with a watch glass and placed on a hot plate at 180°C. After 5 hours, the beaker is removed from the hotplate and allowed to cool and settle. The clear liquid is then decanted into a 250 mL beaker which contains 50 ml

of distilled water and 5 mL 10% ascorbic acid. Using the "Vibro Graver", the sample ID, isotope and date are etched on one side of a silver disc and placed into the larger beaker with the unmarked side up. The beaker with the disc is covered with a watch glass and placed on a hot plate overnight on low heat (80°C). The beaker is removed from the hot plate, allowed to cool to room temperature. The disc was removed with a plastic spatula, rinsed with deionised water and counted using an alpha counter. Each sample was individually counted for ~3-4 days. The International Atomic Energy Agency (IAEA) Reference sample errors ranged from between 0.00372 and 0.0224 Bq/g while sample counting errors ranged between 0.004 and 0.008 on the alpha spectrometer. A correction for the amount of salt retained in the dry sediments was made based on Equation 5. Bq/g were converted to disintegration per minute per gram (dpm/g) by multiplying by 60 (seconds).

3.2.2 ^{137}Cs Analyses

The activities of ^{137}Cs were determined by placing petri dishes containing ~8 g of dried samples on a Micromass Model 602 gamma spectrometer. The gamma spectrum was counted on a lithium doped germanium (Ge (Li)) detector. ^{137}Cs activities were obtained from the 662 keV peak (85%) of Ba-137M and is decay corrected back to the sampling day. ^{137}Cs was counted for 16-24 hours to obtain an energy spectrum (662 keV) and was compared to a certified reference sample having the same counting geometry. ^{137}Cs was calculated as:

$$^{137}\text{Cs activity} = \Sigma\text{Cs} / .85 \times \text{Eff-137} \times 1/e^{-\lambda t} \qquad \text{Equation (3)}$$

Where: Cs activity = activity of ^{137}Cs at time of sampling (dps), ΣCs = counts per second (cps) of 662 keV photo peak, Eff 137 = counting efficiency for ^{137}Cs at 662 keV for the sample

geometry used, λ = decay constant for ^{137}Cs (0.023043 yr^{-1}), t = elapsed time (yrs) between sampling and counting

Counting efficiencies were determined by counting IAEA reference samples (IAEA-65R-67R) within the same sample geometry (i.e., petri dish) as our samples. Average % error in counting ^{137}Cs within samples CI-24 and PLK-NU-15 were 6 and 16%, respectively. In the remaining cores, ^{137}Cs was either not detected or was detected in only one or two sediment sections core slices. The detection limit was 0.1 Bq kg^{-1} for a counting time of 16 hrs. No duplicate samples were analysed, although several samples in which ^{137}Cs was not detected were placed on the gamma spectrometer repeatedly to confirm the results. To correct for the amount of salt retained in the dry sediments, ^{137}Cs activity was multiplied by a salt factor (Equation 5).

3.2.3 Determination of Porosity, Salt Factor, Sedimentation and Mass Accumulation Rates

Porosity (Φ) was used to infer particle size based on (Huettel and Gust 1992), such that higher porosity indicates finer grain sediments. Calculations for determining porosity and salt factor are given in equations 4 and 5 respectively.

<u>Measured parameters</u>

Salinity (S) of bottom water at the time of sediment core sampling = 32.155

Wet weight (ww) of sediments

Dry weight (dw) of sediments

<u>Constant Parameters</u>

Density of water (ρw) = 1.025

Density of sediment (ρs) = 2.650

<u>Calculations</u>

Moisture content (mc) = (ww - dw) / ww

Wet Volume (Vw) = (mc + (mc * S / 1000)) / ρw

Volume of sediment (Vs) = (1 - mc - (mc * S / 1000)) / ρs

$\Phi = Vw / (Vw + Vs)$ Equation (4)

$$\text{Salt Factor (SF)} = \frac{1\text{-mc}}{(1\text{-mc}) - (\text{mc} * S)/1000}$$ Equation (5)

$^{210}Pb_{ex}$ was calculated as the difference between $^{210}Pb_t$ activity in each core slice and the $^{210}Pb_{sp}$ value (i.e. the low constant activities deep in the cores) (Kuzyk et al. 2015). Sedimentation and mass accumulation rates were determined from the profiles of $^{210}Pb_{ex}$ activity by fitting the data to output from a steady-state, advective-diffusive model that explicitly accounts for both sedimentation and mixing rates (Kuzyk et al. 2015). For this modelling approach, the sediments were considered as having a SML (i.e. determined by eye) with a mixing rate, Kb_1 overlying a more slowly-mixed deep layer with mixing rate Kb_2 ~0. This two-layer, advective-diffusive model, is based on Equation 6:

$\boldsymbol{\lambda}C = \omega\delta C/\delta z - \delta/\delta z\,(Kb\delta C/\delta z)$ Equation (6)

Where C = $^{210}Pb_{ex}$ surface activity (dpm cm^{-3}), z = depth (cm, positive downwards), Kb_1 = surface mixing rate (cm^2yr^{-1}), Kb_2 is deep layer with mixing rate below SML (~0), and $\boldsymbol{\lambda}$ = ^{210}Pb decay constant (0.03114 yr^{-1}). Kb_1, and C were obtained by adjusting their values to obtain the best least squares fit between the measured and model output. Details of this advective-diffusive model may be found in Kuzyk et al. (2013, 2014).

Assuming a constant rate of supply, sedimentation velocities (ω) for each core were calculated from the slope (m) of the linear regression of the natural logarithm of the $^{210}Pb_{ex}$ activity (dpm/cm^3) at depths below SML (Equation 6). The mass accumulation rate (r) was calculated from the sedimentation velocity as shown in Equation 8.

$\omega = -\boldsymbol{\lambda}/m$ Equation (7)

$r = \rho s\,(1-\Phi)\,\omega$ Equation (8)

Where ρs is the density of sediment solids (density was taken to be = 2.65 g cm^{-3}). Confidence limits (95%) on the slope of ln ($^{210}Pb_{ex}$ activity) versus depth was determined to evaluate the 'error margins' of the sedimentation velocities. $^{210}Pb_{ex}$ and ^{137}Cs inventories (dpm cm^{-2}) in each core were calculated as the sum down to depth where activity was no longer detectable of the products of mass-depth (g cm^{-2}) and activities (Kuzyk, Macdonald, and Johannessen 2015).

3.2.4 Validating ^{210}Pb Sedimentation Rates and Dating Sediment Cores with Mixed Surface Layers

To validate ^{210}Pb derived rates, models of ^{137}Cs distribution was developed using an advective-diffusive model in MATLAB (Johannessen and Macdonald 2012). The model was run assuming the sedimentation velocities, mixing rates (K_b) and depths determined from the $^{210}Pb_{ex}$ profiles in the cores (Smith 2001). A ^{137}Cs input function that included deposition beginning in 1954 and peaking in 1963 was added and run to obtain a good fit between observed and predicted depth of onset of ^{137}Cs in the sediments (Kuzyk, Macdonald, and Johannessen 2015).

While it is not possible to assign specific dates to core sections or depths that have mixed surface layers (Johannessen and Macdonald 2012; Kuzyk, Macdonald, and Johannessen 2015), timeframes corresponding to, for example, to pre- and post-industrialisation can be assigned. To achieve this assignation, the SML, mixing coefficients and ω determined from $^{210}Pb_{ex}$ profiles in the cores were used in a tracer experiment using the advective–diffusion model in MATLAB (Johannessen and Macdonald 2012). A tracer starting in 1900 was entered into the model to determine two sediment domains or timeframes, i.e. the relative depths of ≥ 90% pre-

1900 and ≥ 90 post-1900 sediments contained in each core (Bailey et al. 2013). The model was allowed to run until the date of core collection, ~2016.

3.3 Total Carbon Analyses

Organic materials in sediments were measured as organic carbon. First, samples were analysed for total carbon (%TC) and total inorganic carbon (%TIC) contents. Then, %TOC was obtained by the difference between TC and TIC.

%TC and %TIC analysis was performed using an Eltra Helios Elemental Analyser. Aliquots (~0.5 g) of the homogenised sediments were weighed in a ceramic crucible and placed into a preheated oven at an elevated temperature. After a few minutes of combustion in a constant carrier gas (oxygen) flow, total carbon was detected and measured as %TC. For TIC analysis, samples were preheated in a flask at a low temperature for ~2 minutes and treated with ~7 mL of 10% (volume) hydrochloric acid (HCl) to remove water and organic carbon. The TIC content was then detected and measured. Average reproducibility of the %TIC and %TC duplicate samples was 2% and 4% respectively are shown in Table 3.2, while percent recoveries of standard reference materials are shown in Table 3.3.

Table 3.2: Percent Differences between duplicate (dup) samples from Carbon Analyses

Sample ID	TC (%)	% Difference	TIC (%)	% Difference
CI-08 0-1 cm	1.43	17		
CI-08 0-1 cm dup	1.20			
CI-08 10-12 cm	1.11	3		
CI-08 10-12 cm dup	1.08			
NU-WAB-10 10-12 cm	2.22	0		
NU-WAB-10 10-12 cm dup	2.23			
PLK-NU-15 9-10 cm	1.76	0		
PLK-NU-15 9-10 cm dup	1.76			
PLK-NU-15 12-14 cm	1.64	1		
PLK-NU-15 12-14 cm dup	1.62			
NU-WAB-08 16-18 cm	3.11	3	1.20	2
NU-WAB-08 16-18 cm dup	3.02		1.22	
CI-08 3-4 cm			0.47	4
CI-08 3-4 cm dup			0.45	
CI-08 9-10 cm			0.44	4
CI-08 9-10 cm dup			0.42	
NU-WAB-10 12-13 cm			0.63	2
NU-WAB-10 12-13 cm dup			0.62	
NU-WAB-08 3-4 cm			0.96	1
NU-WAB-08 3-4 cm dup			0.97	
NU-WAB-08 12-14 cm dup			1.11	1
NU-WAB-08 12-14 cm dup			1.10	
PLK-NU-15 3-4 cm			0.36	0
PLK-NU-15 3-4 cm dup			0.36	

Table 3.3: Percent Recoveries of Standard Reference Materials from Carbon Analyses

%TC Standard (AR1034) (n = 14)		% TIC Standard (B2150) (n = 9)	
Measured Concentration	7.17 ± 0.09	Measured Concentration	12.00 ± 0.02
Known Concentration	7.19	Known Concentration	11.94
Percent Recovery	100	Percent Recovery	100
Standard Deviation	0.06	Standard Deviation	0.05

3.4 Major and Trace Element Analyses

Dried and ground samples were submitted to ACME Labs (Bureau Veritas, Vancouver BC) for analyses of Mn, Fe, S, Mo and Al. A total of 47 samples were analysed using method AQ250. This method involves Aqua regia digestion of 0.5 g of each sample (digestion in nitric and hydrochloric acids) and analysis by ultra-trace inductively coupled plasma mass spectrometry (ICP-MS). All elements were normalised to Al in order to eliminate mineralogical and clay mineral effects (i.e. element/Al) (Loring and Asmund 1996; Newman and Watling 2007; Ho et al. 2012). Accumulation rates of authigenic elements were then calculated by multiplying their concentrations by the sedimentation rate (Equation 9).

$$r_{auth} = rC_{auth} \qquad \text{Equation (9)}$$

Where authigenic concentration (C_{auth}) is defined as the average concentration of the stable portions of element sediment core profile and r is sedimentation rate obtained from ^{210}Pb (Zheng et al. 2000).

Differences between duplicate (dup) samples < 14% (Table 3.4) while recovery of standard samples (DS10 and OREAS45EA) ranged between 96 and 111 %. The concentrations in blank samples were below detection limits (Table 3.5).

Table 3.4: Percent differences between duplicate samples from Trace and Major Elements Analyses

Sample ID	Mo (ppm)	Mn (ppm)	Fe (%)	S (%)
Detection Limit	0.01	1	0.01	0.02
Cl-08 1-2 cm	0.88	98	0.98	0.15
Cl-08 1-2 cm dup	0.82	96	0.99	0.15
Percent difference	7	2	1	0
PLK-NU-15 3-4 cm	0.72	261	2.12	0.25
PLK-NU-15 3-4 cm dup	0.82	272	2.23	0.28
Percent difference	13	4	5	11

Table 3.5: Percent recoveries of SRMs and blank concentrations from Trace and Major Elements Analyses

Standard Reference Materials (SRM)	Mo (ppm)	Mn (ppm)	Fe (%)	S (%)
DS10 (n = 2)				
Average concentration	14.95	894.5	2.75	0.29
Expected concentration	13.60	875	2.72	0.29
Percent recovery	110	102	101	98
OREAS45EA (n = 2)				
Average concentration	1.54	402.5	22.29	0.04
Expected concentration	1.60	400	23.51	0.04
Percent Recovery	96	101	95	111
Blanks concentrations				
Blank 1	<0.01	<1	<0.01	<0.02
Blank 2	<0.01	<1	<0.01	<0.02

3.5 Hydrocarbon Analyses

3.5.1 Hydrocarbon Extraction and Fractionation

Perdeuterated n-alkane recovery standard containing seven deuterated compounds was obtained from Chiron AS (Table 3.6). Each perdeuterated compound contained in the standard solution had a concentration of 1.0 mg/mL. This was further diluted with iso-octane to a concentration of 500 pg/µL and then added to 2 g of sediment and blank samples. No n-alkane SRM was not obtained for use in the analyses. A deuterated PAH standard containing sixteen compounds was purchased from Cambridge Isotope Laboratories, Incorporated (Table 3.10). Each deuterated PAH compound had a concentration of 200 µg/mL. The deuterated PAH standard was diluted with iso-octane to concentrations reflective of the samples (250 and 5000 pg/µL). 20 µl of the 250 pg/µL solution was added to 2 g the grounded freeze-dried sediment and blank samples and 20 µl of the 5000 pg/µL solution was added to NIST 1941b SRM (The SRM had a 20x higher concentration relative to the predicted sediment concentrations). The blank used for the analyses was a sea-washed sand purchased from ACROS Organics. Prior to use, the sand was baked at 550°C for 10 hours. The analyses of all the sediment, SRM and

blank samples were performed in the same manner to reduce variability of the method and ensure the accuracy of the results.

A 30 mL of a hexane/acetone solution (1:1, v/v) was added to all the spiked samples and vortexed for 30 seconds. Extraction of HCs from the samples (sediments, blanks and NIST 1941b SRM) was performed using a CEM MARS 6 microwave extractor operated at 120°C for 20 minutes based on methods outlined under US EPA 3546 (U.S EPA 2007). Acid washed copper was prepared and added to the sample extracts to remove any sulfur that may be present in them. The copper was prepared by weighing roughly 10 g of 106 µm copper powder and adding 100 mL of 10% nitric acid (to remove oxides). After 30 minutes, the acid was decanted and the remaining copper rinsed 3 times with acetone followed by, 3 times with hexane. The copper was added to the sample extracts, which were then reduced down to 1-2 mL in a 35 ºC rotary and nitrogen evaporators.

A silica gel chromatography column (30cm x 20mm id) was used to elute hydrocarbon fractions from sediment extracts using a modified version of US EPA method 3630C (U.S EPA 1996). In brief, a piece of glass wool was placed at the bottom of the column and washed with Dichloro Methane (DCM). A slurry consisting of 5 g of deactivated Fisher brand silica gel (chromatographic grade 923; mesh size 100-200, pre-baked at 160ºC for 8 hours) and ~ 20 mL DCM was poured into the column and allowed to settle. The column was then topped off with 1 g sodium sulphate that had previously been baked at 550 ºC for 5 hours and rinsed with 50 and 25 mL of DCM and hexane, respectively. Sample extracts were loaded onto the top of the column using a pipette. The low polarity aliphatic compounds were eluted off the column first (fraction 1) using 25 mL of hexane. The PAH compounds were then eluted using 25 mL of 1:1, v/v DCM/hexane (fraction 2). Each fraction was collected into a 25 mL flat bottom flask and concentrated down using rotary and nitrogen evaporators. Sediment and blank samples were

concentrated to a pre-injection volume of 0.2 mL while NIST 1941b SRM were reduced to a pre-injection volume of 1.0 mL in iso-octane.

3.5.2 Analyses and Identification of n-alkanes

n-alkane analyses were conducted using a Pegasus® 4D GC x GC HRT coupled to a time of flight mass spectrometer (TOFMS). The mass spectrometer was operated at 70 eV in full scan mode (FSM). The mass range was 50-305 m/z and the resolution set at 25,000. The injection port, transfer line and ion source temperatures were set at 275°C, 320°C and 300°C, respectively. Operating in 1-D, the GC oven temperature was initially set at 80°C. After 1.5 minutes it was increased by 20°C/min to 120°C followed by 3°C/min to 250°C and 2°C/min to 300°C, where it was held for 11.50 minutes. Average sample run time was 83.33 minutes. The chromatography was performed using a 60 m x 0.25 mm ID and 0.10 µm film thickness Rxi-PAH fused-silica capillary column followed by a 2 m x 0.25 mm ID x 0.25 µm film. Rxi-5ms column was used for 2-D analysis. Ultra-High Purity (UHP) Helium was used as the carrier gas and operated at a constant flow rate of 1.4 mL/min. 1 µL sample extract volumes were injected using the splitless mode.

Compound identification was performed based on mass spectral data, comparison of GC retention data, reference standards, and the NIST mass spectra library (Liao et al. 2010).

Quantification and semi-quantification of n-alkanes (n-C_{11} to n-C_{36}) was performed using their per-deuterated analogues (Table 3.6) on a LECO ChromaTOF HRT® (software, version 1.90.60.0.4326).

3.5.3 n-alkane QA/QC

The samples were extracted in three batches. Batch one consisted of three blank samples and twenty-four sediment samples (out of the twenty-four sediment samples, eight were

duplicate samples). Batch two was made up of three blank samples, twenty-four sediment including seven duplicate samples. Batch three comprised of twenty-three sediment samples, (plus six duplicates) and two blank samples. A total of seventy-one samples, twenty-one duplicates and eight blanks were analysed for n-alkanes. Geometric mean (GM) herein also referred to as 'mean' was calculated for all n-alkanes instead of arithmetic mean in order to normalise the positively skewed data.

The differences between duplicate samples ranged from 0 to 66% (Table 3.7). The mean (confidence interval) of n-alkane compounds in blank samples from all three extraction batches ranged from 0 to 22.63 (19.27-26.58) ng/g dw (Table 3.8). The Limits of detection (LOD), were determined from blanks as the concentration equivalent to the average blank value plus three times standard deviation of the same (Ma et al. 2017). Concentrations ranged from 0 to 49.73 ng/g dw. Three per-deuterated compounds (D-26-Dodecane, D-34 Hexadecane, D-42 Eicosane) were detected in the first and second extraction batches, while five per-deuterated; D-34 Hexadecane, D-42 Eicosane, D-50 Tetracosane, D-58 Octacosane, D-66 Dotriacontane) were detected in the third batch. The mean recoveries (SE) concentrations of all per-deuterated standards in each batch were 77 % (6 %), 78 % (4 %) and 119 % (3 %) respectively.

Table 3.6: n-alkane compounds, abbreviations and associated deuterated standards

Compound	Carbon #	Associated Deuterated in Run 1	Associated Deuterated in Run 2	Associated Deuterated in Run 3
Undecane	n-C_{11}	D-26 Dodecane	D-26 Dodecane	D-34 Hexadecane
Dodecane	n-C_{12}	D-26 Dodecane	D-26 Dodecane	D-34 Hexadecane
Tridecane	n-C_{13}	D-26 Dodecane	D-26 Dodecane	D-34 Hexadecane
Tetradecane	n-C_{14}	D-34 Hexadecane	D-34 Hexadecane	D-34 Hexadecane
Pentadecane	n-C_{15}	D-34 Hexadecane	D-34 Hexadecane	D-34 Hexadecane
Hexadecane	n-C_{16}	D-34 Hexadecane	D-34 Hexadecane	D-34 Hexadecane
Heptadecane	n-C_{17}	D-34 Hexadecane	D-34 Hexadecane	D-34 Hexadecane
Octadecane	n-C_{18}	D-34 Hexadecane	D-34 Hexadecane	D-34 Hexadecane
Nonadecane	n-C_{19}	D-42 Eicosane	D-42 Eicosane	D-42 Eicosane
Eicosane	n-C_{20}	D-42 Eicosane	D-42 Eicosane	D-42 Eicosane
Heneicosane	n-C_{21}	D-42 Eicosane	D-42 Eicosane	D-42 Eicosane
Docosane	n-C_{22}	D-42 Eicosane	D-42 Eicosane	D-42 Eicosane
Tricosane	n-C_{23}	D-42 Eicosane	D-42 Eicosane	D-50 Tetracosane
Tetracosane	n-C_{24}	D-42 Eicosane	D-42 Eicosane	D-50 Tetracosane
Pentacosane	n-C_{25}	D-42 Eicosane	D-42 Eicosane	D-50 Tetracosane
Hexacosane	n-$C2_6$	D-42 Eicosane	D-42 Eicosane	D-50 Tetracosane
Heptacosane	n-C_{27}	D-42 Eicosane	D-42 Eicosane	D-58 Octacosane
Octacosane	n-C_{28}	D-42 Eicosane	D-42 Eicosane	D-58 Octacosane
Nonacosane	n-C_{29}	D-42 Eicosane	D-42 Eicosane	D-58 Octacosane
Triacontane	n-C_{30}	D-42 Eicosane	D-42 Eicosane	D-58 Octacosane
Hentriacontane	n-C_{31}	D-42 Eicosane	D-42 Eicosane	D-66 Dotriacontane
Dotriacontane	n-C_{32}	D-42 Eicosane	D-42 Eicosane	D-66 Dotriacontane
Tritriacontane	n-C_{33}	D-42 Eicosane	D-42 Eicosane	D-66 Dotriacontane
Tetratriacontane	n-C_{34}	D-42 Eicosane	D-42 Eicosane	D-66 Dotriacontane
Pentatriacontane	n-C_{35}	D-42 Eicosane	D-42 Eicosane	D-66 Dotriacontane
Hexatriacontane	n-C_{36}	D-42 Eicosane	D-42 Eicosane	D-66 Dotriacontane

Per-deuterated Standards included: D-26 Dodecane, D-34 Hexadecane, D-42 Eicosane, D-50 Tetracosane, D-58 Octacosane, D-66 Dotriacontane, and D-72 Hexatriacontane

Table 3.7: QA/QC of n-alkanes showing percent (%) differences between duplicate samples (n = 22)

Compound	n-C_{11}	n-C_{12}	n-C_{13}	C_{14}	n-C_{15}	n-C_{16}	n-C_{17}	n-C_{18}	n-C_{19}	n-C_{20}	n-C_{21}	n-C_{22}	n-C_{23}
Batch 1													
CI-08 14-16 cm	nd	nd	5.01	35.87	57.85	97.01	14.9	nd	18.38	25.66	33.69	78.53	102.21
CI-08 14-16 cm dup	nd	nd	4.31	21.29	37.03	70.93	12.16	nd	16.12	20.48	33.37	93.67	137.15
% difference	nd	nd	15	51	44	31	20	nd	13	22	1	18	29
CI-24 2-3 cm	nd	4.45	8.73	40.66	17.82	28.5	15.25	nd	nd	15.18	15.15	26.22	22.91
CI-24 2-3 cm dup	nd	4.01	8.63	41.12	17.87	29.36	15.5	nd	nd	15.97	17.31	31.22	35.31
% difference	nd	10	1	1	0	3	2	nd	nd	5	13	17	43
CI-24 3-4 cm	nd	nd	5.94	32.98	42.07	79.73	15.41	4.55	15.05	18.8	28.92	77.69	106.32
CI-24 3-4 cm dup	nd	nd	5.86	33.67	42.57	79.47	15.75	4.57	15.61	18.88	28.33	75.3	103.18
% difference	nd	nd	1	2	1	0	2	0	4	0	2	3	3
CI-24 7-8 cm	nd	3.58	8.02	53.4	46.21	72.13	14.22	4.57	13.3	24.26	25.01	66.08	75.16
CI-24 7-8 cm dup	nd	3.77	7.99	53	46.79	73.26	14.71	5.32	13.41	24.53	25.44	69.57	74.06
% difference	nd	5	0	1	1	2	3	15	1	1	2	5	1
CI-24 8-9 cm	nd	nd	nd	nd	nd	69.08	10.13	3.75	10.45	15.94	23.87	61.72	90.53
CI-24 8-9 cm dup	nd	nd	nd	nd	nd	48.92	11	3.94	11.91	15.49	24.57	63.8	86.09
% difference	nd	nd	nd	nd	nd	34	8	5	13	3	3	3	5
NU-WAB-08 6-7 cm	1.67	5.15	6.65	61.36	11.76	24.03	23.41	9.42	22.91	37.09	55.25	117.32	180.96
NU-WAB-08 6-7 cm dup	1.48	5.02	6.53	61.24	11.98	23.84	21.82	8.82	21.07	33.84	50.87	109.9	168.82
% difference	12	3	2	0	2	1	7	7	8	9	8	7	7
NU-WAB-08 8-9 cm	60.31	289.51	181.7	191.91	27.22	37.49	41.38	13.77	37.57	54.02	55.95	126.94	167.61
NU-WAB-08 8-9 cm dup	57.8	289	184.35	191.87	26.89	36.65	40.72	13.99	36.21	53.58	55.63	123.47	159.73
% difference	4	0	1	0	1	2	2	2	4	1	1	3	5
NU-WAB-08 25-27 cm	nd	317.69	128.08	252.31	43.45	52.69	90.06	10.53	26.92	28.61	28.58	47.23	65.84
NU-WAB-08 25-27 cm dup	nd	305.53	120.49	242.76	38.64	48.77	84.31	10.62	28.58	29.69	31.3	51.43	79.17
% difference	nd	4	6	4	12	8	7	1	6	4	9	9	18
Batch 2													
NU-WAB-10 10-12 cm	nd	5.96	5.36	51.18	17.4	27.92	33.93	9.89	33.46	49.86	55.93	117.7	164.89
NU-WAB-10 10-12 cm dup	nd	6.23	5.23	52.9	17.84	28.5	34.76	10.43	37.17	49.04	54.8	111.92	172.88
% difference	nd	4	2	3	2	2	2	5	11	2	2	5	5

Compound	n-C_{11}	n-C_{12}	n-C_{13}	C_{14}	n-C_{15}	n-C_{16}	n-C_{17}	n-C_{18}	n-C_{19}	n-C_{20}	n-C_{21}	n-C_{22}	n-C_{23}
NU-WAB-14 2-3 cm	12.73	171.74	56.44	249.97	29.08	43.7	nd	nd	nd	24.92	nd	100.67	68.34
NU-WAB-14 2-3 cm dup	11.33	168.12	57.87	247.36	29.45	44.16	nd	nd	nd	25.3	nd	83.62	51.72
% difference	12%	2	3	1	1	1%	nd	nd	nd	2	nd	19	28
NU-WAB-14 8-9 cm	nd	3.82	11.58	69.94	26.96	33.91	18.6	5.21	12.84	15.06	17.65	32.85	54.85
NU-WAB-14 8-9 cm dup	nd	4.02	11.43	68.84	26.92	33.62	18.45	5.22	14.21	15.12	18.49	34.19	58.98
% difference	nd	5	1	2	0	1	1	0	10	0	5	4	7
NU-WAB-16 2-3 cm	nd	37.5	16.23	nd	6.88	14.95	7.35	6.3	9.26	18.68	23.38	57.7	103.46
NU-WAB-16 2-3 cm dup	nd	52.27	16.3	nd	5.89	11.17	6.77	6.38	10.97	23.02	24.37	68.64	98.07
% difference	nd	33	0	nd	16	29	8	1	17	21	4	17	5
NU-WAB-16 3-4 cm	nd	4.97	8.41	45.37	8.75	17.28	15.14	8.07	19.21	25.5	28.04	49.87	82.63
NU-WAB-16 3-4 cm dup	nd	5.33	8.44	45.54	8.64	17.57	15.17	8.33	18.93	25.52	27.71	52.86	82.31
% difference	nd	7	0	0	1	2	0	3	1	0	1	6	0
NU-WAB-16 4-5 cm	nd	nd	nd	nd	nd	nd	8.18	5.98	10.51	17.91	24.07	51.58	112.64
NU-WAB-16 4-5 cm dup	nd	nd	nd	nd	nd	nd	6.51	4.65	11.99	18.04	22.39	55.57	78.13
% difference	nd	nd	nd	nd	nd	nd	23	25	13	1	7	7	36
PLK-NU-15 8-9 cm	nd	nd	nd	4.77	4.91	4.87	6.9	5.88	8.73	15.38	20.28	51.75	61.31
PLK-NU-15 8-9 cm dup	nd	nd	nd	6.96	4.4	5.31	5.53	8.17	5.67	18.34	19.23	49.96	60.41
% difference				37	11	9	22	33	43	18	5	4	1
Batch 3													
PLK-NU-15 10-12 cm	nd	66.7	61.52	46.11	11.17	9.78	13.13	5.18	19.57	26.8	42.04	96.21	163.92
PLK-NU-15 10-12 cm dup	nd	70.18	65.17	48.35	11.44	10.05	14.01	5.27	19.52	27.42	43.29	96.77	165.31
% difference	nd	5	6	5	2	3	6	2	0	2	3	1	1
PLK-NU-15 16-18 cm	1.67	25.84	26.86	91.26	11.66	20.14	14.94	8.56	16.89	36.73	42.98	107.54	258.45
PLK-NU-15 16-18 cm dup	1.73	24.64	26.15	89.98	11.6	20.84	14.24	8.26	15.52	32.33	40.34	102.01	239.21
% difference	4	5	3	1	1	3	5	4	8	13	6	5	8
CI-08 7-8 cm	nd	31.12	16.98	39.71	29.31	27.22	11.46	13.79	17.51	21.91	25.58	44.5	40.21
CI-08 7-8 cm dup	nd	32.14	17.73	39.7	31.65	33.88	13.38	16.21	11.79	18.24	22.58	42	42.69
% difference	nd	3	4	0	8	22	15	16	39	18	12	6	6
NU-WAB-10 20-25 cm	nd	363.06	217.89	388.58	63.05	69.74	299.07	51.08	45.67	41.78	36.88	nd	126.92
NU-WAB-10 20-25 cm dup	nd	333.99	197.15	362.79	64.07	69.72	308.15	35.45	45.74	41.41	42.95	nd	124.29

Compound	n-C_{11}	n-C_{12}	n-C_{13}	C_{14}	n-C_{15}	n-C_{16}	n-C_{17}	n-C_{18}	n-C_{19}	n-C_{20}	n-C_{21}	n-C_{22}	n-C_{23}
% difference	nd	8	10	7	2	0	3	36	0	1	15	nd	2
NU-WAB-10 3-4 cm	nd	nd	nd	nd	44.37	63.14	78.39	24.52	23.72	28.34	45.25	nd	113.28
NU-WAB-10 3-4 cm dup	nd	nd	nd	nd	40.87	49.76	110.22	17.42	19.19	26.62	43.44	nd	113.4
% difference	nd	nd	nd	nd	8	24	34	34	21	6	4	nd	0
NU-WAB-10 9-10 cm	nd	439.39	243.66	368.18	101.37	130.36	119.74	31.51	37.55	38.66	50.24	nd	136.37
NU-WAB-10 9-10 cm dup	nd	447.17	268.36	386.43	98.98	129.2	98.98	34.76	40.34	41.22	54.16	nd	143.93
% difference	nd	2	10	5	2	1	19	10	7	6	8	nd	5

Compound	n-C_{24}	n-C_{25}	n-C_{26}	n-C_{27}	n-C_{28}	n-C_{29}	n-C_{30}	n-C_{31}	n-C_{32}	n-C_{33}	n-C_{34}	n-C_{35}	n-C_{36}
Batch 1													
CI-08 14-16 cm	nd	nd	nd	441.33	357.39	655.76	nd	523.43	55.38	nd	nd	nd	nd
CI-08 14-16 cm dup	nd	nd	nd	599.81	488.69	826.44	nd	437.67	56.19	nd	nd	nd	nd
% difference	nd	nd	nd	30	31	23	nd	18	1	nd	nd	nd	nd
CI-24 2-3 cm	22.94	nd	nd	nd	nd	nd	37.69	nd	nd	nd	nd	nd	nd
CI-24 2-3 cm dup	32.43	nd	nd	nd	nd	nd	50.3	nd	nd	nd	nd	nd	nd
% difference	34	nd	nd	nd	nd	nd	29	nd	nd	nd	nd	nd	nd
CI-24 3-4 cm	144.07	336.23	276.53	517.38	290.7	697.1	147.05	559.43	62.27	nd	nd	nd	nd
CI-24 3-4 cm dup	133.33	322.91	285.45	510.21	291.98	707.82	146.46	540.69	58.2	nd	nd	nd	nd
% difference	8	4	3	1	0	2	0	3	7	nd	nd	nd	nd
CI-24 7-8 cm	83.62	194.76	157.42	345.36	187.84	492.81	111.49	426.98	47.74	nd	nd	nd	nd
CI-24 7-8 cm dup	78.68	198.26	150.98	332.67	184.59	466.02	102.71	375.12	49.18	nd	nd	nd	nd
% difference	6	2	4	4	2	6	8	13	3	nd	nd	nd	nd
CI-24 8-9 cm	106.81	244.05	201.84	414.71	339.64	840.4	292.92	565.32	72.91	nd	nd	nd	nd
CI-24 8-9 cm dup	103.21	217.02	179.01	342.45	211.2	558.88	190.19	436.42	51.5	nd	nd	nd	nd
% difference	3	12	12	19	47	40	43	26	34	nd	nd	nd	nd
NU-WAB-08 6-7 cm	136.09	334.71	239.17	622.43	263.42	1061.65	175.89	881.94	70.2	nd	nd	nd	nd

Compound	n-C_{24}	n-C_{25}	n-C_{26}	n-C_{27}	n-C_{28}	n-C_{29}	n-C_{30}	n-C_{31}	n-C_{32}	n-C_{33}	n-C_{34}	n-C_{35}	n-C_{36}
NU-WAB-08 6-7 cm dup	123.79	306.73	215.87	552.42	231	875.25	152.3	708.36	56.68	nd	nd	nd	nd
% difference	9	9	10	12	13	19	14	22	21	nd	nd	nd	nd
NU-WAB-08 8-9 cm	130.84	293.32	204.19	466.85	176.22	608.14	59.96	469.16	42.1	nd	nd	nd	nd
NU-WAB-08 8-9 cm dup	125.96	282.83	197.77	476.52	176.22	623.5	59.37	488.44	44.15	nd	nd	nd	nd
% difference	4	4	3	2	0	2	1	4	5	nd	nd	nd	nd
NU-WAB-08 25-27 cm	54.12	109.61	77.07	204.78	99.68	369.54	71.98	392.93	55.11	nd	nd	nd	nd
NU-WAB-08 25-27 cm dup	62.35	129.85	93.8	237.58	117.94	432.38	88.9	493.61	58.65	nd	nd	nd	nd
% difference	14	17	20	15	17	16	21	23	6	nd	nd	nd	nd
Batch 2													
NU-WAB-10 10-12 cm	132.17	292.65	193.33	494.23	176.03	731.38	86.77	605.61	45.63	nd	nd	nd	nd
NU-WAB-10 10-12 cm dup	140.11	312.43	206.03	547.77	189.94	793.36	97.04	683.84	49.59	nd	nd	nd	nd
% difference	6	7	6	10	8	8	11	12	8	nd	nd	nd	nd
NU-WAB-14 2-3 cm	229.47	365.98	686.88	181.35	519.52	153.63	1212.11	440.65	nd	nd	nd	nd	nd
NU-WAB-14 2-3 cm dup	189.68	286.3	491.2	166.56	467.86	138.82	930.85	877.47	nd	nd	nd	nd	nd
% difference	19	24	33	9	10	10	26	66	nd	nd	nd	nd	nd
NU-WAB-14 8-9 cm	44.65	105.08	62.97	146.04	53.44	188.27	38.75	199.9	nd	nd	nd	nd	nd
NU-WAB-14 8-9 cm dup	45.83	104.62	65.42	152.68	60.41	203.21	37.67	201.92	nd	nd	nd	nd	nd
% difference	3	0	4	4	12	8	3	1	nd	nd	nd	nd	nd
NU-WAB-16 2-3 cm	115.12	240.92	216.26	474.28	213.2	122.81	57.3	834.08	104.71	nd	nd	nd	nd
NU-WAB-16 2-3 cm dup	119.28	192.85	221.8	336.28	217.56	175.56	91.42	857.61	68.82	nd	nd	nd	nd
% difference	4	22	3	34	2	35	46	3	41	nd	nd	nd	nd
NU-WAB-16 3-4 cm	68.36	148.39	116.46	248.97	119.53	341.71	61.28	221.57	44.13	nd	nd	nd	nd
NU-WAB-16 3-4 cm dup	62.93	148.69	113.88	242.49	117.72	314.7	59.78	194.56	41.81	nd	nd	nd	nd
% difference	8	0	2	3	2	8	2	13	5	nd	nd	nd	nd
NU-WAB-16 4-5 cm	97.4	172.04	178.65	340.04	315.35	883.8	145.13	650.68	100.27	nd	nd	nd	nd
NU-WAB-16 4-5 cm dup	91.45	158.4	185.3	307.13	222.62	480.31	107.85	491.91	85.47	nd	nd	nd	nd

Compound	n-C_{24}	n-C_{25}	n-C_{26}	n-C_{27}	n-C_{28}	n-C_{29}	n-C_{30}	n-C_{31}	n-C_{32}	n-C_{33}	n-C_{34}	n-C_{35}	n-C_{36}
% difference	6	8	4	10	34	59	29	28	16	nd	nd	nd	nd
PLK-NU-15 8-9 cm	63.05	122.23	110.56	209.77	125.72	306.32	71.08	291.98	49.35	nd	nd	nd	nd
PLK-NU-15 8-9 cm dup	82.52	123.56	137.52	209.48	172.78	350.71	40.37	310.2	57.92	nd	nd	nd	nd
% difference	27	1	22	0	32	14	55	6	16	nd	nd	nd	nd
Batch 3													
PLK-NU-15 10-12 cm	162.61	315.29	302.24	581.49	286.96	776.44	122.47	640.14	62.79	nd	nd	nd	nd
PLK-NU-15 10-12 cm dup	167.41	322.08	322.98	650.16	340.82	968.77	157.26	903.89	89.02	nd	nd	nd	nd
% difference	3	2	7	11	17	22	25	34	35	nd	nd	nd	nd
PLK-NU-15 16-18 cm	182.6	501.56	325.86	977.45	456.03	1734.25	493.28	897.33	78.29	nd	nd	nd	nd
PLK-NU-15 16-18 cm dup	178.5	479.23	310.3	946.37	443.11	1649.96	476.9	811.51	69.59	nd	nd	nd	nd
% difference	2	5	5	3	3	5	3	10	12	nd	nd	nd	nd
CI-08 7-8 cm	35.5	65.04	42.73	82.78	45.13	105	43.01	128.05	36.34	60.26	nd	nd	nd
CI-08 7-8 cm dup	38.78	77.56	52.38	95.29	49.36	113.7	43.71	131.77	37.31	56.55	nd	nd	nd
% difference	9	18	20	14	9	8	2	3	3	6	nd	nd	nd
NU-WAB-10 20-25 cm	84.35	175.75	99.91	nd	nd	355.65	267.95	376.54	59.57	151.29	nd	nd	nd
NU-WAB-10 20-25 cm dup	82.22	166.67	94.74	nd	nd	352.12	265.68	383.94	64.3	140.19	nd	nd	nd
% difference	3	5	5	nd	nd	1	1	2	8	8	nd	nd	nd
NU-WAB-10 3-4 cm	75.66	163.31	95.83	225.43	90.21	287.48	96.27	347.5	87.92	165.66	68.03	41.12	62.15
NU-WAB-10 3-4 cm dup	75.95	167.35	102.86	237.72	100.48	311.61	97.99	368.09	97.88	167.65	74.57	50.86	70.09
% difference	0	2	7	5	11	8	2	6	11	1	9	21	12
NU-WAB-10 9-10 cm	124.89	227.59	180.69	295.45	153.1	339.76	123.69	355.24	72.54	145.33	nd	37.51	nd
NU-WAB-10 9-10 cm dup	139.65	290.02	236.05	379.97	198.06	430.72	160.39	446.86	91.41	192.41	nd	43.05	nd
% difference	11	24	27	25	26	24	26	23	23	28	nd	14	nd

nd – Not Detected, dup – Duplicate

Table 3.8: QA/QC of n-alkanes showing blank values (ng/g dw), mean blanks (CI) and LOD (ng/g dw) (n=8)

Compound	Blank 1a	Blank 1b	Blank 1c	Blank 2a	Blank 2b	Blank 2c	Blank 3a	blank 3b	LOD	Mean (CI)
n-C_{11}	4.76	nd	7.15	nd	nd	nd	nd	17.45	30.01	8.41(3.96-17.83)
n-C_{12}	nd	nd	nd	nd	7.32	nd	21.30	14.02	35.18	12.98(7.06-23.86)
n-C_{13}	10.03	nd	2.88	nd	3.44	nd	26.74	21.53	45.24	8.94(3.65-21.91)
n-C_{14}	nd	2.98	nd	9.60	nd	9.20	nd	nd	18.39	6.41(3.03-13.57)
n-C_{15}	nd	3.43	2.68	8.02	9.28	9.91	nd	16.42	23.28	6.93(3.99-12.04)
n-C_{16}	nd	4.09	5.52	14.24	16.01	nd	nd	25.46	39.09	10.55(5.38-20.69)
n-C_{17}	5.87	3.28	2.34	3.85	3.88	nd	21.93	17.32	32.01	5.92(3.13-11.20)
n-C_{18}	nd	3.83	3.79	nd	3.83	nd	16.20	16.98	29.93	6.87(3.39-13.91)
n-C_{19}	nd	4.77	5.20	5.08	5.73	7.27	10.39	9.92	14.00	6.59(5.18-8.38)
n-C_{20}	11.40	9.79	12.78	9.16	9.15	13.86	16.72	10.23	19.64	11.39(9.80-13.24)
n-C_{21}	5.89	6.30	8.40	nd	5.84	11.49	12.27	8.91	16.39	8.10(6.44-10.19)
n-C_{22}	15.59	18.49	18.55	15.30	11.80	16.44	9.57	1.99	30.19	11.48(6.85-19.22)
n-C_{23}	12.61	14.28	9.02	10.60	9.79	8.00	10.43	10.22	16.58	10.46(9.23-11.87)
n-C_{24}	nd	nd	15.73	22.30	19.93	13.66	28.07	21.29	35.48	19.62(5.97-24.11)
n-C_{25}	22.03	22.64	15.78	18.45	13.84	16.12	nd	nd	28.84	17.86(15.26-20.89)
n-$C2_6$	nd	nd	26.43	nd	21.94	19.99	nd	nd	32.70	22.63(19.27-26.58)
n-C_{27}	nd	nd	nd	nd	nd	14.82	nd	nd	nd	nd
n-C_{28}	nd	nd	nd	nd	21.18	17.57	nd	nd	27.04	19.29(16.06-23.17)
n-C_{29}	nd	nd	nd	nd	20.15	17.57	nd	nd	24.34	18.81(16.45-21.52)
n-C_{30}	nd	nd	28.03	nd	27.26	11.91	nd	nd	49.67	20.88(12.05-36.20)
n-C_{31}	nd	nd	31.40	nd	nd	9.55	nd	27.31	34.85	20.16(9.65-42.09)
n-C_{32}	nd	nd	nd	nd	nd	8.82	nd	21.60	27.12	13.81(5.74-33.21)
n-C_{33}	nd	nd	nd	nd	nd	7.07	22.63	14.48	38.07	13.23(6.81-25.71)

Compound	Blank 1a	Blank 1b	Blank 1c	Blank 2a	Blank 2b	Blank 2c	Blank 3a	blank 3b	LOD	Mean (CI)
n-C_{34}	nd	nd	nd	nd	nd	8.85	18.26	13.10	27.53	12.84(8.52-19.35)
n-C_{35}	nd	nd	nd	nd	nd	5.91	9.80	5.86	13.97	6.98(5.00-9.74)
n-C_{36}	nd	nd	nd	nd	nd	nd	nd	nd	nd	nd

nd – Not detected, CI – Confidence Limits

3.5.4 Analyses and Identification of PAHs

Extracts were analysed for PAHs using an Agilent 7890B gas chromatography (GC) with automated backflush capability for removal of high-boiling components coupled to an Agilent 7010B triple quadrupole mass spectrometer (QQQ-MS) equipped with a high efficiency source (HES). Chromatography was performed using a 60 m x 0.25 mm ID x 0.10 µm d_f fused silica GC capillary column and a 5.5 m x 0.18 mm ID x 0 µm d_f deactivated fused silica back-flash pre-column. The carrier gas (ultra-high purity helium, 99.9995%) was operated at a constant flow rate of 1.1 mL/min for the 60 m column and 1.2 mL/min for the 5.5 m column. The injection port, transfer line and ion source temperatures were set to 280°C, 320°C and 280°C, respectively. The oven temperature was initially set at 80°C. After 1.5 minutes, the temperature was increased by 40°C/min to 120°C followed by 4°C/min to 320°C, where it was held for 25 minutes. The total run time of each sample was 82.5 minutes (20 minutes backflush). A 2 µL volume of the extracted sample was injected using the splitless mode. The ion source electron ionisation (EI) energy was 70 eV. Analysis was conducted using Multiple Reaction Monitoring (MRM) Agilent Mass Hunter Workstation, quantitative analysis version B.08.00.

Compound identification was based on mass spectral data, comparison of GC retention data, reference standards, and the NIST mass spectra library (Liao et al. 2010). Quantification of the PAHs was performed using isotope dilution and the average relative response factors (ARRF) of detected parent PAHs relative to their deuterated analogues (DPAHs) using the formula below (Idowu et al. 2018).

$$\text{ARRF} = \left(\frac{\text{Area PAH}}{\text{Area DPAH}}\right) / \left(\frac{\text{Conc PAH}}{\text{Conc DPAH}}\right) \qquad \text{Equation (10)}$$

PAHs without calibration standards were quantified semi-quantitatively using response factors derived from their isomers (Idowu et al. 2018). For example, C1- and C2-Naphthalenes

were quantified using the ARRF for Naphthalene or Benzo[e]pyrene using D12-Benzo(a)pyrene (Table 3.9).

Table 3.9: PAH compounds, abbreviations, associated deuterated standards and QQQ qualification parameters

Analytes	Abbre-viation	Associated D-PAH	Transition	CE (eV)	Gain
Naphthalene	Na	D8-Naphthalene	128.0/128.0; 128.0/102.0; 128.0/78.0	1; 26; 28	20
C1-Naphthalene	N1	D8-Naphthalene	142.0/142.0; 142.0/141.0; 142.0/115.0	1; 16; 36	20
C2-Naphthalene	N2	D8-Naphthalene	156.0/156.0; 156.0/141.0; 156.0/115.0	1; 22; 30	20
Acenaphthylene	Ayl	D8-Acenaphthylene	152.0/152.0; 152.0/151.0; 152.0/126.0	1; 22; 30	30
Acenaphthene	Aen	D10-Acenaphthene	154.0/154.0; 154.0/153.0; 154.0/128.0	1; 14; 28	30
Fluorene	F	D10-Fluorene	166.0/166.0; 166.0/165.0; 166.0/116.0	1; 22; 30	30
Phenanthrene	Pn	D10-Phenanthrene	178.0/178.0; 178.0/176.0; 178.0/152.0	1; 28; 36	30
C1-Phenanthrene/Anthracene	P1	D10-Phenanthrene	192.0/192.0; 192.0/191.0; 192.0/165.0	1; 14; 42	30
C2-Phenanthrene/Anthracene	P2	D10-Phenanthrene	206.0/206.0; 206.0/190.0; 206.0/165.0	1; 28; 50	30
Fluoranthene	Fl	D10-Fluoranthene	202.0/202.0; 202.0/200.0; 202.0/176.0	1; 36; 42	30
Pyrene	Py	D10-Pyrene	202.0/202.0; 202.0/200.0; 202.0/176.0	1; 36; 42	30
C1-Fluoranthene/Pyrene	F1	D10-Fluoranthene	216.0/216.0; 216.0/215.0; 216.0/189.0	1; 28; 50	30
Chrysene/Triphenylene	Ch	D12-Chrysene	228.0/228.0; 228.0/226.0; 228.0/202.0	1; 28; 38	40
Benzo(b,j,k)fluoranthene	BF	D12-Benzo[b]fluoranthene	252.0/252.0; 252.0/250.0; 126.0/126.0	1; 44; 1	50
Perylene	Per	D12-Perylene	252.0/252.0; 252.0/250.0; 126.0/126.0	1; 44; 1	50
Benzo(a)pyrene	BaPy	D12-Benzo[a]pyrene	252.0/252.0; 252.0/250.0; 126.0/126.0	1; 44; 1	50
Benzo(e)pyrene	BePy	D12-Benzo[a]pyrene	252.0/252.0; 252.0/250.0; 126.0/126.0	1; 44; 1	50
Benzo (a)Anthracene	BaA	D12-Benzo[a]pyrene	252.0/252.0; 252.0/250.0; 126.0/126.0	1; 44; 1	50
Indeno(1,2,3-c,d)pyrene	IP	D12-Indeno[1,2,3-c,d]pyrene	276.0/276.0; 276.0/274.0	1; 54	50
Dibenz(a,h)anthracene	DA	D14-Dibenz[a,h]anthracene	278.0/278.0; 278.0/276.0	1; 50	50
Benzo(g,h,i)perylene	Bghi	D12-Benzo[g,h,i]perylene	276.0/276.0; 276.0/274.0	1; 54	50
Deuterated Standards					
D8-Naphthalene			136.0/136.0; 136.0/108.0; 136.0/84.0	1; 28; 28	20
D8-Acenaphthyelene			160.0/160.0; 160.0/158.0; 160.0/132.0	1; 28; 36	30
D10-Acenaphthene			164.0/164.0; 164.0/162.0; 164.0/136.0	1; 20; 36	30

Analytes	Abbre-viation	Associated D-PAH	Transition	CE (eV)	Gain
D10-Fluorene			176.0/176.0; 176.0/174.0; 176.0/124.0	1; 22; 30	30
D10-Phenanthrene			188.0/188.0; 188.0/184.0; 188.0/160.0	1; 28; 36	30
D10-Fluoranthene			212.0/212.0; 212.0/208.0; 212.0/184.0	1; 38; 50	30
D10-Pyrene			212.0/212.0; 212.0/208.0; 212.0/184.0	1; 38; 50	30
D12-Chrysene			240.0/240.0; 240.0/236.0; 240.0/212.0	1; 38; 40	40
D12-Benzo(b)fluoranthene			264.0/264.0; 264.0/260.0	1; 50	50
D12-Benzo(k)fluoranthene			264.0/264.0; 264.0/260.0	1; 50	50
D12-Benzo (a)Anthracene			264.0/264.0; 264.0/260.0	1; 50	50
D12-Perylene			264.0/264.0; 264.0/260.0	1; 50	50
D12-Benzo(a)pyrene			264.0/264.0; 264.0/260.0	1; 50	50
D12-Indeno(1,2,3-c,d)pyrene			288.0/288.0; 288.0/284.0	1; 56	50
D14-Dibenz(a,h)anthracene			292.0/292.0; 292.0/288.0	1; 50	50
D12-Benzo(g,h,i)perylene			288.0/288.0; 288.0/284.0	1; 56	50

D-PAH – Deuterated PAHs
CE – Collision Energy

3.5.5 PAH QA/QC

A total of seven NIST 1941b SRM, twelve blanks and eighty-one sediment samples were extracted in three batches. Batch one and two each consisted of two NIST 1941b SRM, four blank samples and twenty-seven sediment samples. Batch three also consisted of three NIST 1941b SRM, four blank samples and twenty-seven sediment sample. Six samples were re-run on the instrument to check the instrument reproducibility of results. Forty-one individual PAHs were detected at low concentrations in all the samples, comprising twenty parent PAHs (PPAHs) and twenty-one alkylated PAHs (APAHs). For analytical purposes, isomers and co-eluting compounds such as chrysene and triphenylene, phenanthrene and anthracene, methyl naphthalenes and phenanthrenes and dimethyl naphthalenes and phenanthrenes have been combined, giving a total of twenty-one PPAHs and APAHs. Similar to n-alkanes, geometric mean herein also referred to as 'mean' was calculated for all PAHs instead of arithmetic mean to normalise the dataset as the distribution was found to be positively skewed. The complete set of PAH data is included in Appendix B.

The recoveries of F in all seven NIST 1941b SRM was consistently low. Mean recoveries (SE) in all seven SRM was 28% (3%). The mean recoveries (SE) of PAH compounds excluding F, ranged between 58% (4%) and 92% (8%) (See Table 3.9 for abbreviations and their meanings and Table 3.10 for NIST 1941b SRM recoveries). The difference between sample re-runs (duplicates) ranged between 1% and 60% (Table 3.11 and Table 12). Most compounds were not detected in the blank samples or were present at low concentrations with the exception of Na, N1 and N2, which were present in all twelve blank samples (See table 3.13). The Mean (confidence limits) of blank concentrations in ng/g dw of the Na, N1 and N2 compounds was 0.77 (1.48-2.50), 0.50 (1.05-4.28) and 0.46 (1.03-4.82) respectively. Mean (confidence interval) for all remaining compounds ranged from 0.00 ng/g dw to 0.047 (0.02-0.11) ng/g dw. LOD of PAH compound in each sample was determined as described in section 3.5.3 above.

LOD ranged from 0.002 ng/g dw to 2.993 ng/g dw (Table 3.13). After blank correcting, Na and it alkylated compounds were found to be present in only 32-46% of all the analysed samples. They were therefore included in sums of PPAH (ΣPPAH) and sums of APAH (ΣAPAH) excluded from PCA statistical analyses due to the high number of non-detects.

Table 3.10: QA/QC of PAHs showing NIST 1941b SRM recoveries (n=7)

PAH	NIST 1941b 1a	NIST 1941b 1b	NIST 1941b 2a	NIST 1941b 2b	NIST 1941b 3a	NIST 1941b 3b	NIST 1941b 3c
Na	47%	60%	82%	54%	nd	126%	nd
Ayl	67%	109%	143%	69%	60%	nd	nd
Aen	41%	43%	52%	40%	nd	45%	77%
F	23%	33%	28%	28%	23%	26%	42%
Pn	59%	63%	63%	57%	49%	51%	80%
Fl	62%	66%	65%	62%	55%	51%	82%
Py	52%	56%	55%	52%	47%	44%	73%
Ch	65%	59%	65%	69%	60%	57%	104%
BF	nd	70%	44%	46%	61%	43%	75%
IP	66%	60%	39%	58%	69%	54%	95%
DA	102%	106%	131%	88%	96%	93%	146%
Bghi	43%	61%	47%	55%	63%	55%	98%

nd – not detected

Table 3.11: QA/QC of Alkylated PAHs showing percent differences between samples re-runs (n = 6)

Sample ID	N1	N2	P1	P2	F1
CI-08 0-1 cm	0.00	0.19	0.06	0.02	nd
CI-08 0-1 cm re-run	0.01	0.16	0.03	0.01	nd
% difference	9	13	60	47	nd
NU-WAB-08 5-6 cm	nd	nd	0.79	0.17	0.01
NU-WAB-08 5-6 cm re-run	nd	nd	0.80	0.17	0.01
% difference	nd	nd	1	0	1
NU-WAB-10 3-4 cm	nd	nd	0.66	0.03	0.01
NU-WAB-10 3-4 cm re-run	nd	nd	0.70	0.03	0.00
% difference	nd	nd	5	4	10
NU-WAB-14 3-4 cm	nd	nd	0.08	0.01	0.00
NU-WAB-14 3-4 cm re-run	nd	nd	0.08	0.01	0.00
% difference	nd	nd	1	57	48
NU-WAB-16 2-3 cm	nd	nd	0.07	0.02	0.01
NU-WAB-16 2-3 cm re-run	nd	nd	0.06	0.01	0.01
% difference	nd	nd	9	29	15
PLK-NU-15 8-9 cm	6.39	6.46	0.06	0.01	0.00
PLK-NU-15 8-9 cm re-run	6.37	6.39	0.05	0.01	0.00
% difference	0	1	5	43	12

Table 3.12: QA/QC of Parent PAHs showing percent differences between samples re-runs (n = 6)

Sample ID	Na	Ayl	Aen	F	Pn	Fl	Py	BaA	Ch	BF	BePy	BaPy	Per	DA	IP	Bghi
CI-08 0-1 cm	0.01	0.09	nd	0.03	0.01	nd	nd	nd	nd	0.00	nd	nd	nd	nd	nd	0.00
CI-08 0-1 cm re-run	0.01	0.09	nd	0.03	0.01	nd	nd	nd	nd	0.00	nd	nd	nd	nd	nd	0.00
%difference	1	7	nd	1	24	nd	nd	nd	nd	22	nd	nd	nd	nd	nd	16
NU-WAB-08 5-6 cm	0.59	0.39	0.20	0.56	0.16	0.08	0.08	0.03	0.07	0.19	0.18	0.06	0.31	0.02	0.19	0.14
NU-WAB-08 5-6 cm re-run	0.54	0.35	0.18	0.64	0.13	0.08	0.08	0.03	0.05	0.17	0.17	0.05	0.31	0.01	0.22	0.23
%difference	10	13	9	13	23	3	3	13	46	11	9	6	1	23	14	41
NU-WAB-10 3-4 cm	0.80	0.19	0.39	0.31	0.13	0.05	0.05	0.02	0.06	0.06	nd	0.02	0.17	0.01	0.12	0.12
NU-WAB-10 3-4 cm re-run	0.98	0.12	0.28	0.53	0.14	0.06	0.05	0.02	0.10	0.08	nd	0.02	0.17	0.01	0.13	0.10
%difference	19	57	36	46	6	8	1	17	42	30	nd	23	4	5	11	16
NU-WAB-14 3-4 cm	nd	0.02	0.01	0.03	1.11	0.02	0.08	0.01	0.03	0.08	0.04	0.01	0.06	0.00	0.06	0.06
NU-WAB-14 3-4 cm re-run	nd	0.02	0.01	0.03	1.11	0.02	0.07	0.00	0.03	0.07	0.04	0.01	0.10	0.00	0.05	0.05
%difference	nd	1	5	26	0	2	9	26	2	5	5	40	23	6	25	5
NU-WAB-16 2-3 cm	nd	0.01	0.02	0.04	0.15	0.12	0.39	0.01	0.10	0.11	0.03	0.02	0.09	0.00	0.10	0.10
NU-WAB-16 2-3 cm re-run	nd	0.01	0.01	0.03	0.10	0.09	0.28	0.01	0.10	0.12	0.04	0.02	0.09	0.00	0.08	0.14
%difference	nd	8	49	43	49	28	35	34	2	2	14	18	1	41	26	35
PLK-NU-15 8-9 cm	5.79	0.01	0.05	0.03	0.06	0.05	0.18	0.02	0.04	0.10	0.03	nd	0.14	0.00	0.06	0.09
PLK-NU-15 8-9 cm re-run	5.19	0.02	0.03	0.04	0.09	0.09	0.17	0.01	0.04	0.09	0.03	nd	0.12	0.00	0.06	0.06
%difference	11	38	40	25	35	49	5	37	4	11	5	nd	11	65	1	37

Table 3.13: QA/QC of PAHs showing Mean, and LOD of blank samples (n=12)

PAH	Blank 1a	Blank 1b	Blank 1c	Blank 1d	Blank 2a	Blank 2b	Blank 2c	Blank 2d	Blank 3a	Blank 3b	Blank 3c	Blank 3d	LOD	Mean (CI)
Na	1.26	1.16	1.80	nd	0.99	0.33	1.88	0.74	1.05	0.54	0.04	2.00	2.99	0.77(0.40-1.48)
N1	1.32	1.24	1.46	nd	0.32	0.25	0.40	1.39	0.81	0.72	0.02	0.42	2.31	0.50(0.23-1.05)
N2	nd	nd	nd	nd	1.71	0.70	0.73	0.26	1.44	0.31	0.04	0.47	2.46	0.46(0.21-1.03)
Ayl	0.01	0.01	0.00	0.06	nd	0.00	0.22	0.03	0.00	0.06	nd	0.03	0.24	0.016(0.01-0.04)
Aen	0.02	0.03	0.02	0.09	0.04	0.02	0.17	0.06	0.02	0.04	0.03	nd	0.19	0.036(0.02-0.06)
F	0.03	0.03	0.02	0.04	0.31	0.02	nd	0.06	0.02	0.01	0.03	1.28	1.31	0.05(0.02-0.11)
Pn	0.07	0.04	0.04	0.05	0.11	0.03	0.12	0.07	0.03	0.03	0.01	0.04	0.15	0.05(0.03-0.06)
P1	0.16	0.02	0.01	0.02	0.22	0.01	0.42	0.17	0.01	0.10	0.02	0.03	0.47	0.05(0.02-0.10)
P2	0.01	0.00	0.00	0.00	0.04	0.00	0.06	0.89	0.00	0.05	0.01	0.01	0.85	0.01(0.00-0.03)
Fl	0.03	0.01	0.04	0.02	0.03	0.01	0.01	0.02	0.01	0.00	0.00	0.00	0.05	0.01(0.01-0.02)
Py	0.06	0.05	0.14	0.11	0.02	0.02	0.01	0.02	0.03	0.00	0.00	0.00	0.17	0.02(0.01-0.04)
F1	0.00	0.00	0.00	0.00	0.00	0.00	0.00	0.00	0.00	0.00	0.00	0.00	0.00	0.00(0.00-0.00)
BaA	0.01	0.00	0.00	0.00	0.00	0.00	0.00	0.00	0.00	0.00	0.00	0.00	0.01	0.00(0.00-0.00)
Ch	0.02	0.00	0.00	0.00	0.00	0.00	0.01	0.01	0.00	0.01	0.00	0.00	0.02	0.00(0.00-0.01)

PAH	Blank 1a	Blank 1b	Blank 1c	Blank 1d	Blank 2a	Blank 2b	Blank 2c	Blank 2d	Blank 3a	Blank 3b	Blank 3c	Blank 3d	LOD	Mean (CI)
BF	0.04	0.00	0.01	0.01	0.00	0.01	0.01	0.02	0.00	0.00	0.00	0.00	0.04	0.01(0.00-0.01)
BePy	0.02	0.00	0.00	0.01	0.00	0.00	0.01	0.03	0.00	nd	0.00	nd	0.03	0.01(0.00-0.01)
BaPy	0.01	0.01	0.00	0.00	0.00	0.00	0.01	0.01	0.00	nd	nd	nd	0.02	0.01(0.00-0.01)
Per	0.04	0.00	0.00	nd	0.00	0.00	nd	0.00	0.00	nd	nd	0.00	0.04	0.00(0.00-0.01)
DA	0.00	0.00	0.00	0.00	nd	nd	nd	0.00	nd	nd	nd	nd	0.00	0.00(0.00-0.00)
IP	0.04	0.00	0.00	0.00	0.00	0.00	nd	0.01	nd	nd	nd	0.00	0.04	0.00(0.00-0.01)
Bghi	0.02	0.00	0.01	0.01	0.00	0.00	0.01	0.01	nd	nd	nd	nd	0.03	0.01(0.00-0.01)

LOD – Limit of Detection (Mean blank + 3SD)

3.5.6 Statistical Analyses and Principal Component Analyses (PCA)

As previously mentioned in sections 3.5.3 and 3.5.5 sample geometric mean were calculated instead of arithmetic mean, as data is positively skewed. All graphs were plotted using SigmaPlot © 12.5. PCA was used to determine the total variability within the n-alkane and PAH datasets by generating new variables of fewer dimensions called principal components (Johnson 1998). PCA also provided the percent contribution of each principal component that explains the total variance in the data set and helps visualise the specific compounds that contribute most variance to a particular data set (Ma et al. 2017).

For the purpose of this analysis, values below the detection limit within the each dataset were replaced with a random number generated between zero and the minimum LOD of procedural blanks. Cores with more than 30 % non-detected compounds such as n-C_{11}, n-C_{33} to n-C_{36} n-alkanes, and the PAHs Na, N1 and N2 were excluded from the PCA data set (Tables 3.14 and 3.15). The average concentration of perylene was within the range of concentration of other compounds and thus it was retained in PCA analysis. Duplicate samples were averaged and concentrations of co-eluting compounds and homologous groups (chrysene and triphenylene, phenanthrene and anthracene, methyl naphthalenes and phenanthrenes and dimethyl naphthalenes and phenanthrenes) were also combined. Prior to the analysis, the whole dataset was pre-treated by first normalising to the total concentration and dividing by the geometric mean of the concentration-normalised samples to nullify the effects of large differences in concentrations and biases (Yunker et al. 2005). The results were then log transformed to improve normality (Foster et al. 2015; Yunker et al. 2005). PCA was performed on eighteen and twenty-one PAH and n-alkane variables, respectively, with correlation matrix using Systat© 13 and Microsoft Office Excel. Once the PCA results were obtained, the difference among the stations on each PC axes were confirmed using ANOVA followed by Tukey's Honestly-significant-difference test.

Table 3.14: List of n-alkanes detected in the samples and details of whether they were included (Y) or excluded (N) from various calculations and statistical analyses

Compounds	% detected in samples	Included in PCA Model	Included in SCA calculations	Included in LCA calculations
n-C_{11}	45	N	Y	N
n-C_{12}	76	Y	Y	N
n-C_{13}	86	Y	Y	N
n-C_{14}	96	Y	Y	N
n-C_{15}	99	Y	Y	N
n-C_{16}	99	Y	Y	N
n-C_{17}	99	Y	Y	N
n-C_{18}	90	Y	Y	N
n-C_{19}	94	Y	Y	N
n-C_{20}	100	Y	Y	N
n-C_{21}	99	Y	Y	N
n-C_{22}	86	Y	Y	N
n-C_{23}	100	Y	N	Y
n-C_{24}	99	Y	N	Y
n-C_{25}	100	Y	N	Y
n-C_{26}	100	Y	N	Y
n-C_{27}	96	Y	N	Y
n-C_{28}	100	Y	N	Y
n-C_{29}	100	Y	N	Y
n-C_{30}	100	Y	N	Y
n-C_{31}	100	Y	N	Y
n-C_{32}	100	Y	N	Y
n-C_{33}	52	N	N	Y
n-C_{34}	27	N	N	Y
n-C_{35}	28	N	N	Y
n-C_{36}	13	N	N	Y

SCA – Short Chain n-alkanes
LCA – Long Chain n-alkanes

Table 3.15: PAHs detected in the samples and details of whether they were included (Y) or excluded (N) from various summaries and statistical analyses

Compound	% detect	PCA Model	Part of PPAHs calculations	Part of APAHs calculations	Included in 16 priority PAHs calculations
Na	46	N	Y	N	Y
Ayl	95	Y	Y	N	Y
Aen	95	Y	Y	N	Y
F	100	Y	Y	N	Y
Pn	100	Y	Y	N	Y
Fl	99	Y	Y	N	Y
Py	99	Y	Y	N	Y
BaA	99	Y	Y	N	Y
Ch	99	Y	Y	N	Y
BF	100	Y	Y	N	Y
BePy	98	Y	Y	N	N
BaPy	74	Y	Y	N	Y
Per	99	Y	Y	N	N
DA	77	Y	Y	N	Y
IP	99	Y	Y	N	Y
Bghi	100	Y	Y	N	Y
N1	38	N	N	Y	N
N2	32	N	N	Y	N
P1	100	Y	N	Y	N
P2	100	Y	N	Y	N
F1	93	Y	N	Y	N

PPAH – Parent PAHs
APAH – Alkylated PAHs
N1 – 1 Methyl Naphthalene, 2 Methyl Naphthalene
N2 – 1,3 Dimethyl Naphthalene, 1, 4 Dimethyl Naphthalene, 1, 2 Dimethyl Naphthalene 1, 7 Dimethyl Naphthalene 1,5 Dimethyl Naphthalene, 2,3 Dimethyl Naphthalene, 2, 6 Dimethyl Naphthalene)
P1 – 2 Methyl Anthracene, 2 Methyl Phenanthrene, 4 Methyl Phenanthrene, 9,2 Methyl Phenanthrene, 1,2 Methyl Phenanthrene
P2 - 3, 6 Di Methyl Phenanthrene, 1, 8 Di Methyl Phenanthrene, 1, 2 Di Methyl Phenanthrene

CHAPTER 4: RESULTS

4.1 Profiles and Inventories of Porosity, ^{210}Pb and ^{137}Cs

Porosity generally decreased with depth in the sediment cores as expected due to sediment compaction (Figure 4.1). However, in core NU-WAB-10, a notable change in slope was observed from 7 to 8 cm, while the down core profile of porosity was noisy in the short core NU-WAB-16. Among the cores, porosity differences indicate that NU-WAB-08 was the most fine-grained, with average porosity of 0.85±0.05 (n=17), while CI-08 was the most coarse-grained, with average porosity of 0.63±0.03 (n=16) (Table 4.1). CI-24 was the only other core with low porosity (ϕ_{av} = 0.67), while all the cores from Wager Bay (WAB) had average porosities of 0.73-0.85, implying a more quiescent sedimentary environment compared to Chesterfield Inlet (CI).

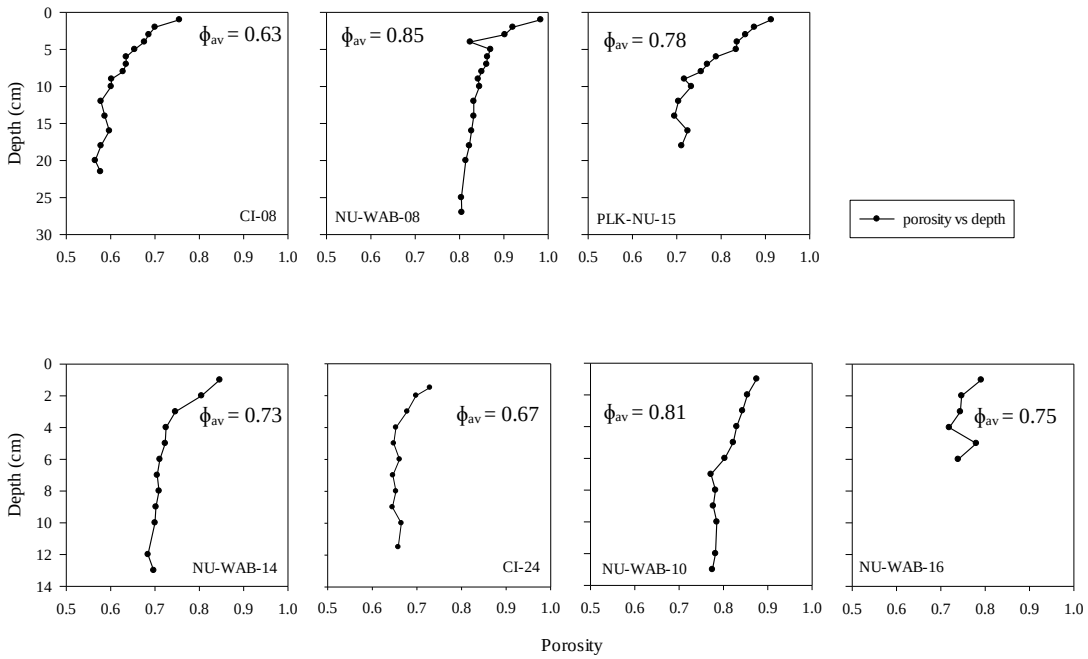

Figure 4.1: Profiles of average porosity within the seven analysed sediment cores. Note varying lengths.

$^{210}Pb_t$ activity in the sediment cores from Chesterfield Inlet (CI-08 and CI-24) generally decreased with depth over the entire core length (Figure 4.2). In contrast, Wager Bay cores showed down-core decreases below the surface to depths ranging from 6 cm in core NU-WAB14 to 16 cm in PLK-NU-15. Activities remained very low and constant thereafter (as indicated by dotted lines). With the exception of NU-WAB-16, which had a quite variable $^{210}Pb_t$ profile (Figure 4.2), the $^{210}Pb_t$ levels measured in the remaining cores were generally consistent with assumptions of steady-state sedimentation and (exponential) ^{210}Pb decay (Kuzyk, Macdonald, and Johannessen 2015). The 'wobbles' in the profiles near the surface reflect surface mixed layers (SML), in which rates of bioturbation or other types of mixing appear to be significant relative to rates of sedimentation. The low constant activities deep in the cores are interpreted as the 'supported' ^{210}Pb activities ($^{210}Pb_{sp}$), i.e., the background contents produced by in situ ^{226}Ra decay. The $^{210}Pb_{sp}$ were significantly lower in CI sediments (1.51-1.80 dpm/g) compared to WAB (3.41-4.21 dpm/g) (Table 4.1).

Figure 4.3 shows profiles of Ln $^{210}Pb_{ex}$ calculated by subtracting $^{210}Pb_{sp}$ activities from $^{210}Pb_t$. No profile of $^{210}Pb_{ex}$ is shown for core NU-WAB-16 because it is uncertain whether supported ^{210}Pb activities were reached over its short length (6 cm). In the remaining cores, $^{210}Pb_{ex}$ generally decreased with depth below the apparent "SML" (SML is the upper portions of the cores where $^{210}Pb_{ex}$ activities did not decrease with depth) (Figure 4.3). The $^{210}Pb_{ex}$ profile in core NU-WAB-10 changes below depth 7-8 cm, similar to the porosity profile in this core, implying a possible difference in sedimentation in the upper and lower portions of this core.

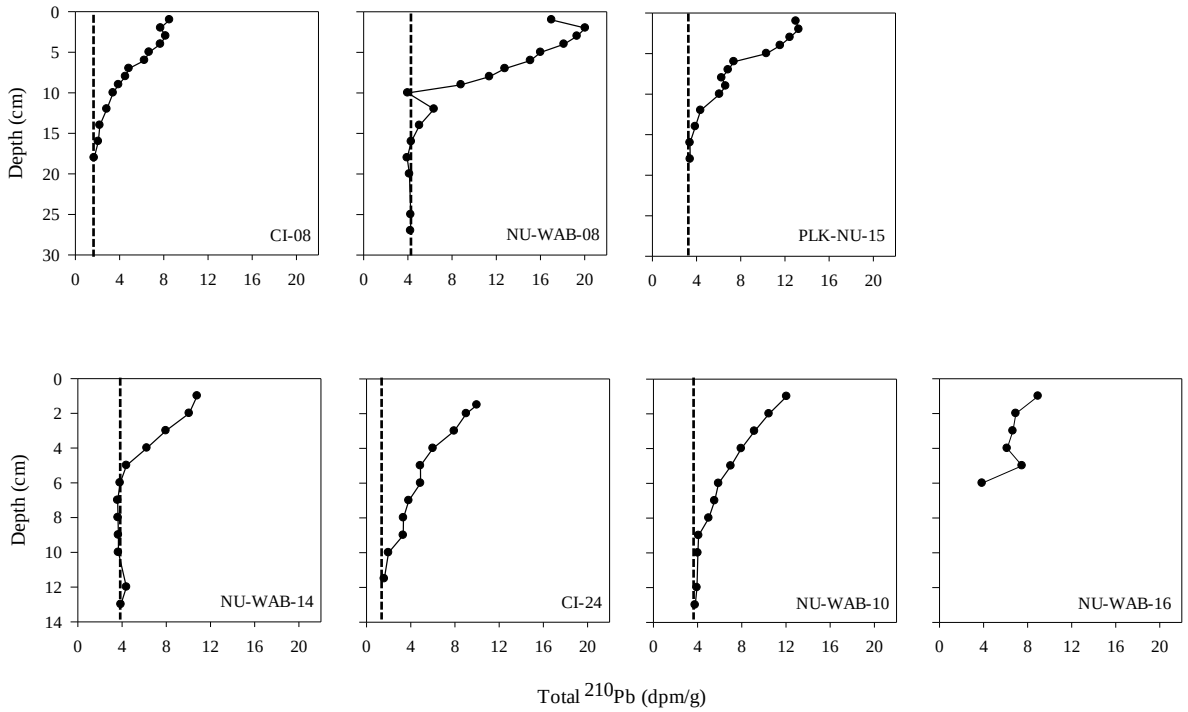

Figure 4.2: Profiles of Total ^{210}Pb (dpm/g). Supported ^{210}Pb activity in each core is shown by the vertical dotted lines.

Inventories of $^{210}Pb_{ex}$ in the cores varied from a minimum of about 10.75 dpm/cm^2 in core NU-WAB-14 to maximum values of 46 and 33 dpm/cm^2 in cores CI-08 and NU-WAB-08, respectively (Table 4.1). The $^{210}Pb_{ex}$ inventories are in the low to middle part of the range previously reported for Hudson Bay sediments (10-76.5 dpm/cm^2, n=15; Kuzyk et al., 2009).

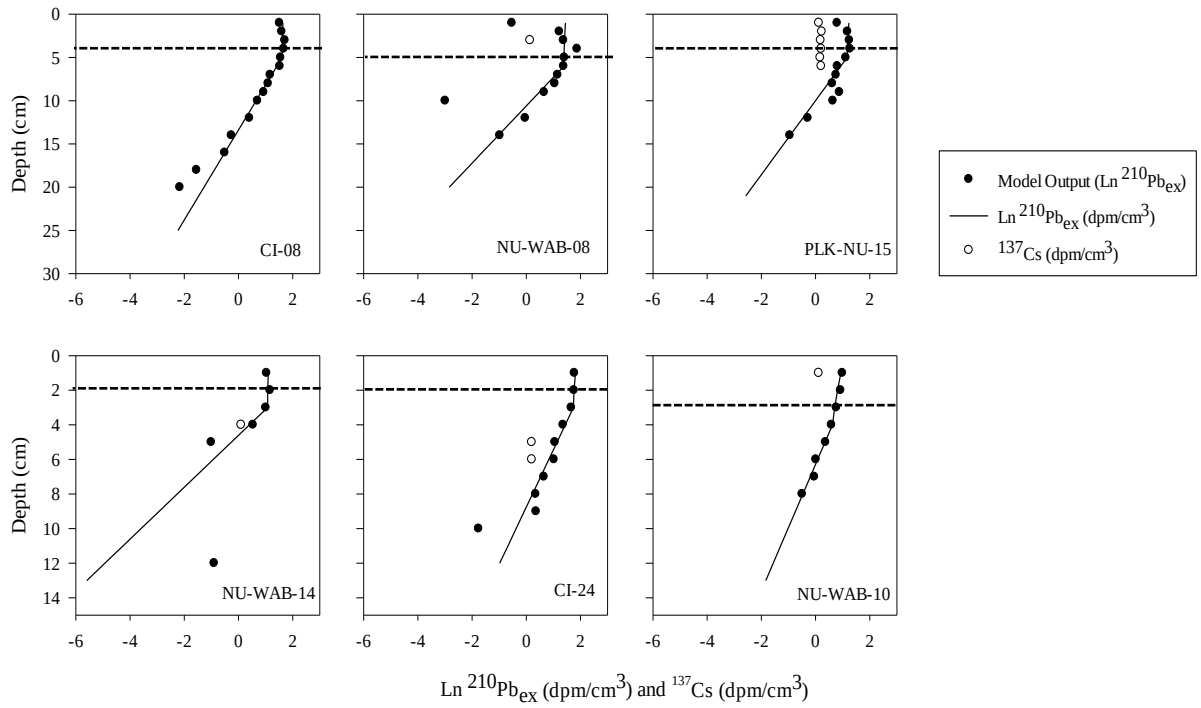

Figure 4.3: Measured (dots) and modeled (lines) profiles of $Ln^{210}Pb_{ex}$ activity versus depth. SML thickness in each core is shown by the horizontal dashed line.

Only two cores, PLK-NU-15 and CI-24, contained detectable ^{137}Cs in more than one core section. ^{137}Cs was present in sediment depths of 1-6 cm in PLK-NU-15, for a total ^{137}Cs inventory of 1.12 dpm/cm^2 and at depths of 4-6 cm in C1-24, for a total ^{137}Cs inventory of 0.41 dpm/cm^2. In the remaining cores (CI-08, NU-WAB-08, NU-WAB-10, NU-WAB-14 and NU-WAB-16), ^{137}Cs was either not detected or detected in only one core section (Table 4.1). Similar findings were reported by Kuzyk et al. (2009). For cores PLK-NU-15 and C1-24, a good fit between observed and predicted depth of onset of ^{137}Cs in the sediment confirmed the sedimentation and mixing rates determined from ^{210}Pb (Figure 4.4). The elevated ^{137}Cs activities in the upper portion of core PLK-NU-15 may be due to continued inputs of ^{137}Cs after the cessation of atmospheric weapons testing. This could result from inputs of terrestrial sediment associated with coastal erosion or ice rafting at this very nearshore site (Kuzyk, Gobeil, and Macdonald 2013). The ^{137}Cs profile in CI-24 is best fit by a model in which there is ^{137}Cs input only between 1954 and 1968.

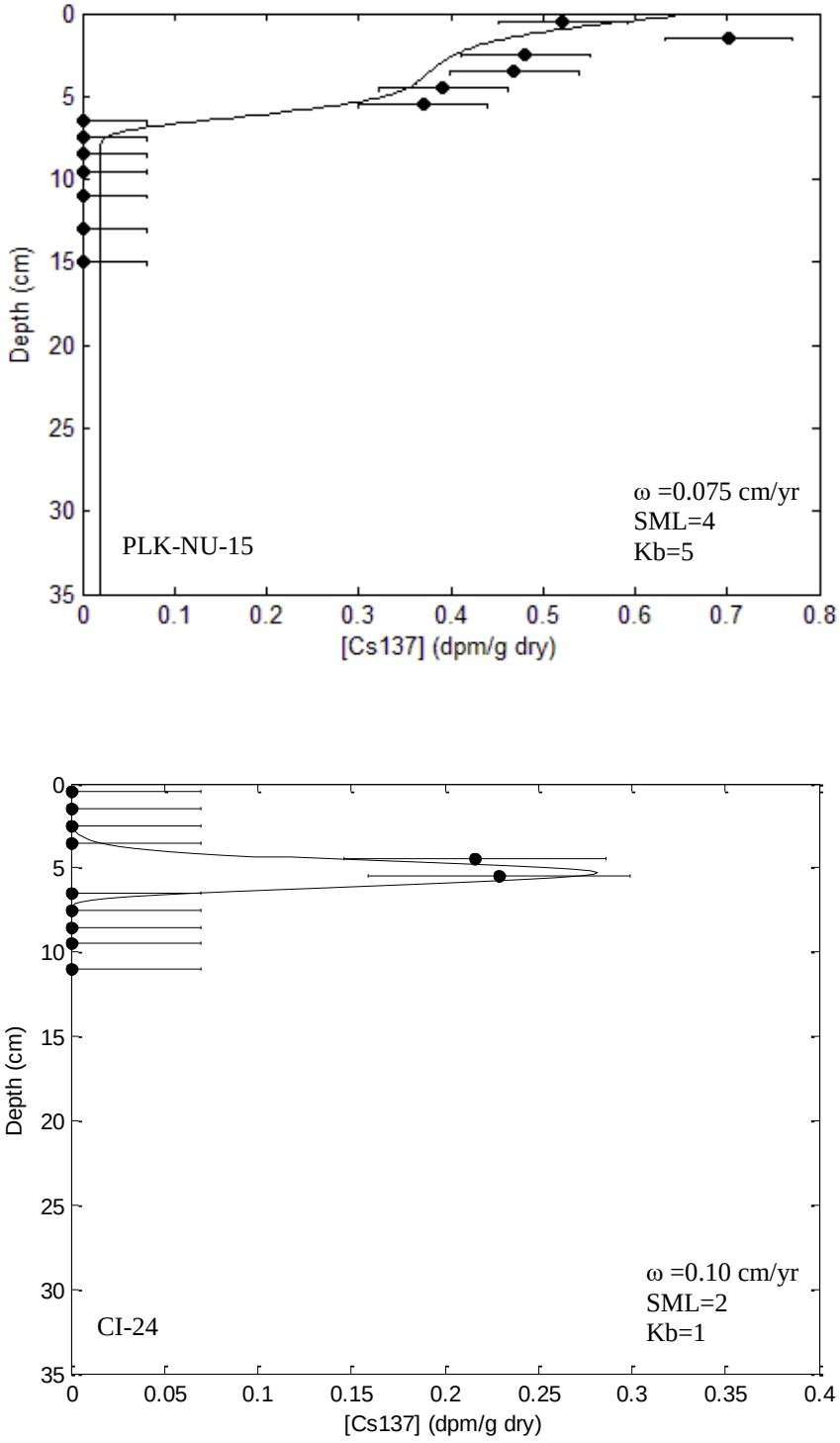

Figure 4.4: Modeled (lines) and observed (dots) ^{137}Cs activities in PLK-NU-15 and CI-24.

Table 4.1: Summary of sediment geochemical properties and sedimentation parameters

	CI-08	CI-24	NU-WAB-08	NU-WAB-10	NU-WAB-14	NU-WAB-16	PLK-NU-15
Average porosity (±SD)	0.63 (±0.05)	0.67 (±0.03)	0.85 (±0.05)	0.81 (±0.04)	0.73 (±0.05)	0.75 (±0.03)	0.78 (±0.07)
Average ^{210}Pb supported (dpm/g)	≤ 1.51	≤ 1.80	4.21	3.96	3.90	≤ 3.88	3.41
ω (CI) (cm/yr)	0.16 (0.14-0.18)	0.10 (0.09-0.37)	0.10 (0.08-0.50)	0.05 (0.02-0.55)	≤0.03	na	0.075 (0.07-0.28)
r (CI) (g/cm^2/yr)	0.17 (0.15-0.19)	0.14 (0.09-0.34)	0.04 (0.03-0.20)	0.03 (0.01-0.31)	≤0.02	na	0.10 (0.07-0.19)
^{210}Pb inventory (dpm/cm^2)	46.12	31.09	32.71	13.14	10.75	na	28.34
Post-1900 ^{210}Pb inventory (dpm/cm^2)	46.11	31.36	22.37	9.14	6.01	na	15.55
SML (cm)	4	2	5	3	2	na	4
^{137}Cs detection depth (cm)	na	5 – 6	3	1	4	na	1 - 6
^{137}Cs inventory (dpm/cm^2)	0.00	0.41	0.14	0.12	0.09	0.00	1.12
Depths of >90 post-1900 material (cm)	0.00 – 15.00	0.00 – 10.00	0.00 – 6.00	0.00 – 4.00	0.00 – 2.00	na	0.00 – 5.00
Depths of >90 pre-1900 material (cm)	> 20.00	> 12.00	> 14.00	> 4.00	> 5.00	na	> 10.00
Intrinsic time resolution (yr)	25.00	20.00	50.00	82.00	50.00	na	53.00

SML - Surface mixed layer, ω - sedimentation velocity (95 confidence limits), r - mass accumulation rate (95 % confidence limits)
nd – Not detected, na - Not analysed, SD – standard deviation, CI – Confidence Interval

4.2 Sedimentation Velocities and Mass Accumulation Rates

The sedimentation velocities obtained by modelling $^{210}Pb_{ex}$ profiles (Figure 4.3), which were validated for cores PLK-NU-15 and CI-24 using ^{137}Cs profiles (Figure 4.4), varied from 0.03 cm/yr in core NU-WAB-14 to 0.16 cm/yr in core CI-08 (Table 4.1). Mass accumulation rates calculated from average porosities and the sedimentation velocities varied from 0.17 g/cm^2/yr in CI-08 to 0.03 g/cm^2/yr in NU-WAB-14. This range of accumulation rates is similar to that previously reported for Hudson Bay (Kuzyk et al. 2010). With low porosity, the two CI cores had relatively high sedimentation rates compared to the WAB cores with the exception of PLK-NU-15. The sedimentation rate in NU-WAB-14 is not well constrained because of the limited number of subsections below the SML (Table 4.1).

Depth limits of the > 90% pre- and > 90% post-1900 timeframes determined from the tracer experiment are reported in Table 4.1. In CI-08 and CI-24, the top 15 and 10 cm, respectively contains > 90% post-1900 sediments. In NU-WAB-08, NU-WAB-10, NU-WAB-14 and PLK-NU-15, the top 6, 4, 2 and 5 cm, respectively, contain > 90% post-1900 sediments (Table 4.1). In CI-08 and CI-24, > 90% pre-1900 sediment lie below 20 and 12 cm respectively, while in NU-WAB-08, NU-WAB-10, NU-WAB-14 and PLK-NU-15, > 90% pre-1900 sediments lie below 14, 4, 5 and 10 cm, respectively.

4.3 TOC Contents and Profiles

Profiles of total organic carbon content (TOC) in selected sections of four cores (CI-08, NU-WAB-08, NU-WAB-10 and PLK-NU-15) are shown in Figure 4.5. The highest TOC content occurs at or near the sediment surface and decreases with depth thereafter. This down-core decrease is consistent with TOC oxidation at or near surface layers where aerobic microbial degradation is significant (Macdonald et al. 2008). Average % TOC in the sediment cores ranged from 0.75 ± 0.10 % in CI-08 to 1.93 ± 0.16 % in NU-WAB-08. Although the

TOC content in NU-WAB-08 is among the very highest recorded for Hudson Bay sediments (Kuzyk et al., 2009), the range of values obtained at CI-08, NU-WAB-10 and PLK-NU-15 compare well with those measured in previous cores from Hudson Bay and in other Arctic regions (Kuzyk et al. 2009; Goñi et al. 2013). High TOC content were measured in the sediment cores having a relatively high porosity (i.e., WAB cores). Conversely, low TOC were measured in the sediment cores having a relatively low porosity (i.e., CI cores). Overall, % TOC content in the analysed sediment sections was strongly positively correlated with sediment porosity (Figure 4.6; r^2=0.96, p<0.001), consistent with the finding from other studies (Goñi, et al. 2003).

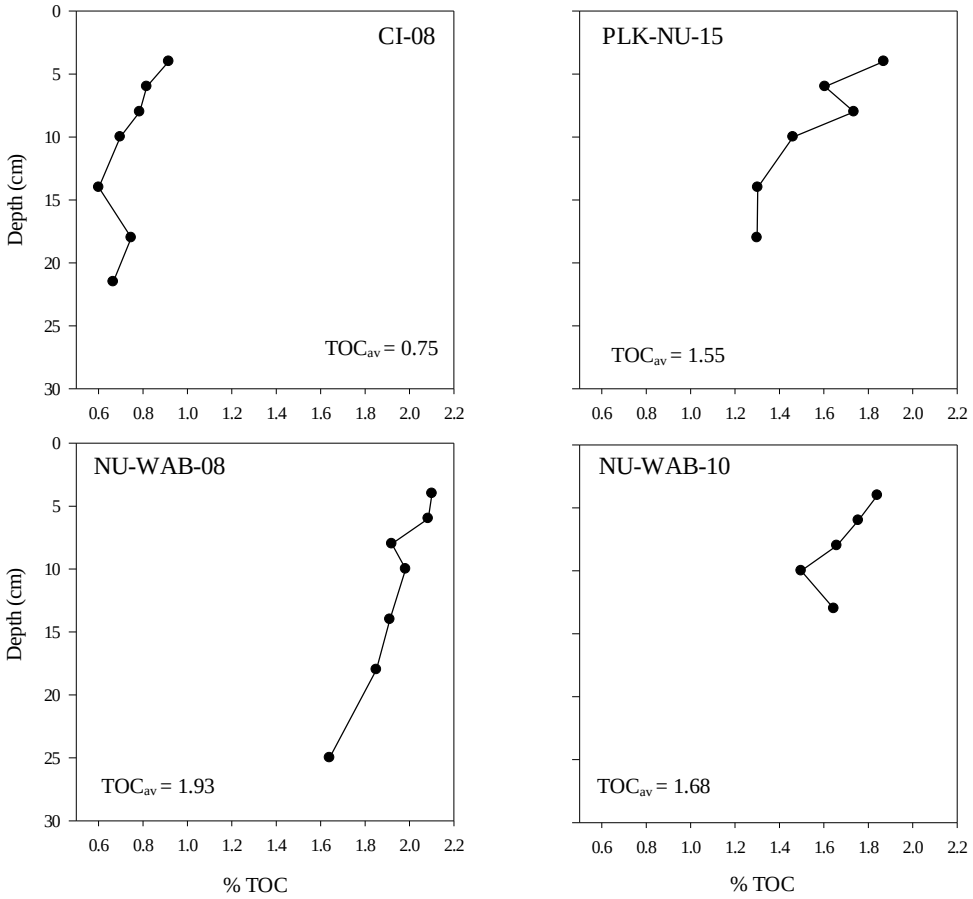

Figure 4.5: Profiles of % TOC in sediment cores and average values for each core. Note that only selected core sections were analysed.

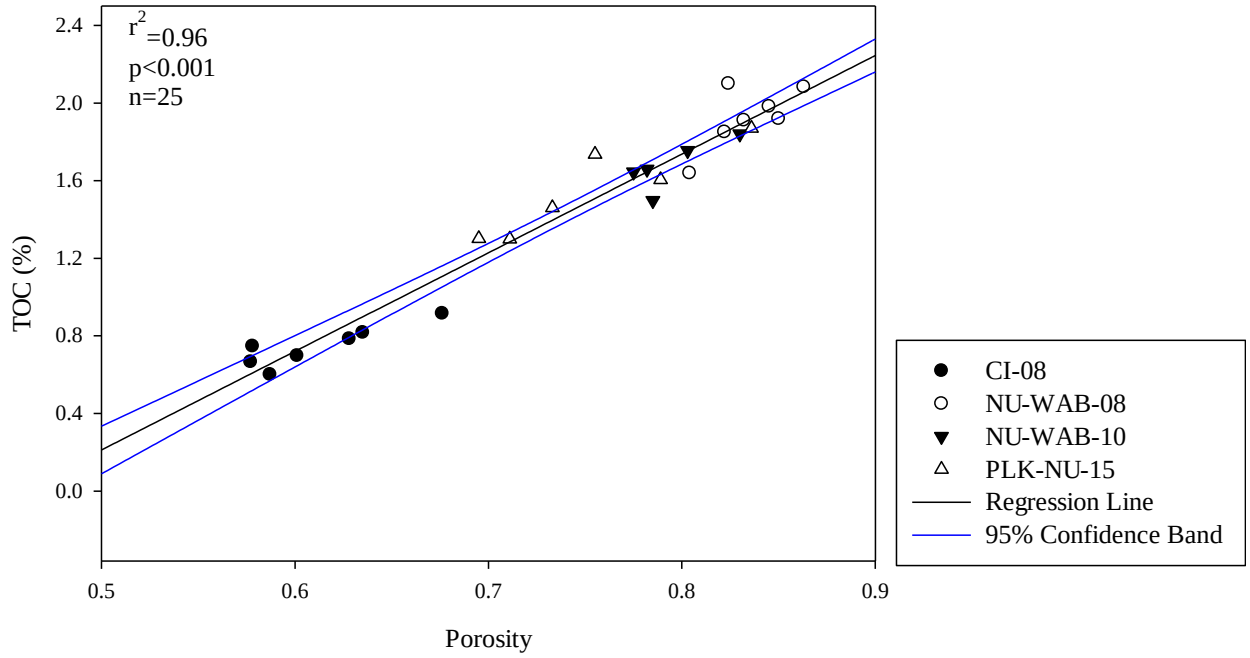

Figure 4.6: Correlation between sediment porosity and TOC (%).

4.4 Profiles and Authigenic Accumulation Rates of Redox Sensitive Elements

Profiles of concentrations of elements normalised to Al, i.e., element/Al ratios (Mn/Al, Fe/Al, S/Al, and Mo/Al), are shown in Figure 4.7. Lithogenic concentrations of the elements need to be accounted for before the distributions of authigenic phases of the redox-sensitive elements can be discussed. Here, we follow previous workers (cf., Kuzyk et al. 2017) in using Al normalization to help account for variation in the lithogenic contribution to S, Mo, and Fe in the sediment samples. In particular, increases in element/Al ratios above typical levels in the sediment cores are interpreted as evidence for precipitation and accumulation of authigenic fractions of the elements in response to redox gradients within the sediments.

4.4.1 Mn Profile

The distribution and re-distribution of Mn is controlled by the thickness of sub-surface oxygen. Mn/Al ratios are high in the top 3 cm of NU-WAB-08, which implies cycling of Mn and precipitation in oxic surface layers (Emerson and Hedges 2003). An isolated example of Mn enrichment below the zone of oxygen enrichment in the 5-6 cm section of NU-WAB-08 probably reflects rapid accumulation of Mn oxides (burial below the oxic zone) and concentrations larger than the capacity of OC to reduce it (Kuzyk et al. 2010). Low concentrations of Mn in deeper sediment sections of core NU-WAB-08 and throughout the remaining cores imply reducing conditions. In sharp contrast to NU-WAB-08, the Al-normalised Mn concentration remains unchanged throughout CI-08, PLK-NU-15 and NU-WAB-10, signifying oxygen-limited and reducing conditions (Emerson and Hedges 2003; Kuzyk et al. 2017).

4.4.2 Fe and S Profiles

Enrichment of Fe is apparent in the top 2-3 cm of the sediment cores with the exception of NU-WAB-10 (Figure 4.7). In NU-WAB-08, PLK-NU-15, and CI-08, minimum Fe/Al ratios are reached at depths of 3-4 cm, after which Fe/Al ratios increase with depth (Figure 4.7). The decrease in Fe in surface and near surface sediments is interpreted as being consistent with Fe reaction following Mn in diagenetic sequence (Kuzyk et al. 2010). The increasing Fe concentrations below 3-4 cm depth are controlled by the distribution of anoxic conditions and the presence of sulphide (S^{2-}), which, in the presence of available Fe, forms various reduced sulphur species including FeS and FeS_2 (Macdonald et al. 2008). Maximum Fe/Al ratios are reached at depths of ~10 cm in most cores and between 10 and 20 cm in PLK-NU-15 (Figure 4.7).

Surface enrichment of S in the first 2 cm of NU-WAB-08 may be due to the presence of particulate organic sulfur which may be enriched in the organic-rich surface sediments (Kuzyk et al. 2010). Below 3-4 cm depth (NU-WAB-08, PLK-NU-15, and CI-08) or immediately below the surface (NU-WAB-10), S/Al ratios tend to increase with depth much like Fe/Al (Figure 4.7). The profiles of S/Al and Fe/Al together are consistent with accumulation of authigenic Fe and S compounds with depth, which implies strongly reducing and sulphidic conditions and long-term capture of Fe sulphides (pyrite) in the subsurface sediments.

4.4.3 Mo Profiles

Elevated concentrations of Mo in marine sediments result from more than one process. The processes include: (i) scavenging by Mn and Fe oxides, i.e., under oxic conditions Mn oxides and/or Fe oxyhydroxides provide reactive surfaces for Mo adsorption (Morford et al. 2009; Malcolm 1985). Elevated concentrations of Mo in the top oxygenated sections of sediment cores reflect association with Mn and Fe in the oxic layer (Macdonald et al. 2008; Kuzyk et al. 2010). Here, we observed a strong correlation between the Mo and Mn enriched surface layers (0-3 cm) within core NU-WAB-08 (r^2=0.85). The Mo profile in upper sediment sections also correlated well with the Fe profile in these sections in all the stations. A second process of Mo enrichment in sediments (ii) involves co-precipitation of Mo with sulphides in anoxic sulfate reduction zones. Mo accumulation under sulphidic conditions is seen as Mo concentrations increasing with depth in parallel with S in the sediments at all stations (Figure 4.7). The increases in Mo/Al with depth in the cores (Figure 4.7) may be an indication of accumulation of sulphide-associated Mo within the sediments with depth, implying strongly reducing and sulfidic conditions (Kuzyk et al. 2010).

4.4.4 Authigenic element accumulation rates in reducing sediments

Average authigenic accumulation rates for Fe and S ($mg/cm^2/yr$) and Mo ($\mu g/cm^2/yr$) calculated from sedimentation rates and average authigenic element concentrations in the reducing portions of the cores (see horizontal dashed lines in Figure 4.7) are shown in Table 4.2. In all the cores, no accumulation of authigenic Mn was observed except for some few portions in NU-WAB-08. The range of authigenic Mo accumulation rates in the WAB and CI cores (0.15-0.57 $\mu g/cm^2/yr$) is similar to that reported previously for Hudson Bay (0.00-0.27 $\mu g/cm^2/yr$; Kuzyk et al. 2011) and other North American Arctic shelves (0.00-0.87 $\mu g/cm^2/yr$; Kuzyk et al. 2017). Authigenic S accumulation rates have not been previously reported for Hudson Bay but the range in the WAB and CI cores (0.11-0.34 $mg/cm^2/yr$) is similar to the average in Lancaster Sound in the Canadian Arctic (0.19 ± 0.13 $mg/cm^2/yr$; Kuzyk et al. 2017). The authigenic Mo and S accumulation rates in the cores are highly correlated ($r^2=0.77$). It is notable that authigenic element accumulation rates are non-zero in all the WAB and CI cores; more than half the rates of authigenic Mo and S accumulation in other Arctic shelf locations have been zero (Kuzyk et al. 2011; 2017). The highest accumulation rates in the WAB and CI cores are in CI-08 (Mo) or PLK-NU-15 (S and Fe) whereas the lowest rates are in NU-WAB-10 (Table 4.2).

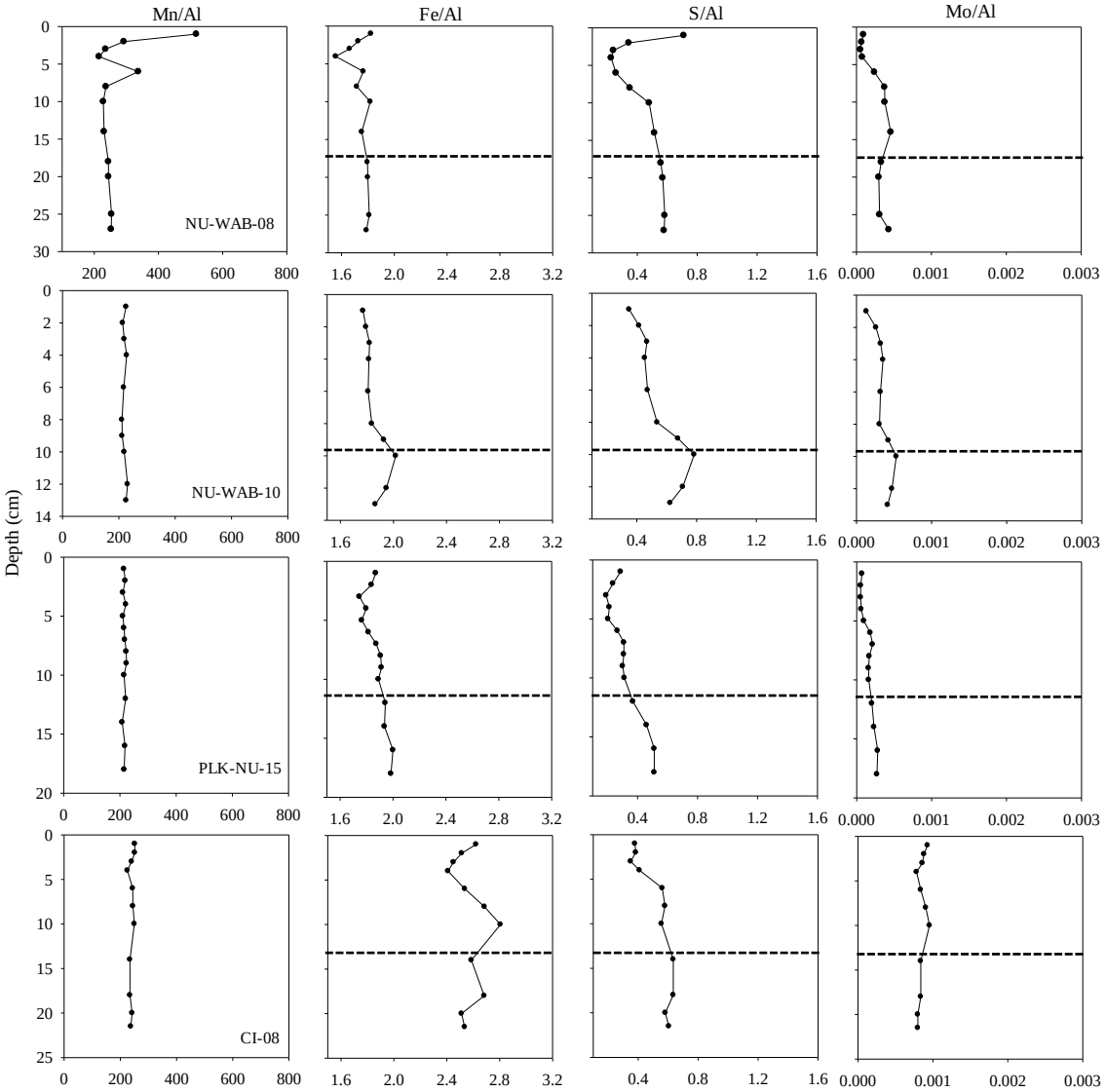

Figure 4.7: Profiles of Al-normalised concentrations of redox-sensitive elements from left to right: Mn/Al, Fe/Al, S/Al and Mo/Al. The horizontal dashed line shows the depth below which the sediments were considered to be reducing for the calculation of the average authigenic element concentrations in reducing sediments.

Table 4.2: Average authigenic element accumulation rates in reducing sediments

Stations	Fe (mg/cm^2/yr)	S (mg/cm^2/yr)	Mo (µg/cm^2/yr)
NU-WAB-08	0.12	0.18	0.18
NU-WAB-10	0.05	0.11	0.15
PLK-NU-15	0.27	0.34	0.34
CI-08	0.12	0.30	0.57

4.5 Concentrations and profiles of n-alkanes

Mean (± confidence intervals) concentrations (ng/g dw) of n-alkanes in the sediment cores (n=6-16 analyzed sections per core; see Appendix 2) are shown in Figure 4.8. The most abundant n-alkanes fell in the n-C_{29} to n-C_{31} range in all the samples (Figure 4.8), apart from NU-WAB-14. A secondary, generally weaker, peak occurred around n-C_{14} to n-C_{16} in the CI cores, n-C_{12} to n-C_{14} in NU-WAB-08, and n-C_{15} to n-C_{17} in NU-WAB-14. Of note is a general predominance of odd-numbered compounds over even-numbered compounds in the sediments (Figure 4.8), except for NU-WAB-14 which shows a reverse trend. This odd-over-even preference particularly in the range n-C_{27} to nC_{31} is clear in all the cores except for NU-WAB-14, which has unusually high abundance of n-C_{32} and n-C_{34}.

Separating the n-alkanes into carbon chain lengths of n-C_{11} to n-C_{22} (short-chain n-alkanes or SCA) *vs*. carbon chain lengths of n-C_{23} to n-C_{36} (long-chain n-alkanes or LCA), it can be seen that LCAs dominate in these sediments, with average concentrations of SCA lower by at least 3-4 times (CI-08, NU-WAB-08, NU-WAB-10, and NU-WAB-14) and, in some cores, as much as ~7-11 times (CI-24, NU-WAB-16, PLK-NU-15) (Table 4.3). The low abundance of SCA relative to LCA obtained here is similar to that reported for the Chukchi Sea (Harvey et al. 2014). Average concentrations of LCA ranged from 1.65 µg/g dw in NU-WAB-14 to 3.18 µg/g dw in PLK-NU-15 and SCA from 0.21 µg/g dw in NU-WAB-16 to 0.86 µg/g dw in NU-WAB-08 (Table 4.3).

The flux of mean n-alkanes in recent post-1900 sediment intervals were highest in the two CI cores (CI-08; 151.33 ng/cm^2/yr and CI-24; 80.71 ng/cm^2/yr, respectively) and much lower in the WAB cores. The flux in WAB ranged from 30.88 ng/cm^2/yr in PLK-NU-15 to 3.66 ng/cm^2/yr in NU-WAB-14 (Table 4.3). However, flux of pre-1900 flux were all within the same range of values for both WAB and CI with the maximum flux of pre-1900 (31.32 ng/cm^2/yr) in PLK-NU-15 and the minimum flux of pre-1900 (7.99 ng/cm^2/yr) in CI-24.

Down-core profiles of LCA and SCA (Figure 4.9) show large variability, with LCA and SCA sometimes changing in parallel (e.g., increase at 7 cm depth in CI-08) and sometimes changing in opposition (increase in SCA with decrease in LCA at 9 cm in NU-WAB-08). There are few significant trends in n-alkane concentrations (LCA or SCA) with depth in the sediment cores (Figure 4.9). For SCA, there was a significant down-core decrease in NU-WAB-16 (r^2 = 0.99, $p<0.004$). For LCA, there was a significant down-core increase in PLK-NU-15 (r^2 = 0.41, $p = 0.06$).

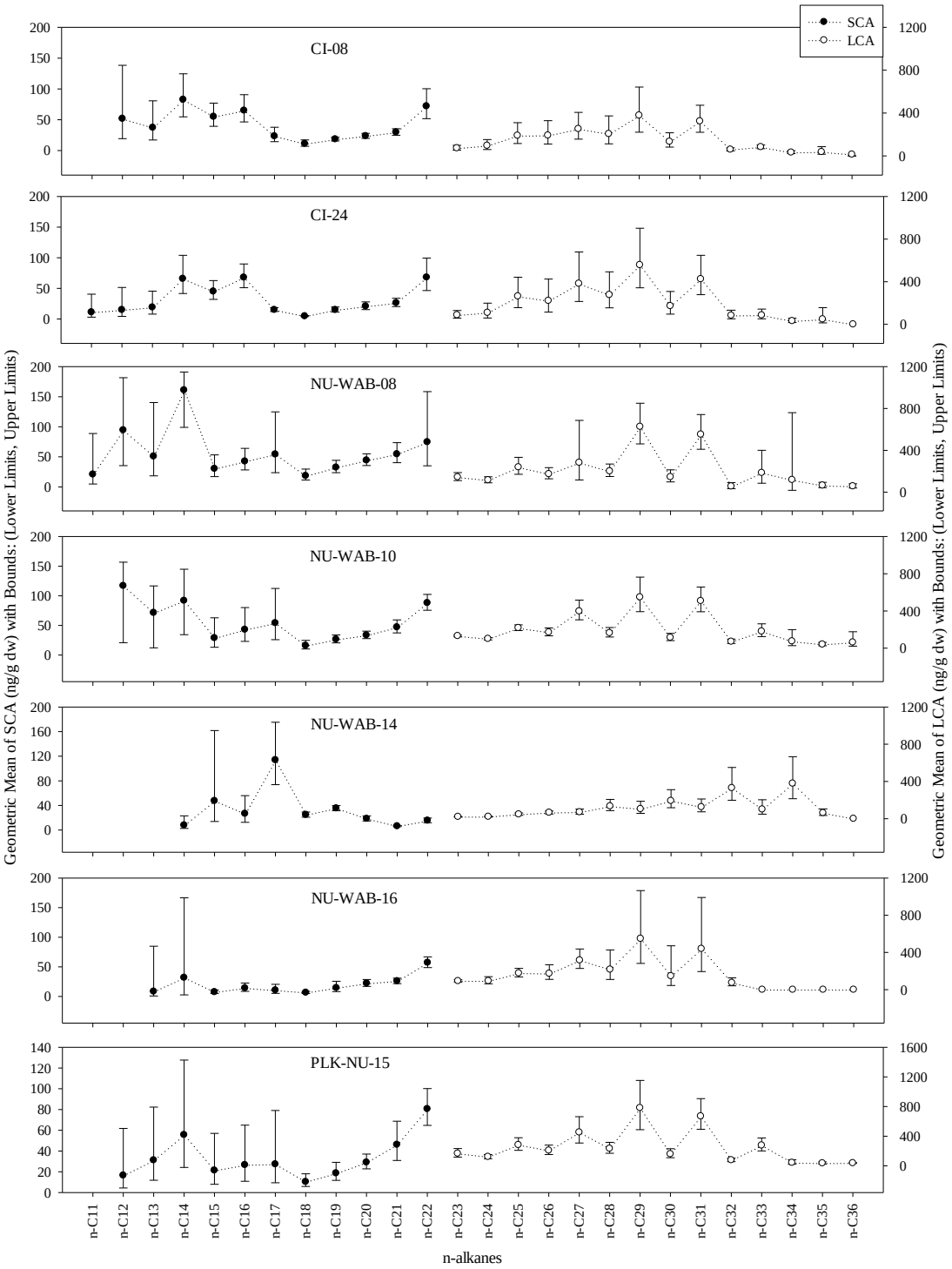

Figure 4.8: Geometric mean (± confidence intervals) concentrations (ng/g dw) of n-alkanes in sediment cores, from top to bottom: C1-24, CI-08, NU-WAB-08, NU-WAB-10, NU-WAB-14, NU-WAB-16, PLK-NU-15. Note the difference in scales for short-chain n-alkanes (SCA, filled circles) and long-chain n-alkanes (LCA, open circles). Number of analysed sediment sections varies among the cores. Absence of symbol indicates that compounds were not detected in the samples.

Table 4.3: Geometric mean (confidence intervals) concentrations and inventories of LCA and SCA

Stations	CI-08	CI-24	NU-WAB-08	NU-WAB-10	NU-WAB-14	NU-WAB-16	PLK-NU-15
Concentrations (µg/g dw)							
SCA	0.51 (0.36-0.72)	0.37 (0.26-0.53)	0.86 (0.62-1.18)	0.66 (0.42-1.06)	0.41 (0.30-0.56)	0.21 (0.10-0.41)	0.43 (0.23-0.79)
LCA	2.05 (1.32-3.18)	2.64 (1.60-4.37)	2.7 (2.11-3.46)	2.64 (2.13-3.28)	1.65 (1.02-2.67)	2.30 (1.30-4.07)	3.18 (2.41-4.19)
Mean n-alkane flux (ng/cm^2/yr)							
Pre-1900	11.34	7.99	14.74	19.12	8.97	NA	31.32
Post-1900	151.33	80.72	26.38	12.89	3.66	NA	30.88

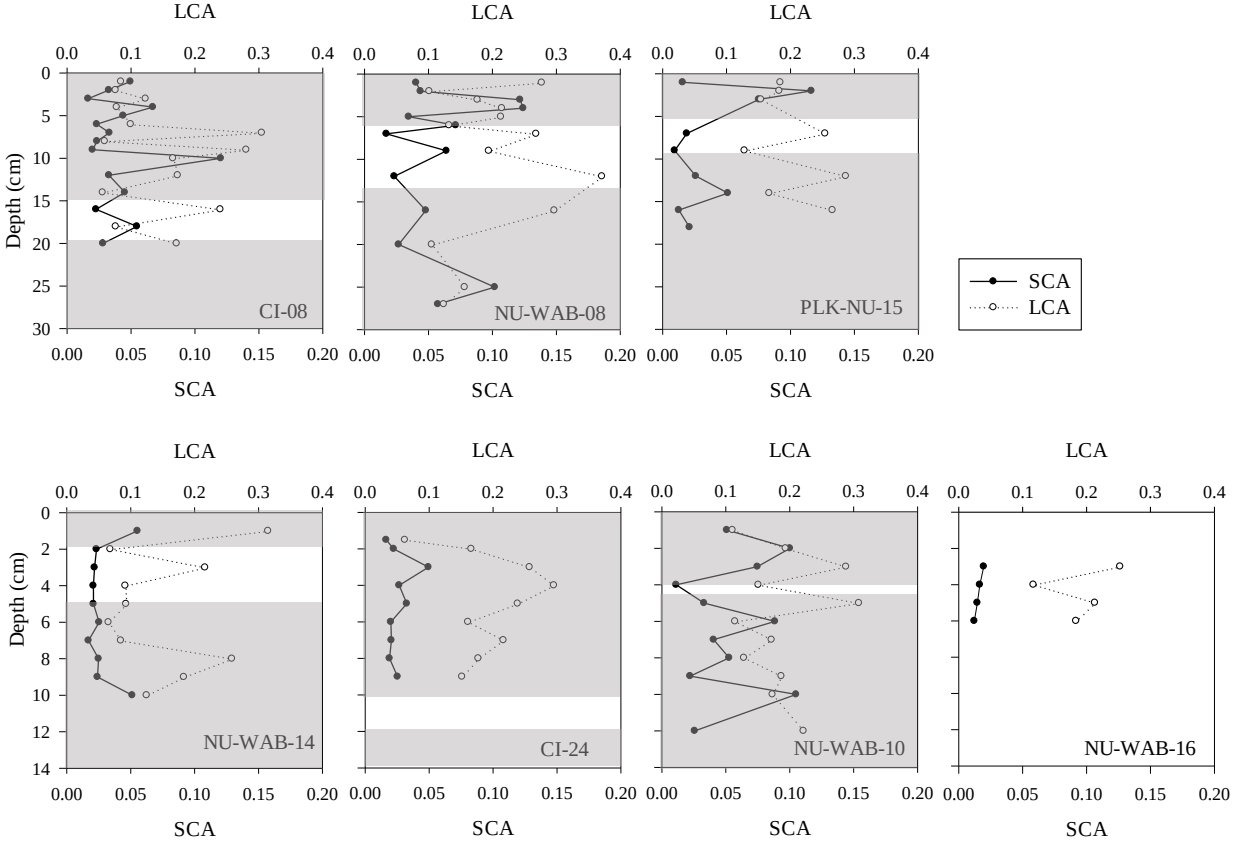

Figure 4.9: Profiles of mean ΣSCA (solid lines) and ΣLCA (dotted lines). Lower and upper shaded portions represent sections of core with more than 90 % of sediments deposited pre- and post-1900, respectively. The non-shaded portions reflect a mixture of sediments deposited during both time periods. Note variation in x- and y-axes scales among the cores.

4.6 Concentrations and Profiles of PAHs

Concentrations of individual PAH compounds compared to concentrations obtained in other arctic regions (Harvey et al. 2014; Foster et al. 2015) were very low in all the sediment samples (Figure 4.10). Concentrations recorded in the WAB and CI sediments are at least 5 to 10 times lower than those in Chukchi Sea sediments (Harvey et al. 2014) and ~100 times lower than the Canadian interim sediment quality guidelines (ISQGs), which are levels believed to be free from association with adverse biological effects to marine life (MacDonald, Ingersoll, and Berger 2000; CCME 2012).

The most abundant compounds in the WAB and CI sediments were Na and its substituted counterparts (N1, N2) and other alkylated compounds (P1, P2, and F1). Alkylated PAHs (APAH) were generally higher than parent PAHs (PPAH) in the cores, with the exception of NU-WAB-08 (Table 4.4). Geometric mean (confidence limits) of PPAHs ranged from 0.83 (0.53-1.32) ng/g dw in CI-08 to 2.65 (1.75-4.00) ng/g in NU-WAB-08. APAH ranged from 2.16 (1.13-4.11) ng/g dw in CI-08 ng/g dw to 6.08 (1.78-20.7) ng/g dw in NU-WAB-14 (Table 4.4). Relatively high concentrations of APAHs compared to PPAHs have also been reported for marine sediments from other sites in the Arctic (Ma et al. 2017; Foster et al. 2015; Harvey et al. 2014; Yunker et al. 1996). Thus, the low concentration of APAH (2.74 ng/g) in NU-WAB-08, which is similar to the concentration of PPAH (2.65 ng/g), may be considered unusual.

The mean concentration of PPAHs was significantly lower in the CI cores than in the WAB cores ($p<0.05$) whereas there was no difference between the two areas in concentrations of alkylated compounds. The flux of post-1900 sediments were much higher in CI-08, CI-24 and NU-WAB-08 (Table 4.4). Pre-1900 flux was highest in PLK-NU-15 (0.03 ng/cm^2/yr) and lowest in CI-24 (3.18E-03) (Table 4.4).

Perylene, which may be produced within marine sediments, was detected at low concentrations in the CI cores (0.03 ng/g dw in CI-08 and 0.07 ng/g dw in CI-24) and at significantly higher concentrations in the WAB cores (0.14-0.37 ng/g dw; Table 4.4). The highest concentrations of Perylene were found in NU-WAB-08 (0.37 ng/g dw) and PLK-NU-15 (0.35 ng/g) (Table 4.4). Despite the potential for perylene to have been produced by diagenesis, the profiles of Perylene (not shown) do not show evidence for increases in perylene with depth in any of the sediment cores.

The down core profiles of PPAH and APAH in relation to pre- and post-1900 sediments (shaded portions) are shown in Figure 4.11. There is a slight down-core decrease in PPAHs in NU-WAB-08 (r^2 = 0.376, p value = 0.012), NU-WAB-10 (r^2 = 0.509, p value = 0.014) and a down-core decrease in both of PPAH and APAH in NU-WAB-14 (PPAHs; r^2 = 0.519, p value = 0.012, APAHs; r^2 = 0.463, p value = 0.021) and no significant change with depth in the remaining three cores (PLK-NU-15, NU-WAB-16, CI-08 and CI-24).

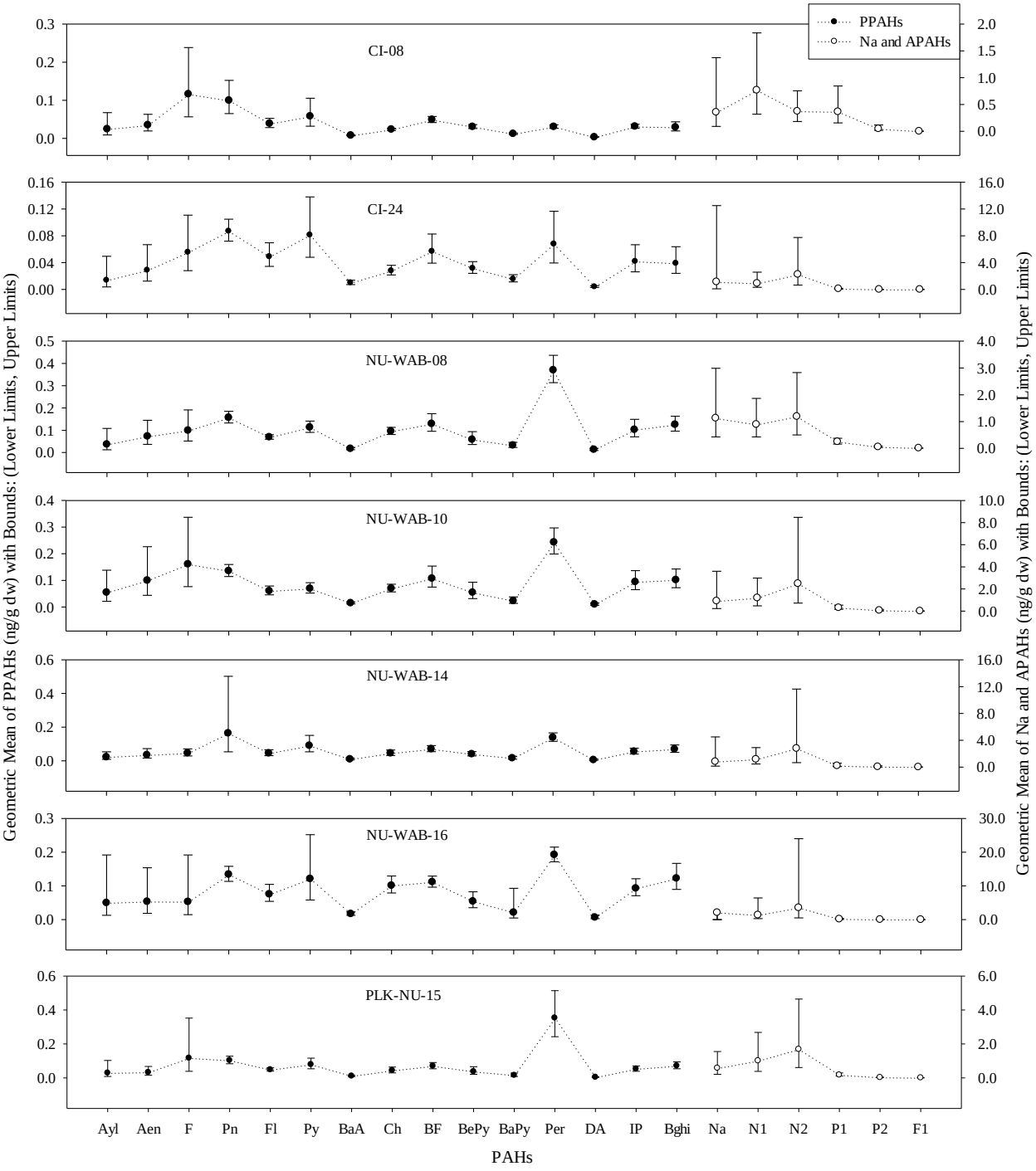

Figure 4.10: Geometric Mean (± CI) concentrations (ng/g dw) of 21 PAHs in sediment cores. Note different scales for Parent PAHs (filled circles) and Na and Alkylated PAHs (open circles). Number of analysed sediment core sections varies from 6 in NU-WAB-16 to 16 in NU-WAB-08 and CI-08.

Table 4.4: Geometric Mean (Confidence Limits) Concentrations and Inventories of PPAHs, APAHs, and Perylene

Stations	CI-08	CI-24	NU-WAB-08	NU-WAB-10	NU-WAB-14	NU-WAB-16	PLK-NU-15
Concentrations (ng/g dw)							
PPAHs	0.83	0.98	2.65	2.31	1.78	1.53	1.59
	(0.53-1.32)	(0.60-1.62)	(1.75-4.00)	(1.32-4.01)	(0.80-3.97)	(0.92-2.53)	(1.02-2.50)
APAHs	2.16	3.58	2.74	5.02	6.08	5.67	3.37
	(1.13-4.11)	(1.20-10.68)	(1.34-5.62)	(1.90-13.31)	(1.78-20.70)	(1.14-28.30)	(1.43-7.92)
Perylene	0.03	0.07	0.37	0.24	0.14	0.19	0.35
	(0.03-0.04)	(0.04-0.12)	(0.31-0.44)	(0.20-0.30)	(0.12-0.17)	(0.17-0.22)	(0.24-0.51)
Mean PAH flux ($ng/cm^2/yr$)							
Pre-1900	0.016	3.18E-03	0.01	0.02	7.3E-03	NA	0.03
Post-1900	0.09	0.07	0.03	0.02	5.45E-03	NA	0.02

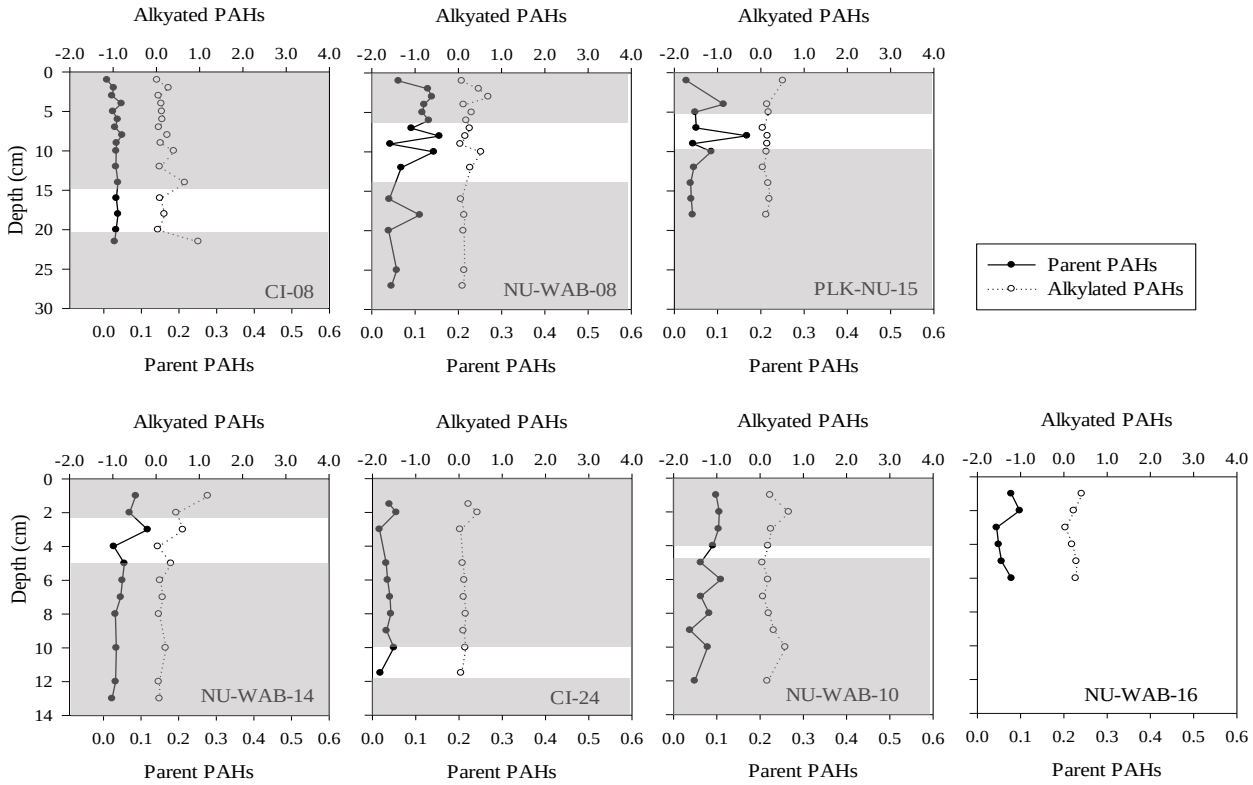

Figure 4.11: Profiles of mean (ng/g dw) of Parent PAH (solid line) and Alkylated PAH (dotted line). Lower and upper shaded portions represent sections of core with more than 90 % of sediments deposited in pre- and post-1900 respectively. The non-shaded portions reflect a mixture of sediments deposited during both time periods. Note variation in y- axis scale among the cores.

CHAPTER 5: DISCUSSION

5.1 Sedimentary Regime as Inferred from Organic Carbon Content, Radioisotope Profiles and Inventories and Sedimentation Rate

Although CI and WAB are situated along the northwest coast of Hudson Bay, there are significant differences in sedimentary regime between the two settings that place important controls on the nature of the HCs found in the sediments. Sediments from CI (CI-08 and CI-24) are coarse-grained and relatively low in TOC (0.75 %) compared to sediments from WAB (Figure 4.5). This set of properties fits well with the setting of CI, including it being a relatively shallow (typically <100 m deep), wave-exposed, tidally-driven inlet, open to Hudson Bay. It is likely that the strong tidal driven current within CI carries finer sediments and organic detritus seaward, leaving behind coarse-textured sediments of low TOC (Table 4.1). Based on the low ^{137}Cs-particle reactivity in seawater (Kuzyk, Gobeil, and Macdonald 2013), the paucity of ^{137}Cs in CI-08 may be an indication that the coastal sediments exhibit a net loss of ^{137}Cs initially deposited with particles (Su and Huh 2002). Furthermore, low atmospheric deposition of ^{137}Cs was previously reported at Saqvaqjuac ($\leq$ 6 dpm/cm^2) (Omelchenko, Lockhart, and Wilkinson 2005). However, the high sedimentation rates in the CI cores imply strong sediment supply to the coring sites, possibly from sediment resuspension along the numerous shoals and islands, and possibly from ice rafting.

WAB, on the other hand, is relatively deeper, protected, almost fjord-like, with a narrow channel separating it from Hudson Bay (Figure 5.1). As a result the sediments from WAB have a higher organic carbon content (>1.5 %) and are more fine grained (ϕ_{av} >0.7) than CI sediments (Table 4.1). There is, however, a lot of variation in properties among the WAB sampling sites including capture of ^{137}Cs, sedimentation rate and inventory of ^{210}Pb in sediments. The short core with incomplete radioisotope profiles (NU-WAB-16) was the most

easterly of the WAB cores (Figure 5.1) and was collected from a separate basin that lies closer to the fast-flowing channel that connects WAB to Hudson Bay. The core with the largest inventory of ^{137}Cs was PLK-NU-15, which was located close to shore between the Paliak Islands and the southern shoreline of WAB (Figure 5.1). Strong terrigenous sediment supply from coastal erosion presumably accounts for the large ^{137}Cs accumulation at this location. The WAB core with the largest inventory of ^{210}Pb (NU-WAB-08; Table 4.1) was located in the deepest part of the main basin close to the southern shoreline of the bay to the west of the Paliak Islands. The high ^{210}Pb inventories in NU-WAB-08 and PLK-NU-15 are probably an indication of sediment focusing (Eadie and Robbins 1987; Simcik et al. 1996). In lacustrine systems, the extent of particle focusing is typically estimated from the degree to which the ^{210}Pb inventory exceeds that expected from direct atmospheric deposition (cf., Muir et al. 2009). Considering that; (i) the average atmospherically-derived inventory of $^{210}Pb_{ex}$ in lake sediments in the Kivalliq region was 11.56 dpm/cm^2 (Omelchenko, Lockhart, and Wilkinson 2005), (ii) the average supply of $^{210}Pb_{ex}$ from the in situ decay of ^{226}Ra was 7.5 ± 1.1 dpm/cm^2 (Kuzyk, 2013), (iii) the range previously reported for Hudson Bay cores was 10-76.5 dpm/cm^2 (Kuzyk et al. 2009) and (iv) the range of observed $^{210}Pb_{ex}$ inventories in the WAB and CI cores was 10.75-33 dpm/cm^2, (Table 4.1), we assume that the ^{210}Pb inventory that may be attributed to direct atmospheric deposition in the WAB and CI cores is probably in the order of 10-15 dpm/cm^2. This implies that any ^{210}Pb inventory in the WAB cores in excess of 10-15 dpm/cm^2 is due to sediment focusing, from which we infer about three-fold focusing in PLK-NU-15 and four- or five-fold focusing in NU-WAB-08. There is no significant focusing at the sites of NU-WAB-10 and NU-WAB-14.

In contrast to WAB, the high ^{210}Pb inventories (three- to five-fold above the inventory arising from direct deposition; Table 4.1) in the CI cores may be attributed to particle scavenging of dissolved ^{210}Pb by, for example, settling marine particulate organic matter

(POM). Particle focusing processes are inconsistent with the relatively flat, gradually sloping bathymetry in CI. We speculate that the source of dissolved ^{210}Pb may be provided by upwelled marine waters.

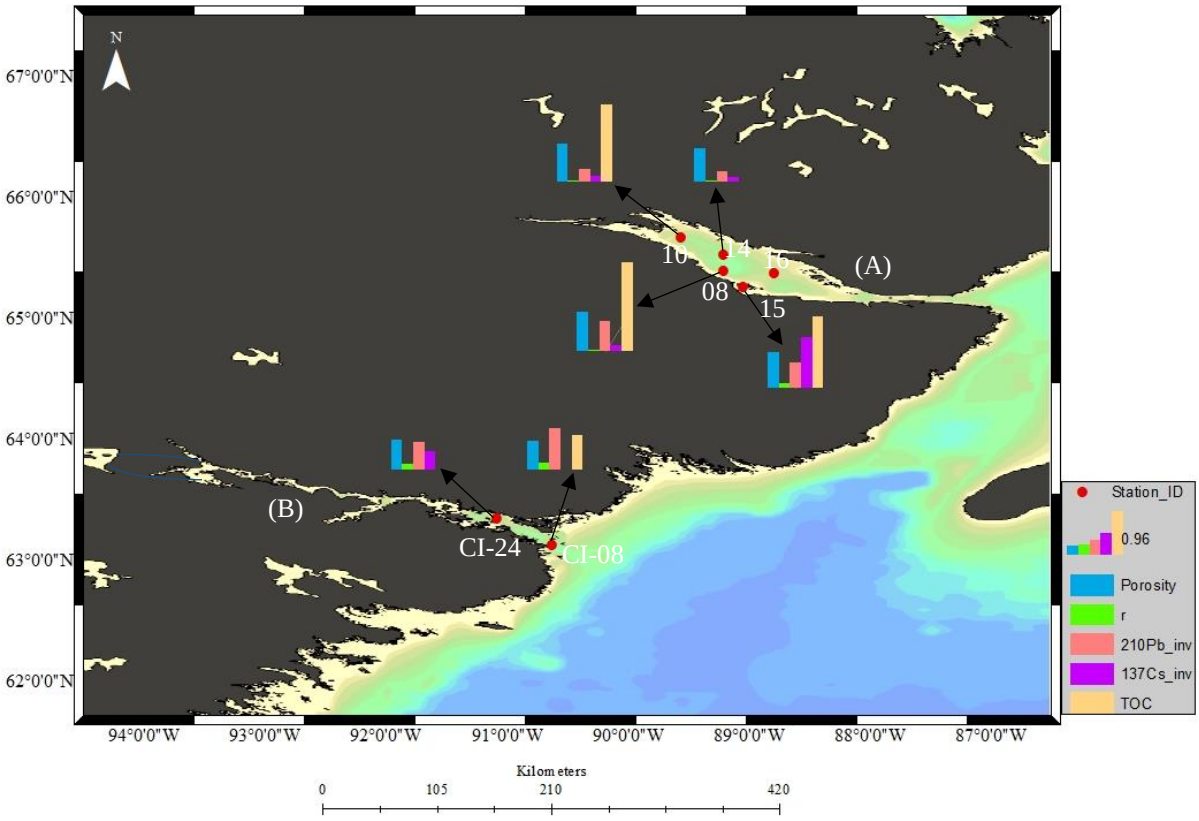

Figure 5.1: Relative porosity, sedimentation rate (r; g/cm^2/yr) inventory of ^{210}Pb$_{ex}$ (dpm/cm^2), inventory of ^{137}Cs (dpm/cm^2), and Organic Carbon Content (% TOC) within sampling stations across Wager Bay (A) and Chesterfield Inlet (B). Note, no inventories and rates are shown for core NU-WAB-16 because ^{137}Cs was not captured and its profile was incomplete.

5.2 Redox Conditions and Labile Carbon Oxidation Inferred from RSE

While TOC contents of sediments sometimes reflect the intensity of organic carbon supply, they are not always reliable indicators because the most labile fraction of the organic carbon may undergo remineralisation. The Al-normalised profiles of redox sensitive elements Mn, Fe, Mo and S (Figure 4.7) can be used to establish the position of redox boundaries within

the sediments and from the position of these boundaries, we can infer the relative intensity of the labile OC flux to the seafloor (Kuzyk et al. 2017).

The pronounced surface Mn enrichment and high Mn/Al ratio in NU-WAB-08, which implies a persistent surface oxic layer several centimetres thick, contrasts strongly with the constant low Mn/Al ratios in the remaining analyzed cores (CI-08, NU-WAB-10 and PLK-NU-15) and reducing conditions throughout. We interpret these differences as indicating lower labile OC fluxes at NU-WAB-08. Indeed, NU-WAB-08 sediments had the highest %TOC content and porosity, and also one of the highest inventories of $^{210}Pb_{ex}$. As proposed above in relation to ^{210}Pb inventories, the organic carbon supplied to the sediments may be associated primarily with focusing of fine-grained particles, winnowed from the surrounding shallows and slopes and delivered into the deepest part of the Bay (Bishop 1989). The most stable fractions reach the sediments at NU-WAB-08, as particle-associated organic carbon are transported to this deeper site. The vertical flux of (labile) marine POC derived from primary production is attenuated with depth (cf., Bishop 1989) and remineralisation can result in a down-core decrease in TOC in NU-WAB-08 (Figure 4.5).

In contrast, Mn is not enriched in surface sediments in the remaining cores, which implies absence of a surface oxic layer and the tendency for both S/Al and Fe/Al to increase with depth in all four cores and the accumulation of authigenic Mo in association with the Fe and S means that there are strong reducing and sulphidic conditions in the sediments. The TOC degradation process must be sufficiently fast to consume oxygen from the surface layers, maintaining reducing conditions throughout the sediment column. Low authigenic Mo inventory in NU-WAB-08 compared to CI-08 (Table 4.2), together with similar high ^{210}Pb inventories in these cores (Table 4.1), generally supports the inference above that stable TOC is supplied to the NU-WAB-08 core site primarily by focusing and labile TOC supplied to the CI-08 core site in association with a vertical marine POC flux.

5.3 n-alkane Sources Inferred from MDR and PCA

Long-chain n-alkanes (LCA: C_{23}-C_{36}), particularly odd numbered LCAs (n-C_{25}, n-C_{27}, n-C_{29}, and n-C_{31}) are present at notably high concentrations in the WAB and CI sediments compared to short-chain n-alkanes (SCA: C_{11}-C_{22}) (Figure 4.8, Figure 4.9). This implies that terrestrial organic carbon sources are dominant in the sediments and particularly at CI-24, NU-WAB-16, and PLK-NU-15, where mean LCA concentrations were greater than 7-fold higher than those of the mean SCA (Table 4.3).This outcome is not surprising considering the coastal setting of the cores. Possible sources of terrestrial OM to the coastal marine environment include river in-flows, coastal erosion, atmospheric deposition and ice transport (Kuzyk et al. 2009).

In addition to the variability noted above there is also a four-fold difference in the TAR index values among the cores (Table 5.1). This result suggests that that there are differences in the terrestrial and/or marine sources among the cores. The lowest TAR values occur in CI-08 and highest values in NU-WAB-16 followed by PLK-NU-15 and CI-24 (Table 5.1). While there is less than two-fold variation in CPI index values, CI-08 again has the lowest value (1.86). The diagnostic ratios thus imply lowest terrestrial source contributions and/or highest marine contributions in CI-08 and highest terrestrial source contributions and/or lowest marine contributions in the most eastern region of Wager Bay and closest proximity to shore. A limitation with ratios is that they may be affected by changes in the numerator or denominator, thus precluding specific assessment of what is causing the variability in TAR and CPI among the cores. The independent variation in concentrations of mean LCA and mean SCA in many sections of the cores (Figure 4.9) implies that both marine and terrestrial OM sources need to be considered in this case.

Table 5.1: Geometric mean (confidence limits) of Molecular Diagnostic Ratios (MDR) of n-alkanes

Station	CPI	TAR
CI-08	1.86 (1.63-2.11)	9.75 (5.43-17.46)
CI-24	2.00 (1.36-2.93)	18.88 (14.16-25.23)
NU-WAB-08	2.69 (2.20-3.29	10.74 (5.51-20.94)
NU-WAB-10	3.08 (2.79-3.40)	12.47 (5.92-26.24)
NU-WAB-14	2.59 (1.76-3.82)	17.66 (10.59-29.38)
NU-WAB-16	2.26 (2.00-2.57)	43.85 (13.09-146.89)
PLK-NU-15	2.83 (2.24-3.57)	24.43 (9.84-60.67)

The n-alkane data were further subjected to principal component analyses to explore the variability among the cores. Prior to the analyses, the data were concentration normalised to emphasise compositional differences among the cores. The overall variance was characterised by two principal components describing 66.9 % of the total variability of the dataset. The first principal component, which is largely made up of SCA (n-C_{12} to n-C16) and LCA (n-C_{22} to n-C_{32}) contributed 50.2 % of the total variability.

From the biplot in Figure 5.2a, it is clear that all the sediments plot over a wide span on PC1. There is a lot of variation in all the cores (except NU-WAB-16, PLK-NU-15 and CI-24 Figure 5.3) along that component. Almost two-thirds of the CI-08, NU-WAB-08, NU-WAB-10 and NU-WAB-14 core sections have low PC1 scores (< 0), while the other one-third appear to be on the high end of PC1 together with cores NU-WAB-16, PLK-NU-15 and CI-24 (Figure 5.2a). It can be inferred that compounds with strong positive PC1 loadings, contribute more strongly to the signatures of n-alkanes in most of the NU-WAB-16, PLK-NU-15 and CI-24 sediments and few sections of cores from CI-08 NU-WAB-08, NU-WAB-10 and NU-WAB-14 core sections. The greater contribution of the LCAs on PC1 to the total variance in the data set confirms that terrigenous organic carbon sources (vascular plants) are the dominant sources of OM to the sediments from primarily NU-WAB-16, PLK-NU-15 and CI-24. Whereas

sections of CI-08, NUU-WAB-8, NU-WAB-10 and NU-WAB-14 have SCAs components derived from marine OM sources.

The second principal component, which is influenced mainly by HMW fractions of SCA (n-C_{17} to n-C_{21}), accounted for 16.7 % of the data variability (Table 5.2, Figure 5.2). There is no significant difference among the stations on this PC (p= 0.79). PC2 appears to also reflect variations among core sections in the relative contribution of n-alkanes from marine organic carbon sources.

Table 5.2: Percent of Total Variance Explained and Component Loadings of Two Significant PCs with reference to Chain Lengths and Molecular Weights of n-alkanes (SCA = n-C_{11} to n-C_{22}; LCA n-C_{23} to n-C_{32})

n-alkanes	Molecular Weight (g/mol)	PC1 (50.2 %)	PC2 (16.7 %)
n-C_{12}	170	-0.789	0.381
n-C_{13}	184	-0.852	0.31
n-C_{14}	198	-0.646	0.245
n-C_{15}	212	-0.485	-0.116
n-C_{16}	226	-0.289	-0.127
n-C_{17}	240	-0.385	-0.592
n-C_{18}	254	-0.206	-0.852
n-C_{19}	268	0.286	-0.831
n-C_{20}	282	0.594	-0.611
n-C_{21}	296	0.568	-0.736
n-C_{22}	310	0.806	0.273
n-C_{23}	324	0.875	-0.217
n-C_{24}	338	0.912	0.091
n-C_{25}	352	0.884	0.194
n-C_{26}	366	0.882	0.274
n-C_{27}	380	0.78	0.273
n-C_{28}	394	0.878	0.324
n-C_{29}	408	0.85	-0.012
n-C_{30}	422	0.742	0.234
n-C_{31}	436	0.841	-0.029
n-C_{32}	450	0.578	0.145

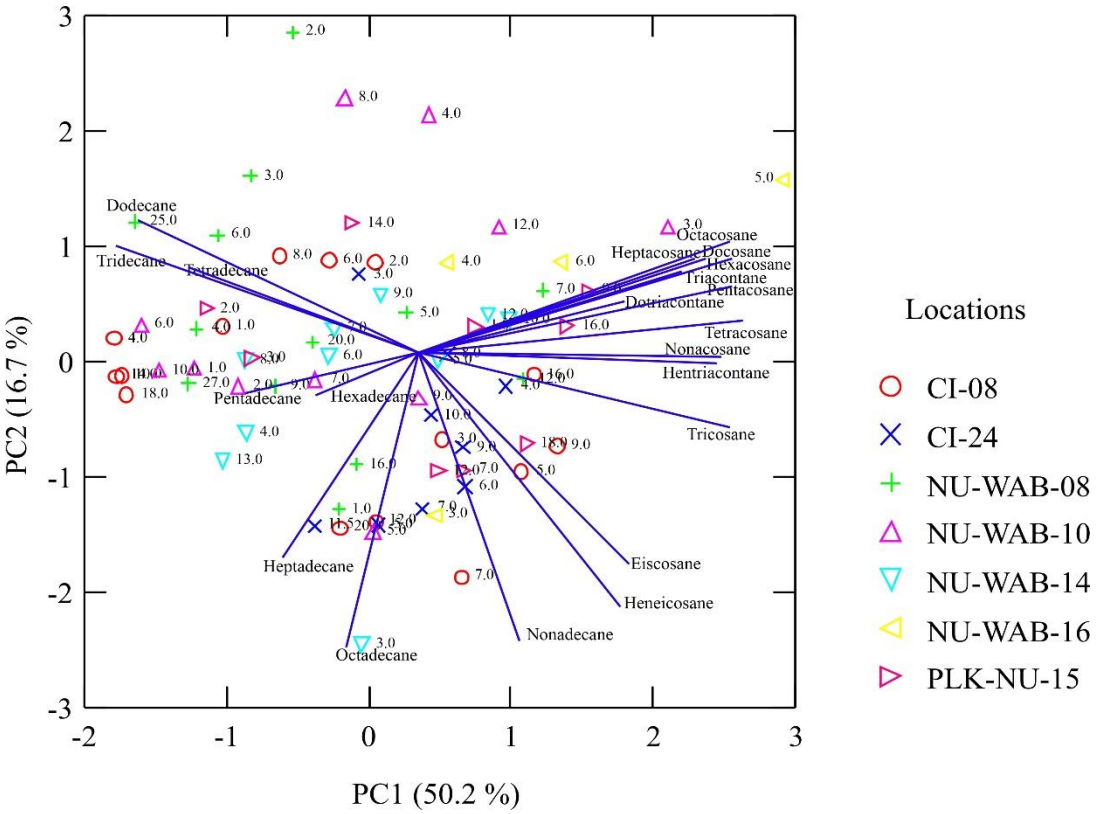

Figure 5.2: Principal Component Analysis of n-alkanes.

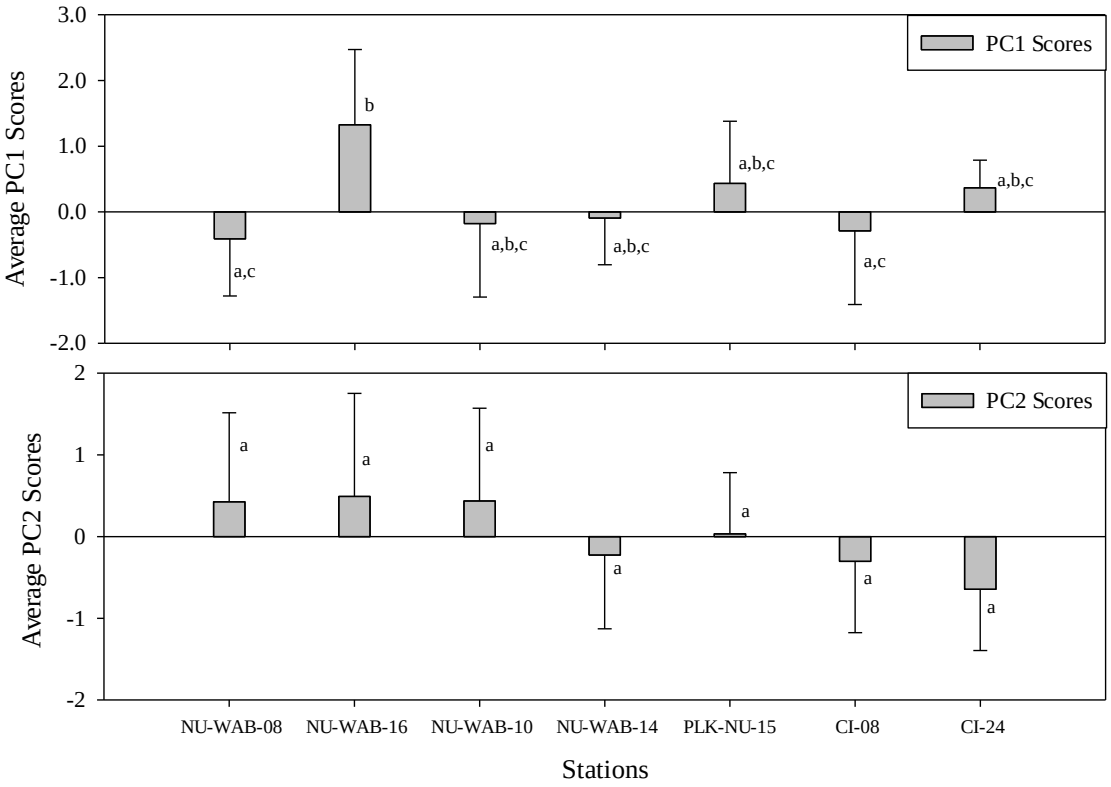

Figure 5.3: Mean ± SD of n-alkane PC scores. Letters (a,b and c) indicate significant difference in scores among the stations.

5.5 Sources of PAHs Inferred from MDR and PCA

Ratios of Fl/(Fl+Py), IP/(IP+Bghi) and BF/(BF+BePy) were used for source interpretation for PAH compounds consistent with previous studies (Yunker et al. 2002). Table 5.4 shows the mean (confidence intervals) of the ratios for all analysed cores. These ratios imply either pyrogenic or mixed (pyrogenic and petrogenic) sources in all cores (see Chapter 2 for details). At stations CI-08, CI-24, NU-WAB-10 and PLK-NU-15, ratios of IP/(IP+Bghi) and BF/(BF+BePy) suggest that combustion of liquid fossil fuel is the dominant source of PAHs. Averagely, petrogenic sources were implied by the Fl/(Fl+Py) index in all the cores except NU-WAB-10, where pyrogenic sources were obtained (Table 5.4). From Figure 5.4, it is seen that some sections of the cores have mixed petrogenic and biomass combustion sources. Stations NU-WAB-14, NU-WAB-16 and to some extent NU-WAB-08, have mixed pyrogenic and petrogenic sources throughout most of their sections according to all three indices (Figure 5.4). Profiles of MDRs of Fl/(Fl+Py), IP/(IP+Bghi) and BF/(BF+BePy) shown in Figure 5.5 indicate no downcore decrease with depth, i.e., no change in source within pre and post 1900 time frames. The only exception to this is the pre-1900 portions of the profile of Fl/(Fl+Py) in PLK-NU-15, in which there is a significant decrease in Fl/(Fl+Py) with depth ($r^2 = 0.6$, $p = 0.025$). The low (Fl/ (Fl+Py) ratio within PLK-NU-15 at depth below 10 cm (pre-1900) makes this core look more petrogenic within pre-1900 sediments. We note that limitations with these ratios is that combinations of two sources may produce ratios consistent with a third source, i.e, it is difficult to interpret sources affected by combination of sources.

Table 5.3: Geometric mean (confidence limits) of Molecular Diagnostic Ratios (MDR) of PAHs

Station	Fl/(Fl+Py)[a]	BF/(BF+BePy) [b]	IP/(IP+Bghi) [c]	Implied Sources ([a/ b/ c])
CI-08	0.39	0.63	0.47	Petrogenic / Pyrogenic / Pyrogenic
CI-24	0.37	0.64	0.52	Petrogenic/ Pyrogenic/ Pyrogenic
NU-WAB-08	0.37	0.65	0.44	Petrogenic/ Pyrogenic/ Pyrogenic
NU-WAB-10	0.46	0.65	0.48	Pyrogenic/ Pyrogenic/ Pyrogenic
NU-WAB-14	0.33	0.62	0.44	Petrogenic/ Pyrogenic/ Pyrogenic
NU-WAB-16	0.38	0.66	0.43	Petrogenic/ Pyrogenic/ Pyrogenic
PLK-NU-15	0.37	0.62	0.42	Petrogenic/ Pyrogenic/ Pyrogenic

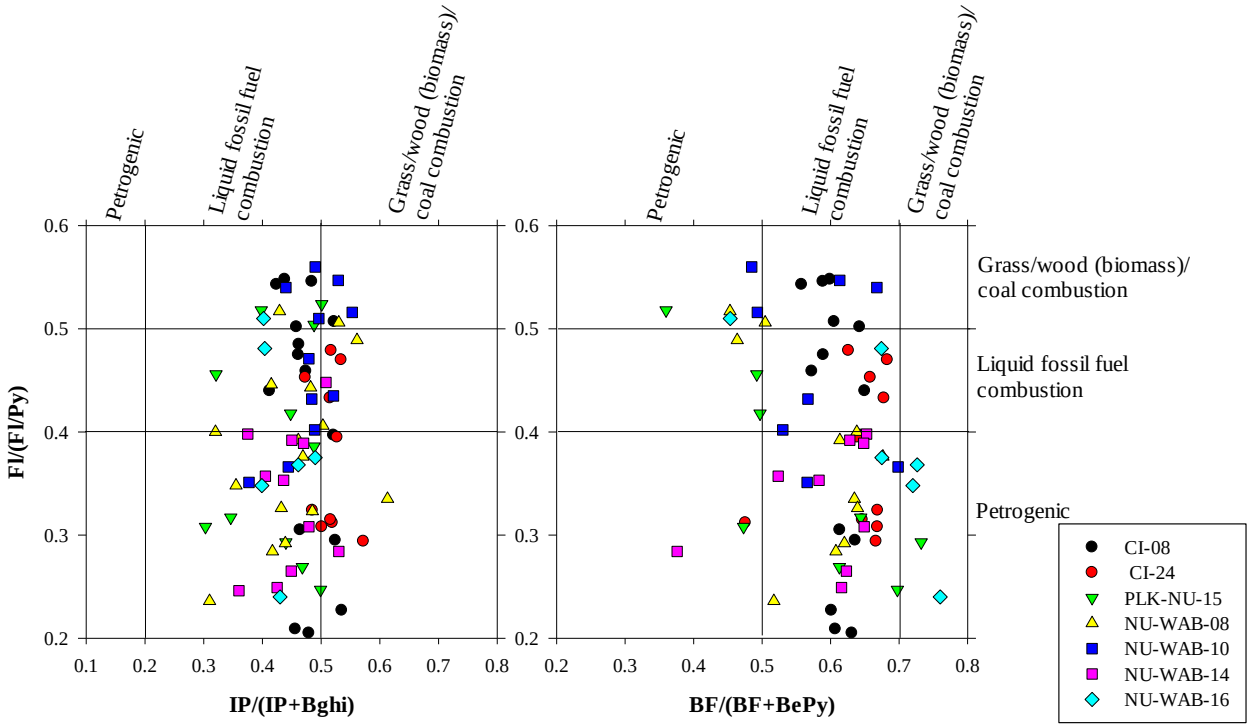

Figure 5.4: PAH cross plots for the ratios of IP/(IP+Bghi) and BF/(BF+BePy) versus Fl/(Fl+Py) in individual core sections.

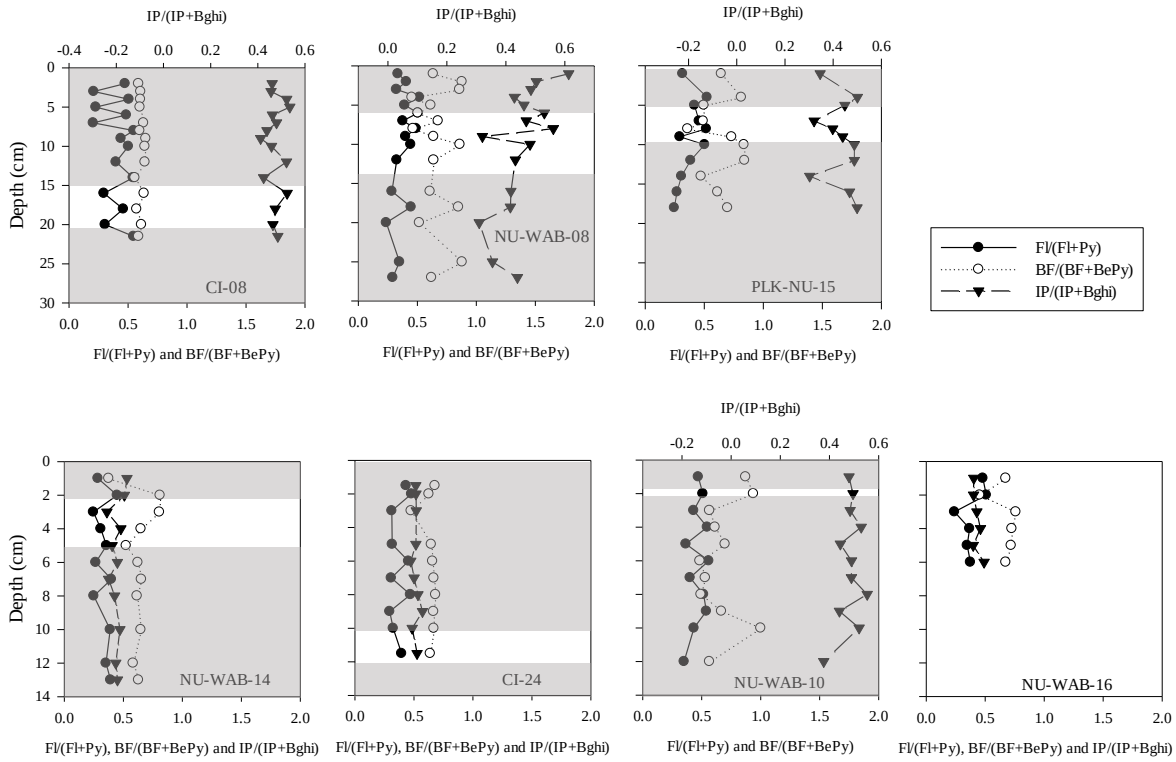

Figure 5.5: Profile of MDRs of Fl/(Fl+Py) (solid lines), IP/(IP+Bghi) (dashed lines) and BF/(BF+BePy) (dotted lines). Lower and upper shaded portions represent sections of core with more than 90 % of sediments deposited pre- and post-1900, respectively. The non-shaded portions reflect a mixture of sediments deposited during both time periods. Note variation in x- and y-axes scales among the cores.

PCA was carried out on the PAH data set to distinguish between petrogenic and pyrogenic sources. Note that data were concentration-normalised to emphasise compositional differences. Excluded from the PCA data set are Na and alkylated Na compounds (N1, N2) because they were only detected in a few core sections. Perylene was included in the data set as its profile does not increase with depth in the cores, which we take as evidence that it is not primarily produced from organic matter but rather supplied with other PAHs to the core sites. The absence of apparent perylene accumulation down core has been used as justification for including perylene in PCAs previously (Bakhtiari et al. 2009).

The overall PAH variance was characterised by three principal components describing 57 % of the total variability of the dataset. The first principal component, highly influenced by HMW PAHs (Ch, BF, DA, IP, Bghi) as well as LMW PAHs (P1, P2, F1, Aen, Ayl, Py, F1 and

F) contributed 30 % to the total variability of the data set (Table 5.5). From the biplot in Figure 5.6a, it is clear that CI-08 sediments plot over a wide span on PC1. Although the average PC1 score for CI-08 sediments is lower than the scores for almost all other cores (NU-WAB-10 excepted; Figure 5.7), there is a lot of variation in CI-08 along that component. Almost half (nine) of the CI-08 core sections have low PC1 scores (-1 or lower), while the other half appear to be on the high end of PC1 together with the CI-24 and WAB cores (Figure 5.6a). Aside from the CI-08 samples, only a few sediment sections from NU-WAB-10 and PLK-NU-15 have similarly negative PC1 scores. It can be inferred that compounds with strong positive PC1 loadings contribute more strongly to the composition of PAHs in most of the WAB and CI-24 sediments and half of CI-08 core sections. Indeed, a cluster of core sections is seen on the right side of Figure 5.6a (circled), and these samples are dominated by HMW pyrogenic PAHs (Ch, IP, Bghi, DA, and BF). These HMW compounds are likely derived from long-range atmospheric transport (Welch et al. 1991; Hung et al. 2005). In contrast, the low PC1 scores observed for some CI-08 core sections are driven by LMW pyrogenic and petrogenic PAHs (Ayl, Aen, F, P1 and P2), which have strong negative loadings on PC1 (Table 5.5). In Figure 5.8, it can be seen that about half of the CI-08 sediments have a greater fractional contribution of LMW pyrogenic and petrogenic PAHs (Ayl, Aen, F, P1 and P2) compared to the WAB sediments. In a sense, the capture of the LMW pyrogenic PPAHs (Ayl, Aen, F) within CI-08 shows fluctuations in input, alternating between high and low inputs, from one slice to the next, implying considerable temporal variability in the pyrogenic source inputs (Figure 5.8). These LMW pyrogenic compounds in CI-08 are likely derived from local sources because these types of compounds are easily depleted during atmospheric transport and thus do not survive transport in the atmosphere over long distances (Welch et al. 1991; Hung et al. 2005). CI-08 is located 7 km southeast of the community of Chesterfield Inlet whereas CI-24 is located approximately 46 km northwest of the community and the WAB cores are all located >100 km

from the nearest community (Naujaat). Therefore, it makes sense that the composition of the PAHs in nearly half of CI-08 is dominated by LMW pyrogenic and petrogenic compounds likely derived from local inputs.

The second and third PCs collectively contribute 27 % to the overall data variability. The second principal component (16%) has strong positive and negative influences from LMW pyrogenic compounds Ayl and Aen, Fl, Py, and Pn, (Figure 5.6, Table 5.5), signifying short range atmospheric PAH inputs. Nearly half of CI-08 sediments have significantly lower PC2 scores while the other half fall into the mid score band. On the average, core section sediments from both CI-08 and CI-24 score lower on PC2 than the WAB sediments and are significantly different from the WAB cores (r^2 = 0.6, $p < 0.001$) (Figure 5.6a, Figure 5.7). A possible explanation for the CI cores being different from the WAB cores is that the CI sediments (both 7 km and 46 km from the community) receive intermittent inputs of these LMW pyrogenic PAHs (Figure 5.8) from local sources such as the community's diesel generator or ship traffic en route to Baker Lake.

The third principal component (11 %) is influenced negatively influenced by the HMW pyrogenic compound, Per, and the intermediate molecular weight compound, petrogenic F1. BaA has a strong positive influence on this PC. From Figure 5.6b and 5.7, it can be seen that many of the sections from the WAB cores have low PC3 scores compared to CI cores. Considering the low fractional contribution of the PC3 factor loading compounds, Per is the only compound that has a significant contribution in both WAB and CI (Figure 5.8). Having established that Per is a HMW compound likely derived from combustion and not diagenesis, one can infer that this compound provides evidence that long-range atmospheric pyrogenic input is also an important contributor to PAH in CI and WAB (Figure 5.7).

Table 5.4: Percent of Total Variance Explained, Component Loadings of Two Significant PCs and Molecular Weights of PAHs

PAHs	Molecular Weight (g/mol)	Number of Rings	PC1 (30%)	PC2 (16 %)	PC3 (11 %)
IP	276	6	0.706	0.416	0.199
F	166	3	-0.667	0.136	0.311
Bghi	276	5	0.665	0.355	-0.044
BF	252	5	0.663	0.056	0.182
Fl	202	4	0.639	-0.556	0.032
DA	278	5	0.615	0.11	0.292
Ch	228	4	0.61	0.405	-0.256
Py	202	4	0.596	-0.581	-0.103
Ayl	152	3	-0.591	0.542	0.195
Aen	154	3	-0.57	0.524	0.218
F1	216	4	0.557	0.099	-0.566
P2	206	3	-0.541	-0.378	-0.463
P1	192	3	-0.499	-0.459	-0.466
BaA	228	6	0.47	-0.235	0.588
Per	252	5	0.444	0.434	-0.526
BePy	252	5	0.166	-0.279	0.154
Pn	178	3	-0.028	-0.55	0.277
BaPy	252	5	0.023	-0.43	0.189

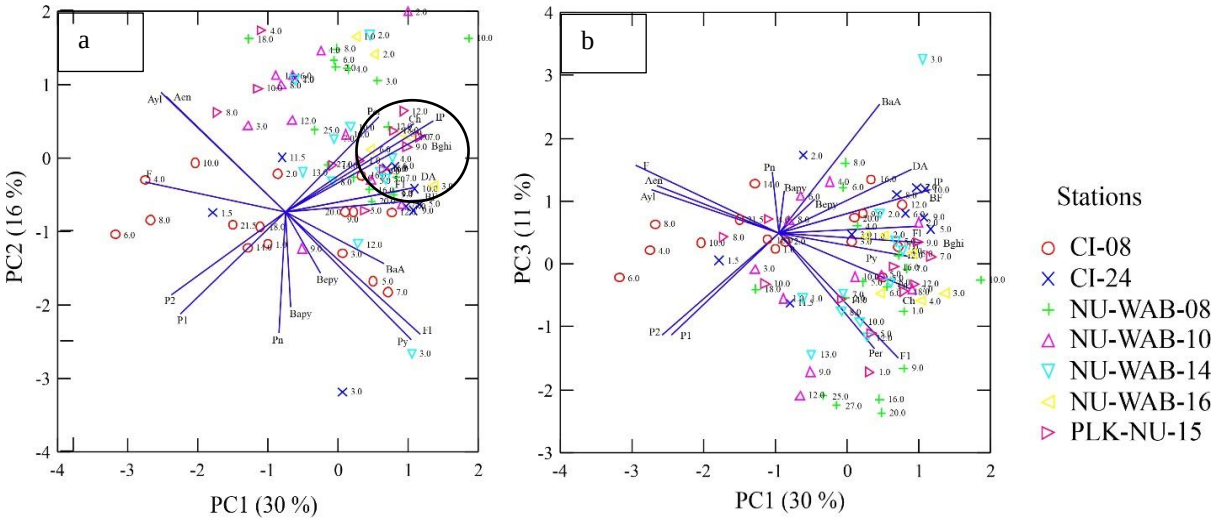

Figure 5.6: Principal components analysis (PCA) of PAHs. Note biplot represent the different core depths and compounds that drive variation among cores. PC1 cluster is highlighted with a black circle.

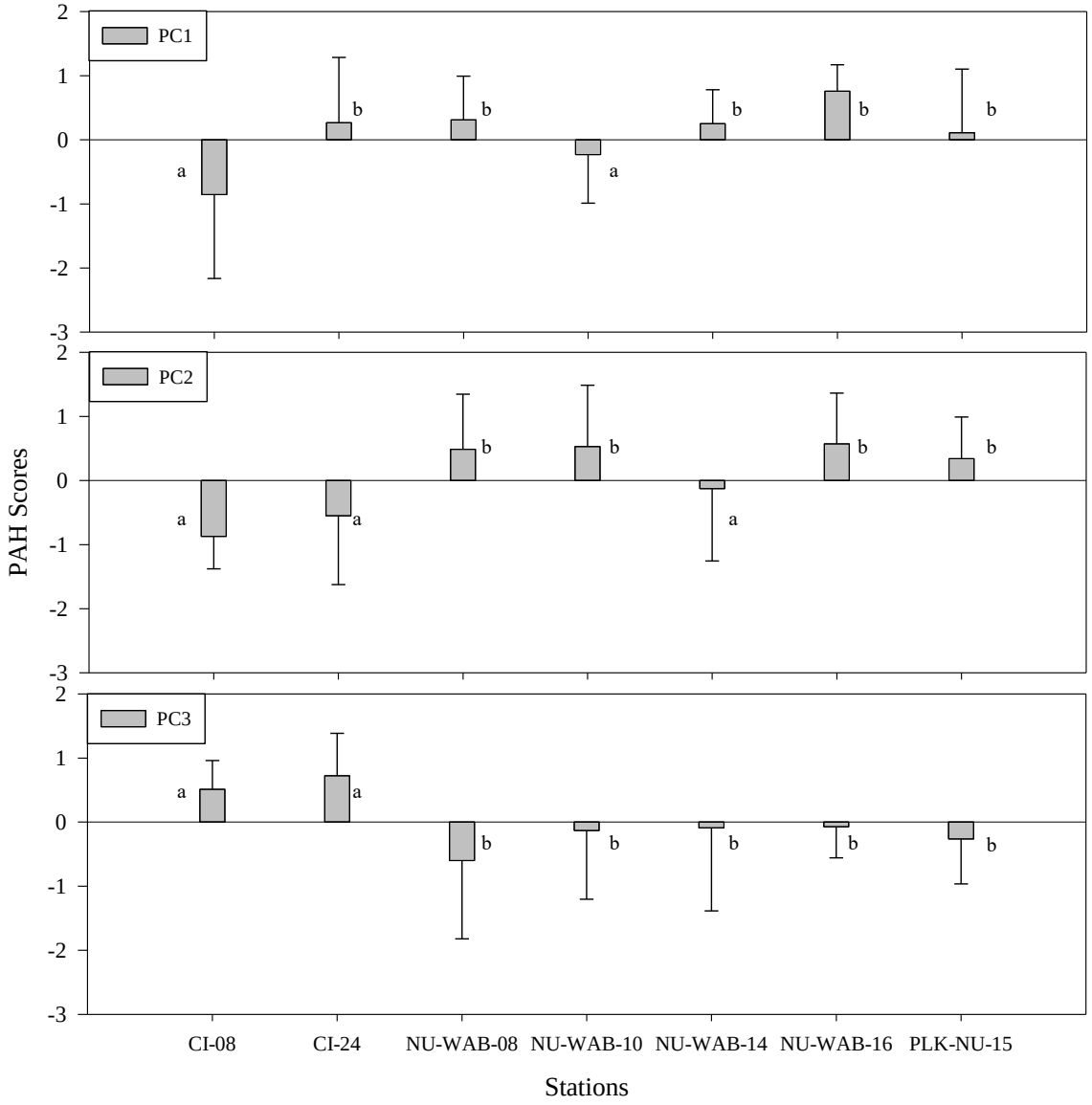

Figure 5.7: Mean ± SD of PAH PC scores. Letters (a and b) represent significant differences among stations.

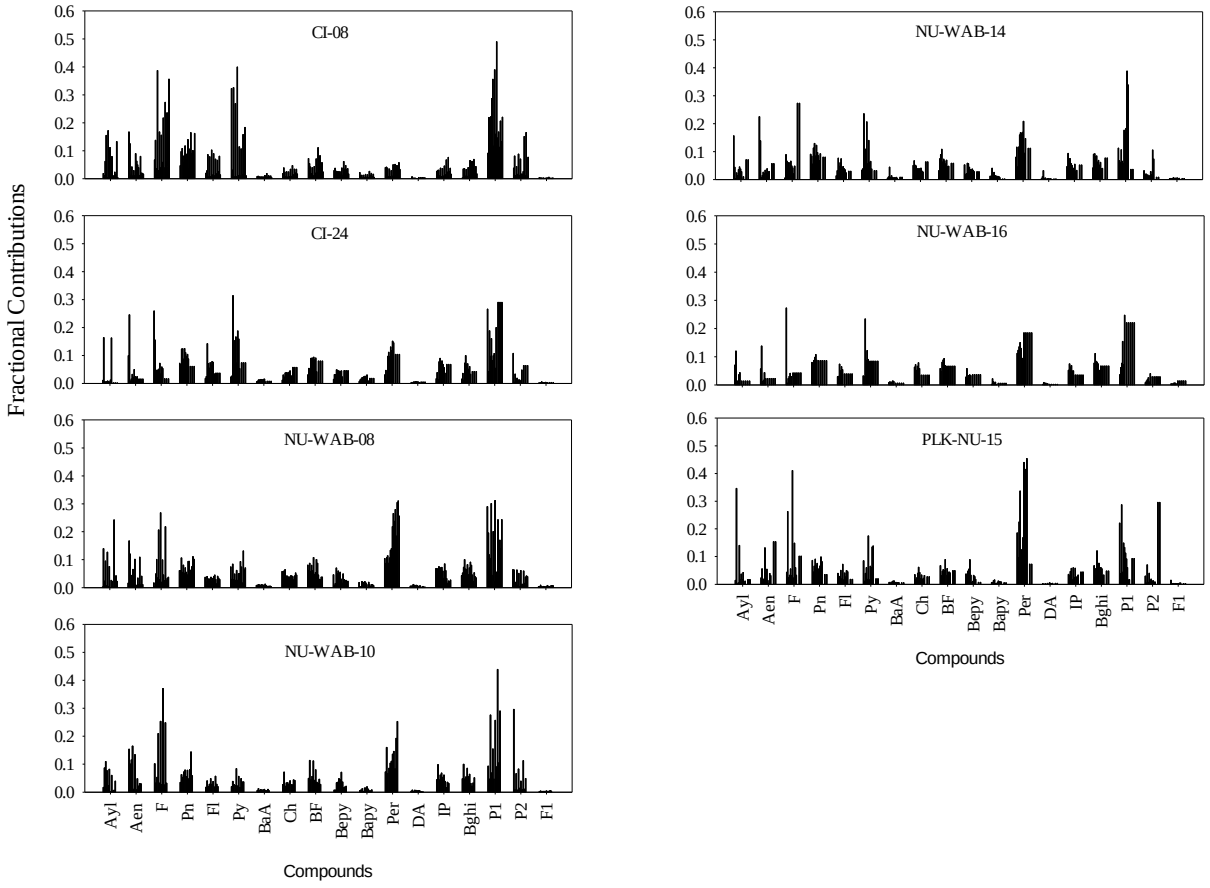

Figure 5.8: Fractional contributions of PAHs within the sections of the seven analysed cores.

5.6 Inferred Origin of Pyrogenic Compounds

Welch et al. (1991) determined regional and local sources of PAHs in brown snow and lake sediment samples collected from the vicinity of Chesterfield Inlet. The elevated presence of HMW PPAH such as IP, Bghi and BF in these samples was attributed to Asian sources influencing northern Canadian coastal area *via* long-range atmospheric transport. LMW PPAHs are typically depleted when transported over long distances. High concentrations of certain LMW PPAHs such as Pn in the lake and snow samples were attributed to local sources (Figure 5.9).

In the present study, the relative proportions of PPAHs, both LMW and HMW, in surficial sediments (1-2 cm) from WAB and CI are similar to those found in lake sediments

and brown snow samples by Welch et al. (1991) (Figure 5.9). Exceptions to this are the higher relative proportions of LMW PPAH compounds such as Aen and F (particularly in CI cores) (Figure 5.9). As noted by Welch et al. (1991), presence of both LMW and HMW compounds in environmental are indicative of both long distance and localised sources of these compounds. Long distance atmospheric transport of pyrogenic PPAH compounds is ubiquitous in the Canadian Arctic as indicated, for example, by their regular detection at air monitoring stations at Alert (Wang et al. 2010). PPAH compounds undergoing short-range atmospheric transport may have been derived from pyrolysis of fuel in the communities of Chesterfield Inlet and Naujaat and from local ship traffic (exhaust).

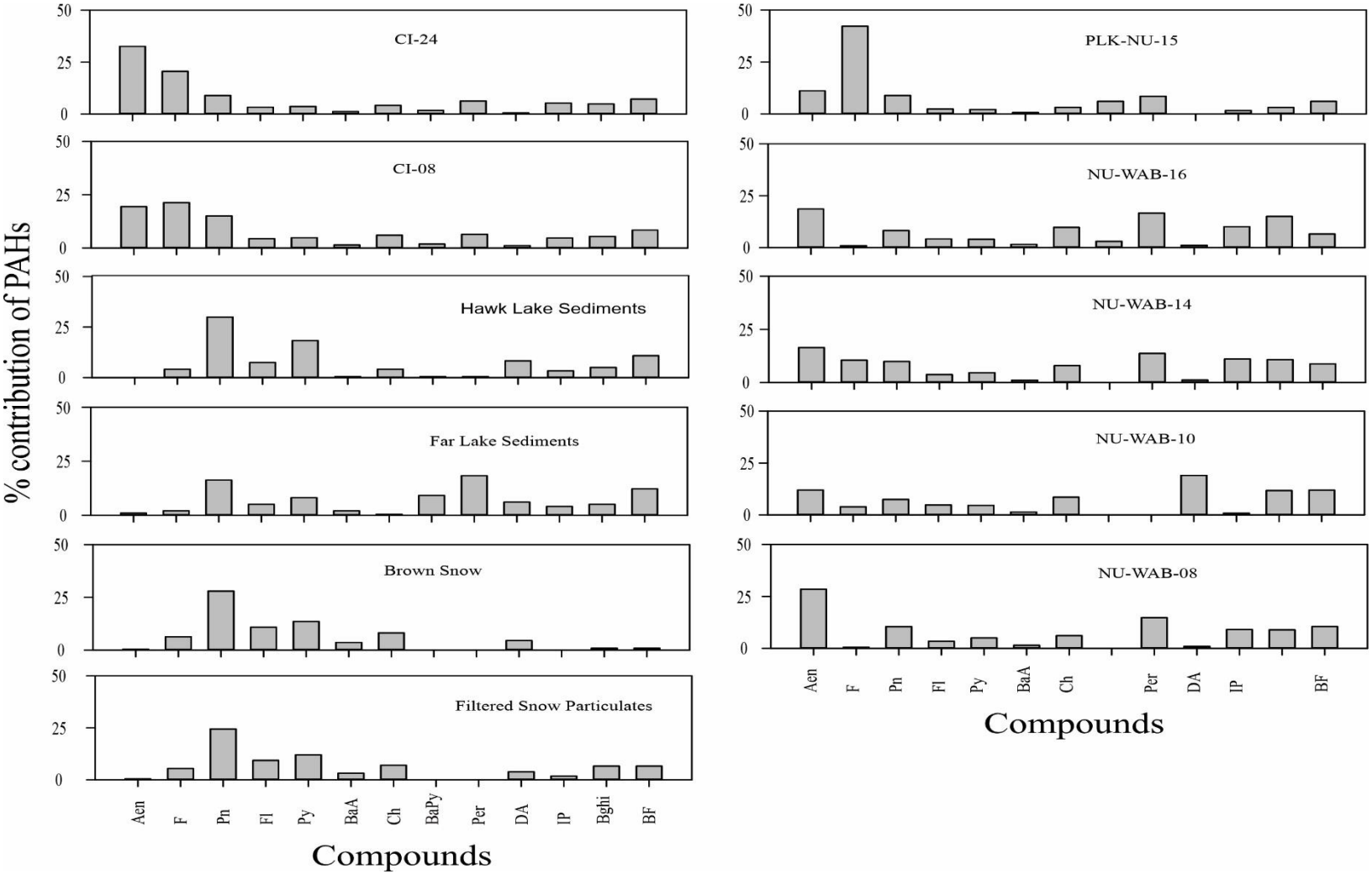

Figure 5.9: Percent contribution of PAHs in surface sediment (1-2 cm) in Chesterfield Inlet and Wager Bay in comparison with brown snow particles (two samples) and surficial lake sediments (0-1.25 cm) from two lakes (Far Lake, Hawk Lake) in the Saqvaqjuac area near Chesterfield Inlet (Welch et al. 1991).

5.7 Pre and post depositional processes that drive sediments in Chesterfield Inlet and Wager Bay

Based on the differences in grain sizes (inferred from porosity), ^{137}Cs profiles, sedimentation rates and ^{210}Pb inventories within WAB (Table 4.1), from which we interpret that focusing is an important process (Eadie and Robbins 1987; Simcik et al. 1996), it is likely that deeper locations within WAB provide a setting for preferential settling and accumulation of pyrogenic PPAHs and terrestrial LCAs on the seafloor.

Post-1900 inventories were used to infer controls on pyrogenic PPAHs and terrestrial LCAs because they may be compared across all cores, regardless of sedimentation rate or the length of the recovered core. A Plot of post-1900 PPAH inventories versus ^{210}Pb inventories is shown in Figure 5.10. The strong correlation implies that variation in ^{210}Pb inventories explains 92 % of the variance in PPAH inventories. The good correlation between post-1900 ^{210}Pb inventories and post-1900 PPAHs inventories in the WAB cores is consistent with delivery of PPAHs with particles focusing into the deeper sites in NU-WAB-08. In CI, the much higher inventories of both ^{210}Pb and PPAHs could be attributed to the rapid direct settling of atmospherically deived compounds (^{210}Pb and PPAHs) to the seabed in this, shallow tidal driven coastal setting.

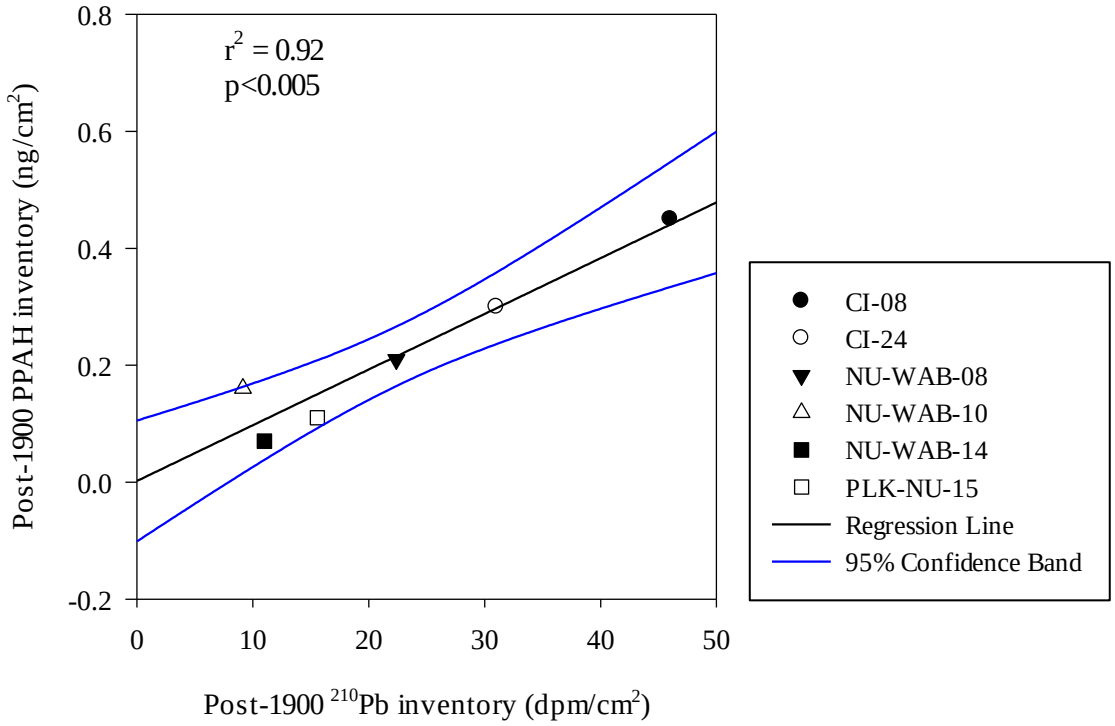

Figure 5.10: Correlation between post-1900 PPAH (ng/cm^2) and ^{210}Pb inventories (dpm/cm^2).

Figure 5.11 is a conceptual map depicting the cycling and focusing of post-1900 HC (PPAHs and LCA) sediments into WAB. High HCs inventories recorded at NU-WAB-08 relative to other WAB sites are interpreted as focusing into the deepest part of the bay (Eadie and Robbins 1987; Simcik et al. 1996).Variations in the inventories of the two other WAB cores (NU-WAB-10 and NU-WAB-14) likely implies that the hydrocarbon concentrations in these shallow depths are affected and reworked as sediments are being transported into deeper depths. The high inventory of ^{137}Cs obtained at PLK-NU-15 is to be expected as this core was sampled close to Paliak Island and receives inputs from coastal sources. In CI, however, higher inventories recorded at CI-08 compared to CI-24 depict scavenging of HC sorbed sediments, and direct delivery to the seafloor with settling particles.

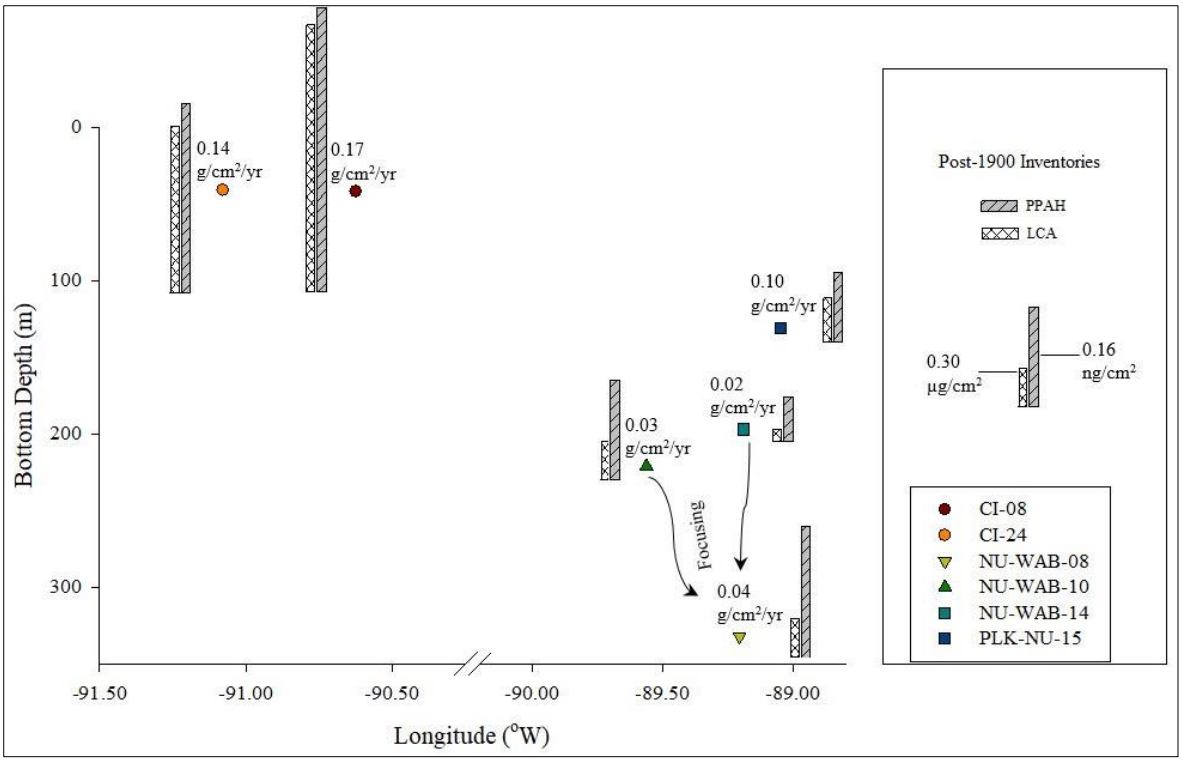

Figure 5.11: Conceptual sketch illustrating the scavenging and focusing of TOC associated pyrogenic PAHs and LCA n-alkanes in post-1900 sediments at Chesterfield Inlet and Wager Bay.

From Figure 4.5, post depositional degradation of OC with depth was identified in TOC profiles and this process is well explained with profiles of RSE. However, no degradational trend was observed in HC profiles in Figure 4.7. The profiles of n-alkanes particularly SCA, although susceptible to degradation, show no significant down-core decrease with depth (Figure 4.9). Similarly, parent and alkylated PAHs also do not decrease with depth (Figure 4.11).

CHAPTER 6: CONCLUSION

Sediment cores from Chesterfield Inlet and Wager Bay were analysed to provide initial baseline data against which future spills can be evaluated and to explore geochemical factors causing variation in baseline concentrations and composition. It was expected that different hydrocarbon source signatures would be present in Chesterfield Inlet and Wager Bay sediments due to their differing degrees of human activity (community and ship traffic servicing Baker Lake at the former, protected National Park area at the latter). In this study we determined that the core (CI-08) closest to the community of Chesterfield Inlet is influenced in a subtle manner (i.e. in composition but not in concentration) by pyrogenic and petrogenic PAHs likely from local sources. The other CI core (CI-24) and all the WAB cores are influenced mostly by HMW pyrogenic PAHs likely derived from distant sources and delivered to the northern coastal area by long-range atmospheric transport (Welch et al. 1991; Hung et al. 2005). Dominance of pyrogenic sources within the sediments from Chesterfield Inlet and Wager Bay is consistent with findings for very remote and pristine Arctic areas such as the Central Canadian Arctic Ocean (Ma et al. 2017). The presence of both LMW and HMW pyrogenic PAHs signifies that pyrogenic PAHs probably have been atmospherically transported from both local and long distance sources. n-alkanes sources in surface sediments in all the cores are from both terrestrial and marine sources. Although degradation processes in the sediments are apparent in TOC profiles, no degradational pattern or change in source is seen in the pre and post-1900 PAH and n-alkanes profiles.

Physical and geochemicals factors affect the baseline PAH composition, concentration and accumulation rates (modern inventories) within the study areas. The TOC-rich sediments from deep sites in Wager Bay contain the highest concentrations of pyrogenic PAHs, while the more coarse-textured, TOC-poor sediment (CI-08) in shallow Chesterfield Inlet contains the lowest concentrations. Rates of accumulation of PAHs in sediments (inventories) do not follow

the same pattern as concentrations in the study area. In CI, higher post-1900 ^{210}Pb inventories and post-1900 pyrogenic PPAHs inventories were recorded than in WAB because of higher sediment accumulation rates. Among the WAB sites, highest inventories were recorded in the deepest site due to focusing. A good correlation was found between post-1900 ^{210}Pb inventories and post-1900 PPAHs inventories, which supports these inferences.

To improve our understanding of the extent and causes of variability in baseline PAH concentrations across Arctic shelves and our ability to predict pre-spill baselines in unsampled areas, there is a need to conduct similar studies in other areas including those lacking seeps, coal beds and other local petrogenic sources. These studies could be used to test the hypothesis emerging from the present work that vertical particle fluxes, for which ^{210}Pb inventories provide a proxy, control the accumulation of PAHs from pyrogenic sources in Arctic sediments. If Arctic shelves become more productive as the ice season is reduced during coming decades, it may be expected that fluxes of pyrogenic PAHs to sediments will increase, regardless of any shipping activity and spills.

CHAPTER 7: REFERENCES

Abdel-Shafy, Hussein I., and Mona S.M. Mansour. 2016. "A Review on Polycyclic Aromatic Hydrocarbons: Source, Environmental Impact, Effect on Human Health and Remediation." *Egyptian Journal of Petroleum* 25 (1). Egyptian Petroleum Research Institute: 107–23. doi:10.1016/j.ejpe.2015.03.011.

AMAP. 1998. "Arctic Monitoring and Assessment Program Report: Arctic Pollution Issues. Chapter 7, Heavy Metals." In *AMAP Assessment Report: Arctic Pollution Issues*, 373–453. http://www.grida.no/amap.

AMAP. 2010. "Sources, Inputs and Concentrations of Petroleum Hydrocarbons, Polycyclic Aromatic Hydrocarbons, and Other Contaminants Related to Oil and Gas Activities in the Arctic." In *AMAP Assessment 2007: Oil and Gas Activities in the Artic - Effects and Potential Effects Volume Twov*, 4_1-4_85. Oslo, Norway: Arctic Monitoring and Assessment Programme (AMAP).

Andrews, Jonathan, Babb. Dave, M. McKernan, B. Horton, and Barber David. 2016. "Climate Change in the Hudson Bay Complex : Opportunities and Vulnerabilities for the Port of Churchill's Marine Operations." *The Centre for Earth Observation Science (CEOS)*, 1–130. doi:10.5203/lwbin.ceos.2016.1.

Bailey, Joscelyn N.-L., Robie W. Macdonald, Hamed Sanei, Peter M. Outridge, Sophia C. Johannessen, Klaus Hochheim, David Barber, and Gary A. Stern. 2013. "Change at the Margin of the North Water Polynya, Baffin Bay, Inferred from Organic Matter Records in Dated Sediment Cores." *Marine Geology* 341 (July): 1–13. doi:10.1016/j.margeo.2013.04.017.

Bakhtiari, Alireza Riyahi, Mohamad Pauzi Zakaria, Mohammad Ismail Yaziz, Mohamad Nordin Hj Lajis, Xinhui Bi, and Mohamad Che Abd Rahim. 2009. "Vertical Distribution

and Source Identification of Polycyclic Aromatic Hydrocarbons in Anoxic Sediment Cores of Chini Lake, Malaysia: Perylene as Indicator of Land Plant-Derived Hydrocarbons." *Applied Geochemistry* 24 (9). Elsevier Ltd: 1777–87. doi:10.1016/j.apgeochem.2009.05.008.

Barber, David, Dave Babb, and Jonathan Andrews. 2015. "From Science to Policy: Climate Related Vulnerabilities and Opportunities for Marine Transportation through Hudson Bay and the Port of Churchill." *CEOS - University of Manitoba, Warming of the North Conference*. www.umanitoba.ca/ceos.

Baskaran, Mark, Joe Nix, Clark Kuyper, and N. Karunakara. 2014. "Problems with the Dating of Sediment Core Using Excess 210Pb in a Freshwater System Impacted by Large Scale Watershed Changes." *Journal of Environmental Radioactivity* 138 (December). Elsevier Ltd: 355–63. doi:10.1016/j.jenvrad.2014.07.006.

Baumard, P., H. Budzinski, Q. Michon, P. Garrigues, T. Burgeot, and J. Bellocq. 1998. "Origin and Bioavailability of PAHs in the Mediterranean Sea from Mussel and Sediment Records." *Estuarine, Coastal and Shelf Science* 47 (1): 77–90. doi:10.1006/ecss.1998.0337.

Becker, Sara, Crispin J. Halsall, Wlodek Tych, Hayley Hung, Susie Attewell, Pierrette Blanchard, Henrik Li, et al. 2006. "Resolving the Long-Term Trends of Polycyclic Aromatic Hydrocarbons in the Canadian Arctic Atmosphere." *Environmental Science and Technology* 40 (10): 3217–22. doi:10.1021/es052346l.

Bennett, R., D .C Campbell, and M. F. A. Furze. 2013. "The Shallow Stratigraphy and Geohazards of the Northern Baffin Island Shelf: Studies to 2012." Vol. 62. doi:10.4095/292614.

Bischoff, J., R. B. Sparkes, A. D. Selver, R. G. M. Spencer, O. Gustafsson, I. P. Semiletov, O. V. Dudarev, et al. 2016. "Source, Transport and Fate of Soil Organic Matter Inferred

from Microbial Biomarker Lipids on the East Siberian Arctic Shelf." *Biogeosciences* 13 (17): 4899–4914. doi:10.5194/bg-13-4899-2016.

Bishop, J.K.B. 1989. "Regional Extremes in Particulate Matter Composition and Flux: Effects on the Chemistry of the Ocean Interior." In *Productivity of the Ocean: Present and Past.*, edited by G W.H., Smetacek, V.S., Wefer, 117–37. Dahlem: J. Wiley & Sons Limited.

Boitsov, Stepan, H. K B Jensen, and Jarle Klungsøyr. 2009. "Natural Background and Anthropogenic Inputs of Polycyclic Aromatic Hydrocarbons (PAH) in Sediments of South-Western Barents Sea." *Marine Environmental Research* 68 (5): 236–45. doi:10.1016/j.marenvres.2009.06.013.

Bourbonniere, R., and P. Meyers. 1996. "Sedimentary Geolipid Records of Historical Changes in the Watersheds and Productivities of Lakes Ontario and Erie." *Limnology and Oceanography* 41 (2): 352–59. doi:10.4319/lo.1996.41.2.0352.

Brandvik, P. J., and F. Leirvik. 2008. "Weathering Properties of the Trestakk Oil." In *Climate Change 2013 - The Physical Science Basis*, edited by Intergovernmental Panel on Climate Change, 63. Cambridge: Cambridge University Press. doi:10.1017/CBO9781107415324.004.

Bridges, Todd S, and Karl Gustavson. 2014. *Processes, Assessment and Remediation of Contaminated Sediments*. Edited by Danny D. Reible. *Environmental Sciences*. Vol. 6. SERDP/ESTCP Environmental Remediation Technology. New York, NY: Springer New York. doi:10.1007/978-1-4614-6726-7.

Budgell, W.P., and B.M. Flemming. 1982. "Chesterfield Inlet Oceanographic Data Report" II (83).

Budzinski, H., I. Jones, J. Bellocq, C. Piérard, and P. Garrigues. 1997. "Evaluation of Sediment Contamination by Polycyclic Aromatic Hydrocarbons in the Gironde

Estuary." *Marine Chemistry* 58 (1–2): 85–97. doi:10.1016/S0304-4203(97)00028-5.

Canfield, Donald E, Erik Kristensen, and Bo Thamdrup. 2005. "The Oxygen Cycle." In *Aquatic Geomicrobiology*, Volume 48:167–204. doi:http://dx.doi.org/10.1016/S0065-2881(05)48006-2.

CCME. 2012. "Canadian Sediment Quality Guidelines for the Protection of Aquatic Life: Summary Tables." *Canadian Council of Ministers of the Environment*, 5.

Corcoran, K. M., and R. J. Kelley. 2006. "Sediment-Tracing Technology : An Overview."

Curtosi, Antonio, Emilien Pelletier, Cristian L. Vodopivez, and Walter P. Mac Cormack. 2007. "Polycyclic Aromatic Hydrocarbons in Soil and Surface Marine Sediment near Jubany Station (Antarctica). Role of Permafrost as a Low-Permeability Barrier." *Science of the Total Environment* 383 (1–3): 193–204. doi:10.1016/j.scitotenv.2007.04.025.

Drexler, Judith Z., Christopher C. Fuller, and Stacey Archfield. 2018. "The Approaching Obsolescence Of137Cs Dating of Wetland Soils in North America." *Quaternary Science Reviews* 199: 83–96. doi:10.1016/j.quascirev.2018.08.028.

Dufresne, Michael, Robert Sim, and Bruce Davis. 2013. "Technical Report And Resource Update For The Angilak Property, Kivalliq Region, Nunavut, Canada."

Duran, Robert, and Cristiana Cravo-Laureau. 2016. "Role of Environmental Factors and Microorganisms in Determining the Fate of Polycyclic Aromatic Hydrocarbons in the Marine Environment." Edited by Corina Brussaard. *FEMS Microbiology Reviews* 40 (6): 814–30. doi:10.1093/femsre/fuw031.

Eadie, Brian J., and John A Robbins. 1987. "The Role of Particulate Matter in the Movement of Contaminants in the Great Lakes." doi:10.1021/ba-1987-0216.ch011.

Emerson, S., and J. Hedges. 2003. "Sediment Diagenesis and Benthic Flux." In *Treatise on Geochemistry*, 6–9:293–319. Elsevier. doi:10.1016/B0-08-043751-6/06112-0.

Foster, Karen L., Gary A. Stern, Jesse Carrie, Joscelyn N.-L. Bailey, Peter M. Outridge,

Hamed Sanei, and Robie W. Macdonald. 2015. “Spatial, Temporal, and Source Variations of Hydrocarbons in Marine Sediments from Baffin Bay, Eastern Canadian Arctic.” *Science of The Total Environment* 506–507 (February): 430–43. doi:10.1016/j.scitotenv.2014.11.002.

Giuliani, Silvia, Mario Sprovieri, Mauro Frignani, Nguyen Huu Cu, Cristian Mugnai, Luca Giorgio Bellucci, Sonia Albertazzi, et al. 2008. “Presence and Origin of Polycyclic Aromatic Hydrocarbon in Sediments of Nine Coastal Lagoons in Central Vietnam.” *Marine Pollution Bulletin* 56 (8): 1504–12. doi:10.1016/j.marpolbul.2008.04.013.

Goñi, Miguel A., Alison E. O’Connor, Zou Zou Kuzyk, Mark B. Yunker, Charles Gobeil, and Robie W. Macdonald. 2013. “Distribution and Sources of Organic Matter in Surface Marine Sediments across the North American Arctic Margin.” *Journal of Geophysical Research: Oceans* 118 (9): 4017–35. doi:10.1002/jgrc.20286.

Goñi, Miguel A., Mark B. Yunker, Robie W. Macdonald, and Timothy I. Eglinton. 2005. “The Supply and Preservation of Ancient and Modern Components of Organic Carbon in the Canadian Beaufort Shelf of the Arctic Ocean.” *Marine Chemistry* 93 (1): 53–73. doi:10.1016/j.marchem.2004.08.001.

Goñi, Miguel A., Mark B. Yunker, Robie W. MacDonald, and Timothy I. Eglinton. 2000. “Distribution and Sources of Organic Biomarkers in Arctic Sediments from the Mackenzie River and Beaufort Shelf.” *Marine Chemistry* 71 (1–2): 23–51. doi:10.1016/S0304-4203(00)00037-2.

Gonzalez-Vila, F.J. 1995. “Alkane Biomarkers. Geochemical Significance and Application In Oil Shale Geochemistry.”

Halsall, C. J., L. A. Barrie, P. Fellin, D. C G Muir, B. N. Billeck, L. Lockhart, F. Ya Rovinsky, E. Ya Kononov, and B. Pastukhov. 1997. “Spatial and Temporal Variation of Polycyclic Aromatic Hydrocarbons in the Arctic Atmosphere.” *Environmental Science*

& Technology 31 (12): 3593–99. doi:10.1021/es970342d.

Hanes, C C Krezek, F Ahern, A Cantin, and M D Flannigan. 2010. “Trends in Large Fires in Canada, 1959-2007.”

Harvey, H. Rodger, Karen A. Taylor, Hannah V. Pie, and Carys L. Mitchelmore. 2014. “Polycyclic Aromatic and Aliphatic Hydrocarbons in Chukchi Sea Biota and Sediments and Their Toxicological Response in the Arctic Cod, Boreogadus Saida.” *Deep Sea Research Part II: Topical Studies in Oceanography* 102 (April): 32–55. doi:10.1016/j.dsr2.2013.07.013.

Hedges, J.I, and R.G Keil. 1995. “Sedimentary Organic Matter Preservation: An Assessment and Speculative Synthesis.” *Marine Chemistry*, 81–115.

Ho, Huu Hieu, Rudy Swennen, Valérie Cappuyns, Elvira Vassilieva, and Tan Van Tran. 2012. “Necessity of Normalization to Aluminum to Assess the Contamination by Heavy Metals and Arsenic in Sediments near Haiphong Harbor, Vietnam.” *Journal of Asian Earth Sciences* 56. Elsevier Ltd: 229–39. doi:10.1016/j.jseaes.2012.05.015.

http://chesterfield-inlet.ca/. n.d. “About Us.” doi:10.1016/B978-0-12-805193-1.00025-2.

Huettel, M., and G. Gust. 1992. “Solute Release Mechanisms from Confined Sediment Cores in Stirred Benthic Chambers and Flume Flows.” *Marine Ecology Progress Series* 82: 187–97. doi:10.3354/meps082187.

Hung, H, P Blanchard, C J Halsall, T F Bidleman, G A Stern, P Fellin, D C G Muir, et al. 2005. “Temporal and Spatial Variabilities of Atmospheric Polychlorinated Biphenyls (PCBs), Organochlorine (OC) Pesticides and Polycyclic Aromatic Hydrocarbons (PAHs) in the Canadian Arctic : Results from a Decade of Monitoring” 342: 119–44. doi:10.1016/j.scitotenv.2004.12.058.

Idowu, Ifeoluwa, Olga Francisco, Philippe J. Thomas, Wesley Johnson, Chris Marvin, Jörg Stetefeld, and Gregg T. Tomy. 2018. “Validation of a Simultaneous Method for

Determining Polycyclic Aromatic Compounds and Alkylated Isomers in Biota." *Rapid Communications in Mass Spectrometry* 32 (3): 277–87. doi:10.1002/rcm.8035.

Ines, Zrafi, Bakhrouf Amina, Rouabhia Mahmoud, and Saidane-Mosbahi Dalila. 2013. "Aliphatic and Aromatic Biomarkers for Petroleum Hydrocarbon Monitoring in Khniss Tunisian-Coast, (Mediterranean Sea)." *Procedia Environmental Sciences* 18. Elsevier B.V.: 211–20. doi:10.1016/j.proenv.2013.04.027.

Jeter, Hewitt W. 1999. "Determining the Ages of Recent Sediments Using Measurements of Trace Radioactivity," 21–28.

Johannessen, S.C., and R.W. Macdonald. 2012. "There Is No 1954 in That Core! Interpreting Sedimentation Rates and Contaminant Trends in Marine Sediment Cores." *Marine Pollution Bulletin* 64 (4). Elsevier Ltd: 675–78. doi:10.1016/j.marpolbul.2012.01.026.

Johnson, R.D., F.R. Joubin, S.J. Nelson, and E. Oslwn. 1986. "Mineral Resources." In *Canadian Inland Seas*, edited by I.P. Martini, 387–402. Department of Land Resource Science, University of Guelph, Guelph, Ont. N 1G 2W1, Canada.

Kamula, C. Michelle, Zou Zou A. Kuzyk, David A. Lobb, and Robie W. Macdonald. 2017. "Sources and Accumulation of Sediment and Particulate Organic Carbon in a Subarctic Fjard Estuary: 210 Pb, 137 Cs, and δ 13 C Records from Lake Melville, Labrador." *Canadian Journal of Earth Sciences* 54 (9): 993–1006. doi:10.1139/cjes-2016-0167.

Kanzari, F., A. D. Syakti, L. Asia, L. Malleret, A. Piram, G. Mille, and P. Doumenq. 2014. "Distributions and Sources of Persistent Organic Pollutants (Aliphatic Hydrocarbons, PAHs, PCBs and Pesticides) in Surface Sediments of an Industrialized Urban River (Huveaune), France." *Science of the Total Environment* 478. Elsevier B.V.: 141–51. doi:10.1016/j.scitotenv.2014.01.065.

Karbassi, a. R., and R. Amirnezhad. 2013. "Geochemistry of Heavy Metals and Sedimentation Rate in a Bay Adjacent to the Caspian Sea." *International Journal of*

Environmental Science & Technology 1 (3): 191–98. doi:10.1007/BF03325832.

Kuzyk, Zou Zou A., Charles Gobeil, Miguel A. Goñi, and Robie W. Macdonald. 2017. "Early Diagenesis and Trace Element Accumulation in North American Arctic Margin Sediments." *Geochimica et Cosmochimica Acta* 203: 175–200. doi:10.1016/j.gca.2016.12.015.

Kuzyk, Zou Zou A., Robie W. Macdonald, and Sophia C. Johannessen. 2015. *Environmental Contaminants*. Edited by Jules M. Blais, Michael R. Rosen, and John P. Smol. *Calculating Rates and Dates and Interpreting Contaminant Profiles in Biomixed Sediments*. Vol. 18. Developments in Paleoenvironmental Research. Dordrecht: Springer Netherlands. doi:10.1007/978-94-017-9541-8.

Kuzyk, Zou Zou A., Robie W. Macdonald, Sophia C. Johannessen, Charles Gobeil, and Gary A. Stern. 2009. "Towards a Sediment and Organic Carbon Budget for Hudson Bay." *Marine Geology* 264 (3–4). Elsevier B.V.: 190–208. doi:10.1016/j.margeo.2009.05.006.

Kuzyk, Zou Zou A., Robie W. Macdonald, Gary A. Stern, and Charles Gobeil. 2010. "Inferences about the Modern Organic Carbon Cycle from Diagenesis of Redox-Sensitive Elements in Hudson Bay." *Journal of Marine Systems* 88 (3). Elsevier B.V.: 451–62. doi:10.1016/j.jmarsys.2010.11.001.

Kuzyk, Zou Zou A, Charles Gobeil, and Robie W. Macdonald. 2013. "210 Pb and 137 Cs in Margin Sediments of the Arctic Ocean: Controls on Boundary Scavenging." *Global Biogeochemical Cycles* 27 (2): 422–39. doi:10.1002/gbc.20041.

Larsen, Randolph K., and Joel E. Baker. 2003. "Source Apportionment of Polycyclic Aromatic Hydrocarbons in the Urban Atmosphere: A Comparison of Three Methods." *Environmental Science & Technology* 37 (9): 1873–81. doi:10.1021/es0206184.

Lavoie, Denis, Nicolas Pinet, Mathieu Duchesne, Shunxin Zhang, Jim Dietrich, Virginia Brake, Esther Asselin, et al. 2011. "Geological Setting and Petroleum Potential of the

Paleozoic Hudson Platform , Northern Canada ± Current Knowledge" 1: 3–6.

Lee, K, M Boudreau, J Bugden, L Burridge, S E Cobanli, S Courtenay, S Grenon, et al. 2011. "State of Knowledge Review of Fate and Effect of Oil in the Arctic Marine Environment 2011," no. August 2015: 1–267.

Li, Pu, Qinhong Cai, Weiyun Lin, Bing Chen, and Baiyu Zhang. 2016. "Offshore Oil Spill Response Practices and Emerging Challenges." *Marine Pollution Bulletin* 110 (1): 6–27. doi:10.1016/j.marpolbul.2016.06.020.

Liao, Chong, Ping Yang, Zhenwei Xie, Yunzhi Zhao, Xiaoyan Cheng, Yu Zhang, Zhaohui Ren, Zhonghua Guo, and Ji Liao. 2010. "Application of GC-Triple Quadrupole MS in the Quantitative Confirmation of Polycyclic Aromatic Hydrocarbons and Phthalic Acid Esters in Soil." *Journal of Chromatographic Science* 48 (3): 161–66. http://www.ncbi.nlm.nih.gov/pubmed/20223080.

Loring, D. H., and G. Asmund. 1996. "Geochemical Factors Controlling Accumulation of Major and Trace Elements in Greenland Coastal and Fjord Sediments." *Environmental Geology* 28 (1): 2–11. doi:10.1007/s002540050072.

Ma, Yuxin, Crispin J Halsall, Zhiyong Xie, Danijela Koetke, Wenying Mi, Ralf Ebinghaus, and Guoping Gao. 2017. "Polycyclic Aromatic Hydrocarbons in Ocean Sediments from the North Pacific to the Arctic Ocean." *Environmental Pollution* 227 (August): 498–504. doi:10.1016/2017.04.087.

MacDonald, D. D., C. G. Ingersoll, and T. A. Berger. 2000. "Development and Evaluation of Consensus-Based Sediment Quality Guidelines for Freshwater Ecosystems." *Archives of Environmental Contamination and Toxicology* 39 (1): 20–31. doi:10.1007/s002440010075.

Macdonald, R. W., S. C. Johannessen, C. Gobeil, C. Wright, B. Burd, A. van Roodselaar, and T. F. Pedersen. 2008. "Sediment Redox Tracers in Strait of Georgia Sediments - Can

They Inform Us of the Loadings of Organic Carbon from Municipal Wastewater?" *Marine Environmental Research* 66 (SUPPL.): 87–100. doi:10.1016/j.marenvres.2008.08.001.

Malcolm, S J. 1985. "Early Diagenesis of Molybdenum in Estuarine Sediments." *Marine Chemistry* 16: 213–25.

Maletic, Snezana, Bozo Dalmacija, and Sran Roncevic. 2013. "Petroleum Hydrocarbon Biodegradability in Soil – Implications for Bioremediation." In *Hydrocarbon*. InTech. doi:10.5772/50108.

Martinsen, Kjetil, Hakon Hustad, and Terje Sverud. 2013. "HFO in the Arctic-Phase 2: 2013-1542-16G8ZQC-5/1." https://pame.is/index.php/document-library/shipping-documents/arctic-marine-shipping-assessment-documents.

Morford, Jennifer L., William R. Martin, Roger François, and Caitlin M. Carney. 2009. "A Model for Uranium, Rhenium, and Molybdenum Diagenesis in Marine Sediments Based on Results from Coastal Locations." *Geochimica et Cosmochimica Acta* 73 (10): 2938–60. doi:10.1016/j.gca.2009.02.029.

Mostafa, Alaa R., Terry L. Wade, Stephen T. Sweet, Abdel Kawi A. Al-Alimi, and Assem O. Barakat. 2009. "Distribution and Characteristics of Polycyclic Aromatic Hydrocarbons (PAHs) in Sediments of Hadhramout Coastal Area, Gulf of Aden, Yemen." *Journal of Marine Systems* 78 (1): 1–8. doi:10.1016/j.jmarsys.2009.02.002.

Muir, D C G, X Wang, F Yang, N Nguyen, T A Jackson, M S Evans, M Douglas, et al. 2009. "Spatial Trends and Historical Deposition of Mercury in Eastern and Northern Canada Inferred from Lake Sediment Cores." *Environ. Sci. Technol.* 43 (13): 4802–9.

Müller, P. J., and E. Suess. 1979. "Productivity, Sedimentation Rate, and Sedimentary Organic Matter in the Oceans-I. Organic Carbon Preservation." *Deep Sea Research Part A, Oceanographic Research Papers* 26 (12): 1347–62. doi:10.1016/0198-

0149(79)90003-7.

Nam, Jae Jak, Orjan Gustafsson, Perihan Kurt-Karakus, Knut Breivik, Eiliv Steinnes, and Kevin C. Jones. 2008. “Relationships between Organic Matter, Black Carbon and Persistent Organic Pollutants in European Background Soils: Implications for Sources and Environmental Fate.” *Environmental Pollution* 156 (3). Elsevier Ltd: 809–17. doi:10.1016/j.envpol.2008.05.027.

NCRP. 2007. “Cesium-137 in the Environment : Radioecology and Approaches to Assessment and Management.” In .

Nemr, Ahmed El, Abeer A Moneer, Safaa Ragab, and Amany El Sikaily. 2016. “Distribution and Sources of N-Alkanes and Polycyclic Aromatic Hydrocarbons in Shellfish of the Egyptian Red Sea Coast.” *The Egyptian Journal of Aquatic Research* 42 (2): 121–31. doi:10.1016/j.ejar.2016.05.003.

Newman, B. K., and R. J. Watling. 2007. “Definition of Baseline Metal Concentrations for Assessing Metal Enrichment of Sediment from the South-Eastern Cape Coastline of South Africa.” *Water SA* 33 (5): 675–91.

Nicolas, Michelle P.B., and D. Lavoie. 2009. “Hudson Bay and Foxe Basins Project: Introduction to the Geo-Mapping for Energy and Minerals, GEM–Energy Initiative , Northeastern Manitoba (Parts of NTS 54),” 160–64.

NRC. 2003. “Bioavailability of Contaminants in Soils and Sediments: Processes, Tools, and Applications Committee.” In , 432 p. Washington, D.C.: National Academies Press. doi:10.17226/661.

“Nunavut’s Energy System.” n.d. https://climatechangenunavut.ca/en/energy/energy-nunavut.

Omelchenko, A, W L Lockhart, and P Wilkinson. 2005. “Depositional Characteristics of Lake Sediments in Canada as Determined by Pb-210 and Cs-137,” 9–50.

Pampanin, Daniela M, and Magne O Sydnes. 2013. “Polycyclic Aromatic Hydrocarbons a

Constituent of Petroleum : Presence and Influence in the Aquatic Environment." *Intech*, 83–118. doi:10.5772/48176.

Parinos, C., A. Gogou, I. Bouloubassi, R. Pedrosa-Pàmies, I. Hatzianestis, A. Sanchez-Vidal, G. Rousakis, D. Velaoras, G. Krokos, and V. Lykousis. 2013. "Occurrence, Sources and Transport Pathways of Natural and Anthropogenic Hydrocarbons in Deep-Sea Sediments of the Eastern Mediterranean Sea." *Biogeosciences* 10 (9): 6069–89. doi:10.5194/bg-10-6069-2013.

ParksCanada. 1977. "Wager Bay Preliminary Marine Resource Analysis - Part II." Section, Marine Studies, Parks System Planning Division.

Petroleum Products Division (PPD). n.d. "Community And." https://www.gov.nu.ca/petroleum-products-division.

Rabalais, Nancy. 2003. "Oil in the Sea III." In *Issues in Science and Technology*, 20:74–78. Washington, D.C.: National Academies Press. doi:10.17226/10388.

Rajesh, Seth, Donald Mackay, and Jane Muncke. 1999. "Estimating the Organic Carbon Partition Coefficient and Its Variability for Hydrophobic Chemicals." *Environmental Science & Technology* 33 (14): 2390–94. doi:10.1021/es980893j.

Ravindra, Khaiwal, Ranjeet Sokhi, and René Van Grieken. 2008. "Atmospheric Polycyclic Aromatic Hydrocarbons: Source Attribution, Emission Factors and Regulation." *Atmospheric Environment* 42 (13): 2895–2921. doi:10.1016/j.atmosenv.2007.12.010.

Readman, J W, R F C Mantoura, and M M Rhead. 1987. "A Record of Polycyclic Aromatic Hydrocarbon (PAH) Pollution Obtained From Accreting Sediments of the Tamar Estuary, U.K.: Evidence For Non-Equilibrium Behaviour of PAH." *The Science of the Total Environment, 66* 66: 73–94.

Roff, C. J., J. R. Pett, F. G. Rogers, and W.P. Budgell. 1980. "A Study of Plankton Ecology in Chesterfield Inlet, Northwest Territories: An Arctic Estuary."

Sanchez-Cabeza, J.A., P. Masqué, I. Ani-Ragolta, J. Merino, Mauro Frignani, F. Alvisi, A. Palanques, and P. Puig. 1999. “Sediment Accumulation Rates in the Southern Barcelona Continental Margin (NW Mediterranean Sea) Derived from 210Pb and 137Cs Chronology.” *Progress in Oceanography* 44 (1–3): 313–32. doi:10.1016/S0079-6611(99)00031-2.

Schulz, Horst D, and Matthias Zabel. 2006. *Marine Geochemistry*. 2nd editio.

Sella, Giovanni F., Seth Stein, Timothy H. Dixon, Michael Craymer, Thomas S. James, Stephane Mazzotti, and Roy K. Dokka. 2007. “Observation of Glacial Isostatic Adjustment in ‘Stable’ North America with GPS.” *Geophysical Research Letters* 34 (2): 1–6. doi:10.1029/2006GL027081.

Short, Jeffrey W., Jonathan J. Kolak, James R. Payne, and Gerald K. Van Kooten. 2007. “An Evaluation of Petrogenic Hydrocarbons in Northern Gulf of Alaska Continental Shelf Sediments – The Role of Coastal Oil Seep Inputs.” *Organic Geochemistry* 38 (4): 643–70. doi:10.1016/j.orggeochem.2006.12.005.

Simcik, Matt F., Steven J. Eisenreich, Katherine A. Golden, Shi-Ping Liu, Elisabeth Lipiatou, Deborah L. Swackhamer, and David T Long. 1996. “Atmospheric Loading of Polycyclic Aromatic Hydrocarbons to Lake Michigan as Recorded in the Sediments” 30 (10): 3039–46.

Smith, John Norton. 2001. “Why Should We Believe 210 Pb Sediment Geochronologies ?” 55: 121–23.

Stein, R., K. Dittmers, K. Fahl, M. Kraus, J. Matthiessen, F. Niessen, M. Pirrung, et al. 2004. “Arctic (Palaeo) River Discharge and Environmental Change: Evidence from the Holocene Kara Sea Sedimentary Record.” *Quaternary Science Reviews* 23 (11–13): 1485–1511. doi:10.1016/j.quascirev.2003.12.004.

Stein, Ruediger. 1990. “Organic Carbon Content/Sedimentation Rate Relationship and Its

Paleoenvironmental Significance for Marine Sediments." *Geo-Marine Letters* 10 (1): 37–44. doi:10.1007/BF02431020.

Stern, G., and M. Evans. 2003. "Persistent Organic Pollutants in Marine and Lake Sediments." In *Sources, Occurrence, Trends and Pathways in the Physical Environment*, edited by T. Bidleman, R. Macdonald, and J. Stow, 100–115. Minister of Public Works and Government Services Canada. www.ainc-inac.gc.ca.

Stewart, D. B., and W. L. Lockhart. 2005. "03.0 Geology and Physiography." *An Overview of the Hudson Bay Marine Ecosystem*, 3-1-3–24.

Stocks, B. J., J. A. Mason, J. B. Todd, E. M. Bosch, B. M. Wotton, B. D. Amiro, M. D. Flannigan, et al. 2002. "Large Forest Fires in Canada, 1959–1997." *Journal of Geophysical Research* 108 (D1): 8149. doi:10.1029/2001JD000484.

Stogiannidis, Efstathios, and Remi Laane. 2015. "Source Characterization of Polycyclic Aromatic Hydrocarbons by Using Their Molecular Indices: An Overview of Possibilities." In *Reviews of Environmental Contamination and Toxicology*, 49–133. doi:10.1007/978-3-319-10638-0_2.

Stout, Scott A, and Zhendi Wang. 2016. "Chemical Fingerprinting Methods and Factors Affecting Petroleum Fingerprints in the Environment." In *Standard Handbook Oil Spill Environmental Forensics*, 61–129. Elsevier. doi:10.1016/B978-0-12-803832-1.00003-9.

Su, C C, and C A Huh. 2002. "210 Pb, 137 Cs and 239,240 Pu in East China Sea Sediments: Sources, Pathways and Budgets of Sediments and Radionuclides." *Marine Geology* 183 (1): 163–78. www.elsevier.com/locate/margeo.

The North is not like other jurisdictions. n.d. "The North Is Not like Other Jurisdictions A Challenge to All of Canada." http://www.canadianfuels.ca/ASR-Fuels-en/Northern-power/.

Tissot, B.P. and Welte, D.H. 1984. *Petroleum Formation and Occurrenc*. doi:10.1088/1751-

8113/44/8/085201.

Tran, Kim, Charlie C Yu, and Eddy Y. Zeng. 1994. “N-Alkane Sources.” *Petrogenic and Biogenic Sources of N-Alkanes off San Diego, California*, p.53.

Tsabaris, C., V. Kapsimalis, G. Eleftheriou, M. Laubenstein, H. Kaberi, and W. Plastino. 2012. “Determination of 137Cs Activities in Surface Sediments and Derived Sediment Accumulation Rates in Thessaloniki Gulf, Greece.” *Environmental Earth Sciences* 67 (3): 833–43. doi:10.1007/s12665-012-1530-5.

U.S EPA. 1996. “EPA Method 3630 C Silica Gel Clean Up,” no. December 1996: 1–15.

U.S EPA.. 2007. “EPA Method 3546 Microwave Extraction,” no. February: 1–13.

Van Cappellen, P, and Y Wang. 1996. “Metal Contaminated Aquatic Sediments.” In , edited by Herbert E. Allen. Atlanta, GA: Ann Arbor Press Inc.

Van Kooten, G, Jeffrey W. Short, and Jonathan J. Kolak. 2002. “Low-Maturity Kulthieth Formation Coal: A Possible Source of Polycyclic Aromatic Hydrocarbons in Benthic Sediment of the Northern Gulf of Alaska.” *Environmental Forensics* 3 (3–4): 227–41. doi:10.1006/enfo.2002.0096.

Venkatesan, M.I. 1988. “Occurrence and Possible Sources of Perylene in Marine Sediments-a Review.” *Marine Chemistry* 25 (1): 1–27. doi:10.1016/0304-4203(88)90011-4.

Vickers, Glenn, Sandra Buzza, Dave Schmidt, and John Mullock. 2000. “Weather Patterns of the Prairies.” In *The Weather of the Canadian Prairies*. Nav Canada.

Vonk, J. E., L. Sánchez-García, B. E. van Dongen, V. Alling, D. Kosmach, a. Charkin, I. P. Semiletov, et al. 2012. “Activation of Old Carbon by Erosion of Coastal and Subsea Permafrost in Arctic Siberia.” *Nature* 489 (7414): 137–40. doi:10.1038/nature11392.

Wang, Jinlong, Mark Baskaran, and John Niedermiller. 2017. “Mobility of 137 Cs in Freshwater Lakes: A Mass Balance and Diffusion Study of Lake St. Clair, Southeast Michigan, USA.” *Geochimica et Cosmochimica Acta* 218 (December). Elsevier Ltd:

323–42. doi:10.1016/j.gca.2017.09.017.

Wang, Rong, Shu Tao, Bin Wang, Yu Yang, Chang Lang, Yanxu Zhang, Jing Hu, Jianmin Ma, and Hayley Hung. 2010. “Sources and Pathways of Polycyclic Aromatic Hydrocarbons Transported to Alert, the Canadian High Arctic.” *Environmental Science & Technology* 44 (3): 1017–22. doi:10.1021/es902203w.

Wang, Zhendi, and Merv F Fingas. 2003. “Development of Oil Hydrocarbon Fingerprinting and Identification Techniques.” *Marine Pollution Bulletin* 47 (9–12): 423–52. doi:10.1016/S0025-326X(03)00215-7.

Wang, Zucheng, Zhanfei Liu, Kehui Xu, Lawrence M Mayer, Zulin Zhang, Alexander S Kolker, and Wei Wu. 2014. “Concentrations and Sources of Polycyclic Aromatic Hydrocarbons in Surface Coastal Sediments of the Northern Gulf of Mexico.” *Geochemical Transactions* 15 (1). Geochemical Transactions: 2. doi:10.1186/1467-4866-15-2.

Welch, Harold E, Derek C G Muir, Brian N Billeck, W Lyle Lockhart, Gregg J Brunskill, Hedy J Kling, Marvin P Olson, and Richard M Lemoineg. 1991. “Welch et Al Brown Snow A Long-Range Transport Event” 25 (2): 280–86.

Wigger, John W, and Bruce E Torkelson. 1997. “Petroleum Hydrocarbon Fingerprinting - Numerical Interpretation Developments.” *Petroleum Hydrocarbon Fingerprinting - Numerical Interpretation Developments*, International Petroleum Environmental Conference. papers2://publication/uuid/01F42CFB-C838-499A-A1A4-0C281A125BBF.

Yuan, Zijiao, Guijian Liu, Chunnian Da, Jie Wang, and Houqi Liu. 2015. “Occurrence, Sources, and Potential Toxicity of Polycyclic Aromatic Hydrocarbons in Surface Soils from the Yellow River Delta Natural Reserve, China.” *Archives of Environmental Contamination and Toxicology* 68 (2): 330–41. doi:10.1007/s00244-014-0085-8.

Yunker, Mark B., Laura L. Belicka, H. Rodger Harvey, and Robie W. Macdonald. 2005.

"Tracing the Inputs and Fate of Marine and Terrigenous Organic Matter in Arctic Ocean Sediments: A Multivariate Analysis of Lipid Biomarkers." *Deep-Sea Research Part II: Topical Studies in Oceanography* 52 (24–26): 3478–3508. doi:10.1016/j.dsr2.2005.09.008.

Yunker, Mark B., Robie W. Macdonald, Roxanne Vingarzan, Reginald H. Mitchell, Darcy Goyette, and Stephanie Sylvestre. 2002. "PAHs in the Fraser River Basin: A Critical Appraisal of PAH Ratios as Indicators of PAH Source and Composition." *Organic Geochemistry* 33 (4): 489–515. doi:10.1016/S0146-6380(02)00002-5.

Yunker, Mark B, and Robie W Macdonald. 1995. "Composition and Origins of Polycyclic Aromatic Hydrocarbons in the Mackenzie River and on the Beaufort Sea Shelf." *Arctic* 48 (2): 118–29.

Yunker, Mark B, Lloyd R Snowdon, Robie W Macdonald, John N Smith, Martin G Fowler, Donald N Skibo, Fiona a Mclaughlin, a I Danyushevskaya, V I Petrova, and G I Ivanov. 1996. "Polycyclic Aromatic Hydrocarbon Composition and Potential Sources for Sediment Samples from the Beaufort and Barents Seas Polycyclic Aromatic Hydrocarbon Composition and Potential Sources for Sediment Samples from the Beaufort and Barents Seas." *Environmental Science & Technology* 30 (4): 1310–20. doi:10.1021/es950523k.

Zeng, E, and C. L. Vista. 1997. "Organic Pollutants in the Coastal Environment off San Diego, California. 2. Petregenic and Biogenic Sources of Aliphatic Hydrocarbons." *Environ. Toxicol. Chem* 16 (2): 189–95.

Zhang, Yan, Xueqiang Lu, Honglei Liu, Qiongqiong Liu, and Dan Yu. 2015. "Identifying the Sources of Organic Matter in Marine and Riverine Sediments of Bohai Bay and Its Catchment Using Carbon and Nitrogen Stable Isotopes." *Chinese Journal of Oceanology and Limnology* 33 (1): 204–9. doi:10.1007/s00343-015-4068-z.

Zheng, Yan, Robert F Anderson, van Geen Alexander, and James Kuwabara. 2000. "Authigenic Molybdenum Formation in Marine Sediments : A Link to Pore Water Sulfide in the Santa Barbara Basin." *Geochimica et Cosmochimica Acta* 64 (24): 4165–78.

Appendix 1

Blank corrected concentrations of PAHs (ng/g dw) in sediment cores of varying lengths collected from 7 stations across Wager Bay and Chesterfield Inlet.

Sediment core PLK-NU-15											
Depth (cm)	0-1	3-4	4-5	6-7	7-8	8-9	9-10	10-12	12-14	14-16	16-18
Naphthalene	nd	1.402	0.303	nd	0.350	nd	0.301	nd	nd	1.352	nd
Acenaphthylene	0.010	1.018	0.002	0.007	0.427	0.017	0.093	0.025	0.061	0.005	0.015
Acenaphthene	0.016	0.164	0.022	0.024	0.000	0.040	0.138	0.020	0.005	0.042	0.041
Fluorene	0.029	0.772	0.039	0.041	2.472	0.032	1.043	0.033	0.212	0.064	0.042
Phenanthrene	0.053	0.118	0.097	0.110	0.201	0.068	0.103	0.072	0.083	0.100	0.101
Anthracene	0.005	0.013	0.009	0.004	0.004	0.009	0.007	0.009	0.011	0.006	0.005
Fluoranthene	0.027	0.035	0.046	0.063	0.059	0.074	0.041	0.059	0.039	0.053	0.059
Pyrene	0.057	0.032	0.064	0.076	0.055	0.178	0.040	0.093	0.087	0.144	0.181
Benz(a)Anthracene	0.005	0.011	0.012	0.011	0.034	0.013	0.014	0.010	0.008	0.007	0.008
Triphenylene	0.011	0.022	0.015	0.024	0.129	0.019	0.028	0.023	0.017	0.010	0.022
Chrysene	0.012	0.025	0.022	0.025	0.057	0.024	0.024	0.025	0.009	0.014	0.019
Benzo[b]fluoranthene	0.021	0.052	0.016	0.025	0.061	0.051	0.046	0.050	0.014	0.031	0.030
Benzo(k)fluoranthene	0.013	0.016	0.031	0.022	0.027	0.017	0.014	0.012	0.014	0.007	0.009
Benzo(j)fluoranthene	0.011	0.022	0.029	0.019	0.064	0.024	0.022	0.019	0.013	0.009	0.014
Benzo(a)fluoranthene	0.003	0.030	0.005	0.005	0.041	0.016	0.026	0.027	0.003	0.003	0.011
Benzo(e)pyrene	0.025	0.021	0.077	0.069	0.270	0.033	0.016	0.015	0.046	0.030	0.023
Benzo(a)pyrene	nd	nd	0.021	0.020	nd	nd	nd	nd	0.014	0.009	nd
Perylene	0.125	0.282	0.363	0.423	0.375	0.128	0.428	0.634	0.571	0.445	0.592
Dibenz[a,h]anthracene	nd	nd	nd	nd	nd	0.004	nd	0.008	0.003	0.003	0.004
Indeno[1,2,3-c,d]pyrene	0.024	0.093	0.075	0.072	0.048	0.061	0.061	0.083	0.035	0.030	0.043
Benzo(g,h,i) perylene	0.046	0.093	0.092	0.152	0.073	0.078	0.064	0.087	0.080	0.034	0.044
2-MethylNapthalene	3.444	0.568	1.495	nd	nd	5.148	0.223	nd	0.699	3.986	1.298
1-MethylNapthalene	2.734	nd	1.196	0.154	0.352	2.308	nd	0.227	nd	1.753	0.166

Depth (cm)	0-1	3-4	4-5	6-7	7-8	8-9	9-10	10-12	12-14	14-16	16-18
2,6-Dimethylnaphthalene	nd	nd	0.404	nd	nd	1.523	nd	nd	nd	1.457	nd
2,7-Dimethylnaphthalene	nd	nd	0.407	nd	nd	1.412	nd	nd	nd	1.448	0.982
1,3-Dimethylnaphthalene	2.012	nd	nd	nd	1.295	0.327	nd	nd	1.560	nd	nd
1,7-Dimethylnaphthalene	nd	nd	1.087	0.166	nd	1.940	nd	nd	1.748	5.334	1.088
1,6-Dimethylnaphthalene	2.956	nd	1.083	nd	nd	0.957	nd	nd	nd	nd	0.088
1,4-Dimethylnaphthalene	1.202	nd	nd	nd	nd	0.272	nd	nd	0.496	nd	nd
2,3-Dimethylnaphthalene	0.966	0.822	nd	nd	nd	nd	0.612	nd	nd	nd	nd
1,5-Dimethylnaphthalene	0.418	nd	1.508	nd	nd	1.202	nd	0.133	nd	nd	nd
1,2-Dimethylnaphthalene	1.177	nd	nd	nd	nd	nd	nd	nd	nd	0.491	nd
3-Methylphenanthrene	0.011	0.056	0.016	0.014	0.075	0.008	0.063	0.011	0.027	0.008	0.012
2-Methylphenanthrene	0.025	0.108	0.041	0.030	0.107	0.011	0.101	0.046	0.070	0.045	0.018
4-Methylphenanthrene	0.025	0.108	0.041	0.030	0.107	0.011	0.097	0.046	0.070	0.045	0.018
2-Methylanthracene	0.003	0.021	0.004	0.003	0.014	0.001	0.010	0.007	0.011	0.004	0.005
9-Methylphenanthrene	0.011	0.069	0.024	0.016	0.064	0.008	0.075	0.017	0.045	0.017	0.016
1-Methylphenanthrene	0.017	0.128	0.023	0.021	0.097	0.014	0.107	0.010	0.063	0.013	0.018
3,6-Dimethylphenanthrene	0.002	0.010	0.002	0.003	0.016	nd	0.014	0.002	0.006	nd	0.006
1,8-Dimethylphenanthrene	0.009	0.055	0.013	0.008	0.073	0.006	0.081	0.009	0.031	0.008	0.010
1,2-Dimethylphenanthrene	0.003	0.016	0.005	0.002	0.024	0.002	0.026	0.003	0.011	0.002	0.003
Methylfluoranthene	nd	0.003	0.005	0.004	0.004	0.003	0.005	0.004	0.004	0.005	0.006

Sediment core NU-WAB-08										
Depth (cm)	0-1	1-2	2-3	3-4	4-5	5-6	6-7	7-8	8-9	9-10
Naphthalene	nd	2.216	0.460	0.448	19.915	nd	2.273	0.496	0.266	4.437
Acenaphthylene	0.005	0.485	0.066	0.225	0.017	0.371	0.008	0.253	0.001	0.061
Acenaphthene	0.035	0.582	0.342	0.104	0.059	0.191	0.034	0.341	0.016	0.000
Fluorene	0.038	0.010	0.140	0.239	0.092	0.603	0.063	0.899	0.035	0.234
Phenanthrene	0.127	0.207	0.288	0.123	0.201	0.146	0.148	0.164	0.072	0.213
Anthracene	0.006	0.007	0.014	0.006	0.012	0.005	0.007	0.021	0.010	0.008
Fluoranthene	0.081	0.071	0.114	0.073	0.083	0.078	0.082	0.083	0.059	0.095
Pyrene	0.160	0.104	0.238	0.068	0.129	0.077	0.135	0.087	0.089	0.120
Benz(a)Anthracene	0.018	0.030	0.030	0.024	0.019	0.031	0.022	0.031	0.011	0.030
Triphenylene	0.069	0.038	0.060	0.077	0.053	0.066	0.036	0.064	0.033	0.054
Chrysene	0.055	0.087	0.109	0.076	0.042	0.057	0.047	0.065	0.034	0.046
Benzo[b]fluoranthene	0.096	0.119	0.151	0.048	0.120	0.042	0.136	0.042	0.048	0.139
Benzo(k)fluoranthene	0.024	0.038	0.035	0.038	0.043	0.066	0.035	0.045	0.020	0.028
Benzo(j)fluoranthene	0.054	0.058	0.061	0.052	0.048	0.069	0.063	0.073	0.029	0.071
Benzo(a)fluoranthene	0.007	0.063	0.081	0.012	0.007	0.013	0.012	0.011	0.005	0.075
Benzo(e)pyrene	0.100	0.030	0.041	0.166	0.133	0.174	0.112	0.185	0.055	0.039
Benzo(a)pyrene	0.040	nd	nd	0.052	0.039	0.056	0.047	0.056	0.020	nd
Perylene	0.226	0.302	0.305	0.270	0.230	0.310	0.291	0.469	0.389	0.626
Dibenz[a,h]anthracene	0.012	0.020	0.019	0.027	0.023	0.020	0.019	0.026	0.006	0.013
Indeno[1,2,3-c,d]pyrene	0.148	0.185	0.195	0.178	0.151	0.209	0.159	0.199	0.059	0.200
Benzo(g,h,i) perylene	0.093	0.182	0.207	0.237	0.176	0.185	0.179	0.156	0.126	0.215
2-MethylNapthalene	0.363	2.809	0.870	nd	2.747	nd	2.548	0.285	0.236	5.612
1-MethylNapthalene	nd	0.855	3.186	0.436	2.304	0.377	2.075	nd	nd	0.522
2,6-Dimethylnaphthalene	nd	nd	nd	0.310	1.497	nd	nd	nd	nd	0.429
2,7-Dimethylnaphthalene	nd	nd	0.183	nd	1.499	nd	nd	nd	nd	0.156
1,3-Dimethylnaphthalene	nd	nd	nd	nd	0.168	nd	nd	0.768	nd	nd

Depth (cm)	0-1	1-2	2-3	3-4	4-5	5-6	6-7	7-8	8-9	9-10
1,7-Dimethylnaphthalene	nd	0.679	2.252	nd	2.801	nd	4.498	nd	0.028	1.399
1,6-Dimethylnaphthalene	nd	nd	0.032	nd	2.807	nd	4.166	nd	0.108	1.124
1,4-Dimethylnaphthalene	nd	2.570	nd	nd	nd	nd	1.003	nd	nd	nd
2,3-Dimethylnaphthalene	nd	nd	nd	nd	1.129	nd	0.002	nd	nd	2.083
1,5-Dimethylnaphthalene	0.351	nd	4.091	nd	nd	0.357	nd	nd	nd	nd
1,2-Dimethylnaphthalene	nd	2.479	3.533	nd	0.019	nd	0.421	nd	nd	0.619
3-Methylphenanthrene	0.022	0.107	0.101	0.040	0.032	0.089	0.022	0.078	0.010	0.071
2-Methylphenanthrene	0.009	0.127	0.144	0.076	0.062	0.194	0.016	0.038	0.017	0.141
4-Methylphenanthrene	0.009	0.127	0.145	0.076	0.062	0.194	0.016	0.038	0.017	0.141
2-Methylanthracene	0.013	0.014	0.015	0.014	0.006	0.024	0.016	0.052	0.003	0.013
9-Methylphenanthrene	0.028	0.116	0.142	0.063	0.041	0.128	0.032	0.112	0.012	0.093
1-Methylphenanthrene	0.028	0.138	0.134	0.066	0.043	0.166	0.027	0.120	0.016	0.098
3,6-Dimethylphenanthrene	0.004	0.019	0.028	0.007	0.004	0.020	0.003	0.015	0.002	0.013
1,8-Dimethylphenanthrene	0.017	0.087	0.127	0.036	0.016	0.106	0.016	0.069	0.008	0.070
1,2-Dimethylphenanthrene	0.005	0.034	0.065	0.013	0.007	0.041	0.006	0.028	0.003	0.027
Methylfluoranthene	0.008	0.013	0.026	0.009	0.008	0.012	0.008	0.010	0.006	0.018

Sediment core NU-WAB-08						
Depth (cm)	10-12	14-16	16-18	18-20	20-25	25-27
Naphthalene	nd	nd	0.505	nd	0.561	nd
Acenaphthylene	0.036	0.002	0.699	0.003	0.056	0.039
Acenaphthene	0.054	0.020	0.314	0.016	0.054	0.019
Fluorene	0.072	0.047	0.627	0.043	0.044	0.066
Phenanthrene	0.141	0.109	0.121	0.114	0.146	0.166
Anthracene	0.007	0.006	0.011	0.007	nd	0.013
Fluoranthene	0.071	0.054	0.039	0.065	0.045	0.051
Pyrene	0.147	0.136	0.048	0.211	0.084	0.125
Benz(a)Anthracene	0.013	0.008	0.015	0.008	0.008	0.008
Triphenylene	0.032	0.035	0.039	0.039	0.027	0.040
Chrysene	0.034	0.038	0.041	0.029	0.042	0.039
Benzo[b]fluoranthene	0.074	0.050	0.046	0.016	0.031	0.039
Benzo(k)fluoranthene	0.020	0.012	0.012	0.015	0.006	0.009
Benzo(j)fluoranthene	0.043	0.022	0.028	0.014	0.013	0.018
Benzo(a)fluoranthene	0.007	0.005	0.029	0.003	0.016	0.003
Benzo(e)pyrene	0.077	0.054	0.015	0.042	0.007	0.041
Benzo(a)pyrene	0.031	0.020	nd	0.018	nd	0.013
Perylene	0.374	0.516	0.532	0.490	0.408	0.451
Dibenz[a,h]anthracene	0.011	0.005	nd	0.007	nd	0.004
Indeno[1,2,3-c,d]pyrene	0.096	0.060	0.046	0.038	0.028	0.048
Benzo(g,h,i) perylene	0.126	0.083	0.065	0.086	0.051	0.062
2-MethylNapthalene	3.450	0.220	0.339	nd	0.463	nd
1-MethylNapthalene	2.685	nd	nd	0.415	nd	0.236
2,6-Dimethylnaphthalene	nd	0.255	0.344	nd	nd	nd
2,7-Dimethylnaphthalene	nd	nd	nd	nd	nd	0.295
1,3-Dimethylnaphthalene	nd	nd	nd	0.815	0.587	nd

Depth (cm)	10-12	14-16	16-18	18-20	20-25	25-27
1,7-Dimethylnaphthalene	nd	nd	nd	nd	nd	nd
1,6-Dimethylnaphthalene	nd	nd	nd	nd	nd	nd
1,4-Dimethylnaphthalene	nd	nd	nd	nd	nd	nd
2,3-Dimethylnaphthalene	4.067	nd	nd	nd	nd	nd
1,5-Dimethylnaphthalene	6.024	nd	nd	nd	nd	nd
1,2-Dimethylnaphthalene	nd	nd	nd	nd	nd	nd
3-Methylphenanthrene	0.023	0.015	0.054	0.025	0.047	0.036
2-Methylphenanthrene	0.010	0.008	0.093	0.007	0.058	0.020
4-Methylphenanthrene	0.010	0.008	0.093	0.007	0.056	0.020
2-Methylanthracene	0.006	0.008	0.014	0.009	0.003	0.018
9-Methylphenanthrene	0.033	0.025	0.087	0.032	0.052	0.045
1-Methylphenanthrene	0.030	0.023	0.106	0.036	0.057	0.047
3,6-Dimethylphenanthrene	0.003	0.002	0.012	0.005	0.007	0.008
1,8-Dimethylphenanthrene	0.018	0.013	0.069	0.028	0.039	0.034
1,2-Dimethylphenanthrene	0.007	0.005	0.028	0.011	0.016	0.014
Methylfluoranthene	0.008	0.008	0.008	0.012	0.010	0.012

Sediment Core NU-WAB-10											
Depth (cm)	0-1	1-2	2-3	3-4	4-5	5-6	6-7	7-8	8-9	9-10	10-12
Naphthalene	0.712	0.322	19.072	nd	nd	0.532	nd	0.983	nd	1.214	0.187
Acenaphthylene	0.055	0.182	0.269	0.155	0.042	0.202	0.005	0.130	0.010	0.010	0.057
Acenaphthene	0.490	0.211	0.283	0.331	0.018	0.331	0.018	0.105	0.045	0.046	0.044
Fluorene	0.323	0.068	0.131	0.421	0.057	0.626	0.057	0.805	0.055	0.365	0.047
Phenanthrene	0.106	0.119	0.120	0.139	0.129	0.134	0.159	0.096	0.139	0.189	0.077
Anthracene	0.006	0.013	0.011	0.007	0.010	0.004	0.006	0.007	0.028	0.023	0.008
Fluoranthene	0.057	0.084	0.051	0.057	0.085	0.069	0.080	0.040	0.118	0.041	0.029
Pyrene	0.064	0.081	0.067	0.047	0.147	0.055	0.120	0.038	0.100	0.054	0.054
Benz(a)Anthracene	0.018	0.025	0.013	0.019	0.013	0.020	0.021	0.013	0.010	0.015	0.007
Triphenylene	0.031	0.062	0.033	0.031	0.024	0.037	0.042	0.029	0.026	0.029	0.031
Chrysene	0.056	0.088	0.019	0.036	0.035	0.032	0.045	0.029	0.028	0.035	0.030
Benzo[b]fluoranthene	0.091	0.140	0.020	0.056	0.104	0.027	0.109	0.027	0.046	0.042	0.009
Benzo(k)fluoranthene	0.020	0.043	0.034	0.024	0.039	0.036	0.027	0.019	0.007	0.008	0.010
Benzo(j)fluoranthene	0.046	0.054	0.055	0.032	0.052	0.041	0.033	0.031	0.013	0.018	0.021
Benzo(a)fluoranthene	0.056	0.079	0.005	0.024	0.006	0.007	0.005	0.004	0.003	0.025	0.004
Benzo(e)pyrene	0.023	0.015	0.083	0.071	0.084	0.110	0.150	0.079	0.033	nd	0.031
Benzo(a)pyrene	nd	nd	0.030	nd	0.026	0.037	0.041	0.024	0.010	nd	0.012
Perylene	0.231	0.334	0.165	0.171	0.181	0.273	0.287	0.317	0.173	0.283	0.368
Dibenz[a,h]anthracene	0.011	0.016	0.006	0.014	0.012	0.013	0.012	0.013	0.003	nd	nd
Indeno[1,2,3-c,d]pyrene	0.141	0.205	0.108	0.123	0.120	0.130	0.130	0.084	0.035	0.052	0.045
Benzo(g,h,i) perylene	0.153	0.209	0.116	0.110	0.150	0.136	0.135	0.067	0.045	0.048	0.075
2-MethylNapthalene	0.716	nd	nd	0.479	nd	nd	0.189	2.170	3.452	6.102	1.577
1-MethylNapthalene	nd	2.550	6.102	nd	0.181	0.321	nd	nd	2.401	nd	nd
2,6-Dimethylnaphthalene	nd	nd	0.633	nd	nd	nd	nd	nd	2.347	nd	0.787
Depth (cm)	0-1	1-2	2-3	3-4	4-5	5-6	6-7	7-8	8-9	9-10	10-12
2,7-Dimethylnaphthalene	nd	nd	5.404	0.707	nd	nd	nd	nd	2.447	nd	0.808

Depth (cm)	0-1	1-2	2-3	3-4	4-5	5-6	6-7	7-8	8-9	9-10	10-12
1,3-Dimethylnaphthalene	nd	nd	2.102	nd	nd	nd	nd	nd	nd	nd	0.056
1,7-Dimethylnaphthalene	2.066	nd	4.903	nd	0.188	nd	nd	nd	7.995	2.741	2.068
1,6-Dimethylnaphthalene	0.266	nd	4.822	nd	nd	nd	nd	0.742	nd	2.741	2.068
1,4-Dimethylnaphthalene	0.200	nd	1.133	nd	nd	0.657	nd	nd	0.966	nd	nd
2,3-Dimethylnaphthalene	0.584	1.774	nd	nd	nd	nd	nd	nd	4.495	0.703	nd
1,5-Dimethylnaphthalene	1.078	nd	0.551	nd	nd	nd	nd	nd	0.298	nd	1.118
1,2-Dimethylnaphthalene	nd	18.874	1.101	nd	nd	nd	0.205	nd	2.100	0.366	nd
3-Methylphenanthrene	0.043	0.050	0.017	0.080	0.015	0.082	0.031	0.059	0.022	0.128	0.012
2-Methylphenanthrene	0.124	0.066	0.008	0.160	0.038	0.298	0.006	0.139	0.051	0.183	0.041
4-Methylphenanthrene	0.122	0.066	0.008	0.160	0.038	0.298	0.006	0.139	0.051	0.183	0.041
2-Methylanthracene	0.018	0.009	0.009	0.018	0.005	0.055	0.005	0.016	0.017	0.021	0.018
9-Methylphenanthrene	0.061	0.049	0.028	0.115	0.020	0.132	0.033	0.078	0.028	0.189	0.025
1-Methylphenanthrene	0.061	0.057	0.027	0.145	0.021	0.149	0.034	0.111	0.026	0.206	0.017
3,6-Dimethylphenanthrene	0.009	0.869	0.002	0.020	0.002	0.018	0.005	0.010	0.003	0.030	0.002
1,8-Dimethylphenanthrene	0.045	0.013	0.106	0.010	0.090	0.022	0.054	0.013	0.145	0.010	nd
1,2-Dimethylphenanthrene	0.016	0.004	0.037	0.003	0.036	0.008	0.020	0.004	0.059	0.004	nd
Methylfluoranthene	0.007	0.004	0.006	0.005	0.007	0.010	0.004	0.006	0.008	0.005	nd

Sediment Core NU-WAB-14											
Depth (cm)	0-1	1-2	2-3	3-4	4-5	5-6	6-7	7-8	9-10	10-12	12-13
Naphthalene	6.900	0.690	nd	nd	0.191	nd	2.592	nd	1.360	nd	0.084
Acenaphthylene	0.322	0.053	0.006	0.016	0.017	0.039	0.043	0.034	0.022	0.002	0.009
Acenaphthene	0.462	0.166	0.015	0.010	0.031	0.023	0.032	0.022	0.030	0.019	0.025
Fluorene	0.012	0.106	0.130	0.029	0.070	0.045	0.063	0.044	0.032	0.032	0.041
Phenanthrene	0.181	0.093	21.396	0.073	0.138	0.085	0.110	0.084	0.061	0.099	0.075
Anthracene	0.006	0.007	1.373	0.004	0.011	0.004	0.007	0.002	0.004	0.004	0.004
Fluoranthene	0.028	0.038	0.152	0.033	0.070	0.079	0.036	0.042	0.030	0.054	0.021
Pyrene	0.070	0.047	0.464	0.073	0.126	0.220	0.054	0.125	0.047	0.098	0.033
Benz(a)Anthracene	0.011	0.012	0.088	0.005	0.016	0.007	0.006	0.006	0.005	0.012	0.004
Triphenylene	0.055	0.023	0.018	0.011	0.032	0.023	0.019	0.018	0.013	0.023	0.010
Chrysene	0.049	0.057	0.083	0.022	0.014	0.017	0.018	0.008	0.018	0.023	0.013
Benzo[b]fluoranthene	0.018	0.054	0.094	0.041	0.015	0.040	0.034	0.029	0.036	0.041	0.028
Benzo(k)fluoranthene	0.021	0.014	0.061	0.015	0.017	0.017	0.016	0.010	0.006	0.012	0.005
Benzo(j)fluoranthene	0.027	0.021	0.023	0.018	0.040	0.022	0.014	0.011	0.011	0.017	0.008
Benzo(a)fluoranthene	0.004	0.032	0.006	0.004	0.006	0.002	nd	0.002	0.003	0.003	0.002
Benzo(e)pyrene	0.109	0.021	0.043	0.040	0.066	0.047	0.034	0.031	0.029	0.050	0.024
Benzo(a)pyrene	0.025	nd	0.080	0.012	0.030	0.016	0.012	0.010	0.009	0.016	0.006
Perylene	0.164	0.138	0.091	0.079	0.185	0.179	0.157	0.151	0.159	0.142	0.125
Dibenz[a,h]anthracene	0.007	0.013	0.063	0.003	0.007	nd	0.003	0.004	0.002	0.005	0.002
Indeno[1,2,3-c,d]pyrene	0.096	0.112	0.103	0.052	0.067	0.054	0.039	0.034	0.042	0.046	0.028
Benzo(g,h,i) perylene	0.085	0.108	0.182	0.056	0.098	0.066	0.065	0.046	0.047	0.060	0.034
2-MethylNapthalene	nd	nd	0.435	nd	2.546	0.944	nd	0.451	4.800	nd	nd
1-MethylNapthalene	6.472	6.472	nd	0.214	nd	nd	1.998	nd	1.580	0.170	0.516
2,6-Dimethylnaphthalene	nd	nd	nd	nd	0.322	nd	0.157	nd	1.786	nd	nd
2,7-Dimethylnaphthalene	nd	nd	nd	nd	0.284	nd	0.163	nd	1.786	nd	nd
1,3-Dimethylnaphthalene	2.687	nd	nd	nd	18.943	nd	nd	nd	0.346	0.160	nd

Depth (cm)	0-1	1-2	2-3	3-4	4-5	5-6	6-7	7-8	9-10	10-12	12-13
1,7-Dimethylnaphthalene	1.159	nd	nd	nd	21.390	nd	2.195	nd	0.981	nd	nd
1,6-Dimethylnaphthalene	1.159	nd	nd	nd	0.454	nd	2.195	nd	0.981	nd	0.740
1,4-Dimethylnaphthalene	nd	nd	nd	nd	2.341	nd	1.097	nd	0.273	nd	nd
2,3-Dimethylnaphthalene	38.886	nd	nd	nd	nd	nd	nd	nd	nd	nd	nd
1,5-Dimethylnaphthalene	nd	nd	nd	nd	nd	1.596	nd	nd	2.256	nd	nd
1,2-Dimethylnaphthalene	nd	48.881	nd	nd	0.158	nd	nd	0.761	0.064	nd	nd
3-Methylphenanthrene	0.083	0.019	2.310	0.013	0.030	0.010	0.016	0.010	0.010	0.020	0.010
2-Methylphenanthrene	0.086	0.061	4.657	0.022	0.009	0.013	0.005	0.005	0.054	0.038	0.042
4-Methylphenanthrene	0.086	0.058	4.657	0.022	0.009	0.013	0.005	0.005	0.054	0.038	0.042
2-Methylanthracene	0.008	nd	0.509	nd	0.009	0.006	0.005	0.009	0.011	0.005	0.006
9-Methylphenanthrene	0.079	0.037	3.307	0.012	0.039	0.017	0.024	0.017	0.024	0.024	0.026
1-Methylphenanthrene	0.080	0.055	2.133	0.011	0.023	0.014	0.020	0.014	0.014	0.025	0.014
3,6-Dimethylphenanthrene	2.611	0.006	0.812	nd	0.006	0.002	0.002	nd	nd	0.003	0.002
1,8-Dimethylphenanthrene	0.058	0.033	1.631	0.006	0.024	0.007	0.012	0.008	0.009	0.016	0.009
1,2-Dimethylphenanthrene	0.007	0.028	0.727	0.002	0.010	0.003	0.004	0.003	0.003	0.007	0.003
Methylfluoranthene	0.008	0.005	0.006	0.002	0.009	0.005	0.005	0.005	0.005	0.006	0.004

Sediment core NU-WAB-16						
Depth (cm)	0-1	1-2	2-3	3-4	4-5	5-6
Naphthalene	nd	2.056	nd	nd	nd	nd
Acenaphthylene	0.127	0.224	0.007	0.018	0.047	0.087
Acenaphthene	0.102	0.257	0.018	0.020	0.056	0.044
Fluorene	0.489	0.012	0.032	0.036	0.053	0.060
Phenanthrene	0.137	0.097	0.119	0.111	0.133	0.162
Anthracene	0.006	0.017	0.005	0.007	0.006	0.012
Fluoranthene	0.054	0.058	0.106	0.060	0.084	0.108
Pyrene	0.058	0.055	0.334	0.104	0.157	0.180
Benz(a)Anthracene	0.016	0.022	0.012	0.013	0.019	0.024
Triphenylene	0.050	0.070	0.039	0.039	0.054	0.057
Chrysene	0.064	0.065	0.035	0.040	0.048	0.059
Benzo[b]fluoranthene	0.046	0.025	0.063	0.068	0.069	0.088
Benzo(k)fluoranthene	0.026	0.034	0.024	0.014	0.025	0.021
Benzo(j)fluoranthene	0.033	0.031	0.028	0.024	0.027	0.029
Benzo(a)fluoranthene	0.024	0.007	0.026	0.019	0.026	0.030
Benzo(e)pyrene	0.051	0.109	0.036	0.040	0.047	0.066
Benzo(a)pyrene	nd	0.041	0.017	nd	0.013	nd
Perylene	0.201	0.229	0.194	0.179	0.167	0.188
Dibenz[a,h]anthracene	0.005	0.017	0.002	0.008	0.005	0.009
Indeno[1,2,3-c,d]pyrene	0.094	0.140	0.091	0.082	0.064	0.100
Benzo(g,h,i) perylene	0.139	0.208	0.120	0.097	0.096	0.103
2-MethylNapthalene	0.447	0.824	nd	1.974	3.344	2.519
1-MethylNapthalene	0.967	nd	0.099	0.172	2.245	2.164
2,6-Dimethylnaphthalene	nd	nd	nd	1.925	4.096	0.518
2,7-Dimethylnaphthalene	nd	1.546	nd	1.889	2.683	1.356
1,3-Dimethylnaphthalene	nd	nd	nd	0.060	nd	0.178

Depth (cm)	0-1	1-2	2-3	3-4	4-5	5-6
1,7-Dimethylnaphthalene	nd	nd	nd	nd	nd	0.930
1,6-Dimethylnaphthalene	nd	nd	0.094	nd	6.172	1.014
1,4-Dimethylnaphthalene	nd	nd	nd	0.100	nd	0.011
2,3-Dimethylnaphthalene	11.490	nd	nd	nd	nd	nd
1,5-Dimethylnaphthalene	nd	nd	nd	0.193	nd	2.026
1,2-Dimethylnaphthalene	nd	3.856	nd	nd	nd	nd
3-Methylphenanthrene	0.079	0.036	0.012	0.016	0.018	0.023
2-Methylphenanthrene	0.128	0.065	0.013	0.023	0.019	0.050
4-Methylphenanthrene	0.128	0.065	nd	0.023	0.019	0.050
2-Methylanthracene	0.019	0.008	0.003	0.007	0.003	0.004
9-Methylphenanthrene	0.100	0.051	0.017	0.024	0.025	0.026
1-Methylphenanthrene	0.131	0.064	0.020	0.022	0.028	0.030
3,6-Dimethylphenanthrene	0.019	0.007	0.002	0.003	0.003	0.004
1,8-Dimethylphenanthrene	0.094	0.040	0.010	0.018	0.019	0.021
1,2-Dimethylphenanthrene	0.046	0.015	0.003	0.006	0.006	0.006
Methylfluoranthene	0.008	0.008	0.006	0.009	0.009	0.009

Sediment core CI-08										
Depth (cm)	0-1	1-2	2-3	3-4	4-5	5-6	6-7	7-8	8-9	9-10
Naphthalene	nd	nd	nd	nd	nd	nd	nd	nd	1.772	0.409
Acenaphthylene	0.009	0.009	nd	0.445	0.004	0.467	0.003	0.282	0.011	0.156
Acenaphthene	nd	0.103	0.010	0.122	0.010	nd	0.011	0.227	0.041	0.097
Fluorene	0.033	0.112	0.027	1.111	0.029	0.455	0.038	0.394	0.038	0.427
Phenanthrene	0.010	0.075	0.074	0.151	0.073	0.280	0.078	0.164	0.079	0.061
Anthracene	nd	0.005	0.005	0.018	0.008	0.039	0.008	0.018	0.012	0.005
Fluoranthene	nd	0.023	0.063	0.022	0.078	0.020	0.099	0.035	0.059	0.020
Pyrene	nd	0.026	0.239	0.022	0.266	0.021	0.387	0.029	0.075	0.020
Benz(a)Anthracene	nd	0.007	0.005	0.006	0.007	0.006	0.007	0.010	0.008	0.006
Triphenylene	nd	0.011	0.005	0.009	0.008	0.006	0.007	0.006	0.007	0.006
Chrysene	nd	0.021	0.012	0.013	0.017	0.010	0.017	0.014	0.015	0.011
Benzo[b]fluoranthene	0.003	0.022	0.019	0.028	0.023	0.020	0.025	0.028	0.027	0.027
Benzo(k)fluoranthene	nd	0.009	0.005	0.012	0.007	0.008	0.006	0.011	0.007	0.009
Benzo(j)fluoranthene	nd	0.013	0.007	0.015	0.009	nd	0.011	0.013	0.012	0.009
Benzo(a)fluoranthene	nd	nd	0.002	0.002	0.003	nd	0.002	0.002	0.002	0.003
Benzo(e)pyrene	nd	0.031	0.020	0.036	0.026	0.021	0.025	0.034	0.025	0.025
Benzo(a)pyrene	nd	0.010	0.009	0.010	0.012	0.011	0.015	0.014	0.010	0.008
Perylene	nd	0.034	0.028	0.024	0.035	0.020	0.028	0.024	0.033	0.018
Dibenz[a,h]anthracene	nd	0.006	0.002	nd	0.003	nd	nd	nd	0.003	0.002
Indeno[1,2,3-c,d]pyrene	nd	0.025	0.023	0.031	0.038	0.021	0.036	0.025	0.030	0.027
Benzo(g,h,i) perylene	0.002	0.029	0.027	0.028	0.033	0.024	0.039	0.032	0.043	0.032
2-MethylNapthalene	0.005	0.340	nd	nd	0.330	nd	0.352	1.051	2.562	1.595
1-MethylNapthalene	nd	2.240	0.347	0.464	1.811	0.325	nd	2.234	0.723	0.713
2,6-Dimethylnaphthalene	nd	nd	0.485	nd	nd	0.281	nd	nd	0.615	nd
2,7-Dimethylnaphthalene	nd	nd	nd	0.218	nd	nd	0.368	nd	nd	0.365
1,3-Dimethylnaphthalene	nd	0.821	nd	nd	nd	nd	nd	nd	nd	nd

Depth (cm)	0-1	1-2	2-3	3-4	4-5	5-6	6-7	7-8	8-9	9-10
1,7-Dimethylnaphthalene	nd	nd	nd	nd	0.153	nd	nd	0.487	nd	nd
1,6-Dimethylnaphthalene	nd	nd	nd	nd	0.703	nd	0.154	0.243	0.257	nd
1,4-Dimethylnaphthalene	0.004	0.012	nd	nd	nd	nd	nd	nd	nd	nd
2,3-Dimethylnaphthalene	nd	nd	nd	nd	nd	0.008	nd	0.011	0.111	nd
1,5-Dimethylnaphthalene	nd	nd	nd	nd	0.127	nd	0.032	0.003	nd	nd
1,2-Dimethylnaphthalene	0.005	0.150	nd	nd	nd	nd	nd	nd	nd	nd
3-Methylphenanthrene	0.008	0.030	0.010	0.070	0.018	0.132	0.010	0.131	0.020	0.089
2-Methylphenanthrene	0.009	0.048	0.027	0.148	0.035	0.271	0.037	0.178	0.019	0.037
4-Methylphenanthrene	0.009	0.048	0.027	0.148	0.035	0.271	0.037	0.178	0.019	0.037
2-Methylanthracene	nd	0.005	0.001	0.026	0.034	0.037	0.003	nd	nd	0.021
9-Methylphenanthrene	0.008	0.024	0.009	0.114	0.129	0.155	0.013	0.272	0.014	0.132
1-Methylphenanthrene	0.011	0.024	0.021	0.133	0.032	0.201	0.012	0.446	0.032	0.646
3,6-Dimethylphenanthrene	0.003	1.616	0.002	0.017	0.002	0.030	0.002	0.021	0.002	0.004
1,8-Dimethylphenanthrene	0.012	0.020	0.005	0.082	0.011	0.161	0.007	0.119	0.007	0.022
1,2-Dimethylphenanthrene	0.005	0.029	0.002	0.027	0.003	0.048	0.002	0.039	0.002	0.006
Methylfluoranthene	nd	0.002	0.002	0.002	0.003	0.002	0.002	0.002	0.002	nd

Sediment core CI-08						
Depth (cm)	10-12	12-14	14-16	16-18	18-20	20-21.5
Naphthalene	nd	0.153	nd	0.462	nd	0.110
Acenaphthylene	0.007	0.018	0.018	0.019	nd	0.006
Acenaphthene	0.031	0.019	0.061	0.027	0.015	0.023
Fluorene	0.030	0.441	0.047	0.309	0.033	0.489
Phenanthrene	0.071	0.234	0.062	0.125	0.070	0.211
Anthracene	0.011	0.032	0.008	0.007	0.008	0.011
Fluoranthene	0.055	0.028	0.051	0.034	0.063	0.019
Pyrene	0.083	0.024	0.121	0.040	0.143	0.016
Benz(a)Anthracene	0.015	0.010	0.009	0.009	0.008	0.006
Triphenylene	0.012	0.010	0.010	0.013	0.010	0.013
Chrysene	0.024	0.013	0.017	0.014	0.016	0.011
Benzo[b]fluoranthene	0.043	0.033	0.037	0.030	0.026	0.017
Benzo(k)fluoranthene	0.014	0.017	0.010	0.014	0.007	0.010
Benzo(j)fluoranthene	0.030	0.021	0.016	0.013	0.012	0.007
Benzo(a)fluoranthene	0.003	nd	0.003	0.002	0.002	nd
Benzo(e)pyrene	0.048	0.056	0.036	0.043	0.028	0.024
Benzo(a)pyrene	0.021	0.020	0.015	0.012	0.013	0.007
Perylene	0.040	0.027	0.037	0.036	0.045	0.046
Dibenz[a,h]anthracene	0.004	0.004	0.003	0.004	nd	nd
Indeno[1,2,3-c,d]pyrene	0.053	0.038	0.059	0.034	0.029	0.022
Benzo(g,h,i) perylene	0.048	0.052	0.053	0.038	0.034	0.024
2-MethylNapthalene	nd	0.248	2.428	0.675	0.347	1.389
1-MethylNapthalene	0.377	0.683	0.858	0.719	nd	0.682
2,6-Dimethylnaphthalene	nd	0.124	nd	nd	nd	nd
2,7-Dimethylnaphthalene	nd	nd	nd	nd	0.148	0.266
1,3-Dimethylnaphthalene	nd	nd	nd	nd	nd	nd

Depth (cm)	10-12	12-14	14-16	16-18	18-20	20-21.5
1,7-Dimethylnaphthalene	nd	nd	0.726	nd	nd	nd
1,6-Dimethylnaphthalene	nd	nd	0.257	nd	nd	nd
1,4-Dimethylnaphthalene	nd	nd	nd	nd	nd	nd
2,3-Dimethylnaphthalene	0.565	nd	nd	nd	nd	nd
1,5-Dimethylnaphthalene	nd	nd	nd	0.3007982	nd	nd
1,2-Dimethylnaphthalene	nd	nd	nd	nd	nd	nd
3-Methylphenanthrene	0.014	0.061	0.005	0.176	0.011	2.352
2-Methylphenanthrene	0.027	0.385	0.026	0.047	0.040	0.160
4-Methylphenanthrene	0.027	0.385	0.026	0.047	0.040	0.160
2-Methylanthracene	nd	0.178	nd	0.048	0.002	1.173
9-Methylphenanthrene	0.013	2.544	nd	0.314	0.011	2.309
1-Methylphenanthrene	0.032	3.163	0.029	0.375	nd	1.205
3,6-Dimethylphenanthrene	0.003	0.023	nd	0.023	nd	0.019
1,8-Dimethylphenanthrene	0.013	0.165	0.006	0.139	0.005	0.158
1,2-Dimethylphenanthrene	0.005	0.056	0.002	0.055	nd	0.041
Methylfluoranthene	0.004	nd	0.002	0.002	0.002	nd

Sediment core CI-24										
Depth (cm)	0-1.5	1.5-2	2-3	4-5	5-6	6-7	7-8	8-9	9-10	10-11.5
Naphthalene	nd	0.384	nd	nd	nd	nd	2.419	nd	1.591	nd
Acenaphthylene	0.287	0.210	0.005	0.004	0.006	0.009	0.005	0.005	0.011	nd
Acenaphthene	0.142	0.314	0.006	0.013	0.029	0.021	0.038	0.021	0.018	0.013
Fluorene	0.436	0.199	0.017	0.039	0.042	0.049	0.055	0.029	0.052	0.029
Phenanthrene	0.100	0.079	0.075	0.090	0.067	0.109	0.075	0.071	0.081	0.044
Anthracene	0.022	0.007	0.013	0.010	0.009	0.010	0.008	0.009	0.011	0.004
Fluoranthene	0.031	0.032	0.103	0.057	0.048	0.070	0.049	0.065	0.067	0.019
Pyrene	0.040	0.035	0.226	0.124	0.058	0.159	0.056	0.155	0.140	0.029
Benz(a)Anthracene	0.011	0.011	0.009	0.010	0.013	0.014	0.010	0.012	0.014	0.003
Triphenylene	0.004	0.012	0.005	0.010	0.011	0.012	0.012	0.012	0.013	0.006
Chrysene	0.017	0.027	0.012	0.021	0.024	0.023	0.018	0.021	0.027	0.009
Benzo[b]fluoranthene	0.036	0.042	0.013	0.042	0.052	0.047	0.040	0.039	0.046	0.015
Benzo(k)fluoranthene	0.007	0.015	0.003	0.012	0.014	0.015	0.011	0.011	0.010	0.003
Benzo(j)fluoranthene	0.010	0.012	0.005	0.019	0.014	0.024	0.020	0.020	0.025	0.005
Benzo(a)fluoranthene	0.002	0.002	nd	0.003	0.003	0.004	0.004	0.004	0.004	nd
Benzo(e)pyrene	0.025	0.041	0.023	0.040	0.041	0.043	0.033	0.035	0.040	0.013
Benzo(a)pyrene	0.012	0.017	0.012	0.017	0.019	0.024	0.020	0.018	0.027	0.005
Perylene	0.053	0.060	0.009	0.079	0.098	0.092	0.099	0.097	0.134	0.079
Dibenz[a,h]anthracene	0.002	0.005	0.002	0.004	0.005	0.006	0.005	0.005	0.005	nd
Indeno[1,2,3-c,d]pyrene	0.029	0.050	0.010	0.063	0.078	0.066	0.061	0.057	0.051	0.020
Benzo(g,h,i) perylene	0.027	0.047	0.009	0.059	0.087	0.066	0.053	0.042	0.054	0.018
2-MethylNapthalene	nd	nd	nd	nd	1.237	nd	2.869	3.985	0.480	nd
1-MethylNapthalene	nd	9.357	nd	nd	nd	nd	0.657	1.708	0.456	nd
2,6-Dimethylnaphthalene	nd	nd	nd	nd	nd	nd	0.261	nd	nd	nd
2,7-Dimethylnaphthalene	nd	nd	nd	nd	nd	nd	0.101	nd	nd	nd
1,3-Dimethylnaphthalene	nd	nd	nd	nd	nd	nd	nd	nd	nd	nd

Depth (cm)	0-1.5	1.5-2	2-3	4-5	5-6	6-7	7-8	8-9	9-10	10-11.5
1,7-Dimethylnaphthalene	nd	0.146	nd	nd	nd	nd	14.156	nd	0.013	nd
1,6-Dimethylnaphthalene	0.039	nd	nd	nd	nd	nd	14.109	nd	0.006	nd
1,4-Dimethylnaphthalene	0.952	nd	nd	nd	nd	nd	nd	nd	nd	nd
2,3-Dimethylnaphthalene	0.747	nd	nd	nd	nd	nd	nd	nd	nd	nd
1,5-Dimethylnaphthalene	0.302	nd	nd	nd	nd	nd	nd	nd	nd	nd
1,2-Dimethylnaphthalene	nd	nd	nd	nd	1.237	nd	2.869	0.011	2.244	0.142
3-Methylphenanthrene	nd	9.357	nd	nd	nd	nd	1.466	1.708	0.456	nd
2-Methylphenanthrene	nd	nd	nd	nd	nd	nd	0.261	nd	nd	nd
4-Methylphenanthrene	nd	nd	nd	nd	nd	3.498	0.101	nd	nd	nd
2-Methylanthracene	nd	9.356	nd	nd	nd	nd	nd	nd	nd	0.195
9-Methylphenanthrene	nd	0.146	nd	nd	nd	nd	11.056	nd	0.013	nd
1-Methylphenanthrene	0.039	nd	0.101	0.530	nd	nd	0.603	nd	0.006	nd
3,6-Dimethylphenanthrene	0.952	nd	nd	nd	nd	nd	nd	2.925	9.005	nd
1,8-Dimethylphenanthrene	0.747	nd	nd	nd	3.686	nd	nd	nd	nd	nd
1,2-Dimethylphenanthrene	4.756	nd	nd	nd	nd	nd	nd	nd	nd	nd
Methylfluoranthene	nd	2.518	nd	nd	nd	nd	nd	nd	nd	nd

Appendix 2

Blank corrected concentrations of n-alkanes (ng/g dw) in sediment cores of varying lengths collected from 7 stations across Wager Bay and Chesterfield Inlet.

Sediment Core PLK-NU-15									
Depth (cm)	0-1	1-2	2-3	6-7	8-9	10-12	12-14	14-16	16-18
Undecane	5.781	364.157	235.547	8.867	nd	nd	nd	1.277	1.700
n-Dodecane	4.364	nd	nd	58.576	nd	68.444	12.392	3.647	25.239
Tridecane	7.292	152.672	99.655	26.875	nd	63.345	31.509	5.668	26.505
Tetradecane	46.121	209.027	158.508	41.913	5.865	47.231	116.500	27.095	90.619
Pentadecane	16.571	144.197	91.536	7.112	4.651	11.304	99.239	9.532	11.629
Hexadecane	31.112	124.738	74.625	10.529	5.089	9.915	128.102	16.257	20.490
Heptadecane	13.965	483.884	79.185	10.022	6.219	13.572	79.184	16.014	14.588
Octadecane	6.572	32.778	20.559	5.811	7.025	5.226	27.660	6.900	8.411
Nonadecane	13.627	48.233	31.251	11.878	7.201	19.547	30.331	16.386	16.204
Eiscosane	22.672	45.044	37.771	24.450	16.860	27.112	39.398	25.177	34.532
Heneicosane	32.459	83.697	94.337	34.675	19.751	42.664	80.262	37.546	41.660
Docosane	56.828	87.693	96.287	83.218	50.857	96.493	nd	86.089	104.776
Tricosane	128.406	183.702	189.120	149.275	60.856	164.616	239.068	244.920	248.831
Tetracosane	87.752	109.759	107.623	134.406	72.786	165.009	137.443	142.177	180.552
Pentacosane	238.966	264.065	250.952	288.835	122.895	318.685	338.100	384.712	490.397
Hexacosane	111.913	182.320	291.058	263.252	124.044	312.607	169.814	217.381	318.080
Heptacosane	405.628	307.231	252.893	628.881	209.625	615.824	492.928	646.671	961.911
Octacosane	153.054	245.402	252.566	310.984	149.254	313.886	132.439	240.006	449.568
Nonacosane	723.513	968.205	nd	nd	328.515	872.605	558.170	938.283	1692.107
Triacontane	114.238	189.182	172.722	141.638	55.725	139.862	94.514	184.872	485.087
Hentriacontane	596.261	990.066	880.235	958.350	301.086	772.016	595.743	453.683	854.420
Dotriacontane	48.854	131.983	131.426	109.456	53.639	75.906	69.258	49.440	73.942
Tritriacontane	nd	309.897	279.284	nd	nd	nd	241.776	nd	nd

Depth (cm)	0-1	1-2	2-3	6-7	8-9	10-12	12-14	14-16	16-18
Tetratriacontane	nd	53.496	45.263	nd	nd	nd	31.978	nd	nd
Pentatriacontane	nd	40.960	30.128	nd	nd	nd	37.657	nd	nd
Hexatriacontane	nd	38.314	37.517	nd	nd	nd	nd	nd	nd

Sediment Core NU-WAB-08							
Depth (cm)	0-1	1-2	2-3	3-4	4-5	5-6	6-7
Undecane	50.521	71.286	nd	nd	137.925	nd	1.575
n-Dodecane	222.511	4.998	nd	428.035	72.038	125.148	5.085
Tridecane	nd	112.326	nd	222.549	5.186	65.311	6.591
Tetradecane	154.954	726.303	204.781	266.616	48.471	156.296	61.302
Pentadecane	14.099	36.289	113.936	164.087	7.860	57.206	11.870
Hexadecane	18.081	39.435	127.003	136.438	25.294	85.303	23.935
Heptadecane	14.070	4.998	797.957	161.093	69.020	144.591	22.612
Octadecane	10.152	48.778	50.175	41.776	9.262	30.581	9.123
Nonadecane	17.818	72.387	75.329	55.116	28.276	37.004	21.993
Eiscosane	50.691	100.423	60.255	52.887	40.702	41.703	35.462
Heneicosane	53.485	134.071	94.965	77.630	52.489	79.976	53.061
Docosane	148.268	4.998	113.883	nd	150.309	nd	113.610
Tricosane	204.628	79.134	143.353	223.420	179.738	196.574	174.890
Tetracosane	154.531	180.440	81.009	157.979	109.055	121.230	129.938
Pentacosane	428.044	nd	178.000	387.884	287.651	205.700	320.722
Hexacosane	344.254	160.178	224.412	217.813	192.552	135.124	227.519
Heptacosane	938.333	4.998	190.352	580.363	515.599	295.197	587.425
Octacosane	393.291	188.618	211.600	175.941	163.311	110.680	247.208
Nonacosane	nd	688.271	802.098	733.367	777.127	341.125	968.450
Triacontane	225.516	165.560	177.195	151.833	78.238	45.826	164.099
Hentriacontane	nd	798.931	868.385	724.412	642.935	217.846	795.148
Dotriacontane	89.566	4.998	172.592	130.214	54.579	31.884	63.436
Tritriacontane	nd	129.651	305.946	405.720	nd	90.919	nd
Tetratriacontane	nd	279.709	76.626	75.452	nd	nd	nd
Pentatriacontane	nd	67.639	52.855	71.065	nd	nd	nd
Hexatriacontane	nd	48.385	58.109	63.708	nd	nd	nd

Sediment Core NU-WAB-08						
Depth (cm)	8-9	10-12	14-16	18-20	20-25	25-27
Undecane	59.056	10.487	41.553	2.577	nd	nd
n-Dodecane	289.253	53.165	240.532	57.331	348.526	311.610
Tridecane	183.023	4.874	111.985	40.716	207.519	124.283
Tetradecane	191.887	41.798	151.907	149.209	375.685	247.535
Pentadecane	27.055	9.497	20.373	25.401	63.562	41.045
Hexadecane	37.073	20.433	26.435	33.574	69.731	50.733
Heptadecane	41.054	23.278	27.951	24.729	303.613	87.188
Octadecane	13.882	8.355	10.254	nd	43.265	10.571
Nonadecane	36.889	22.373	21.708	15.461	45.707	27.749
Eiscosane	53.801	39.058	45.134	22.096	41.593	29.152
Heneicosane	55.790	51.809	48.677	18.940	39.915	29.938
Docosane	125.204	130.926	116.202	39.569	nd	49.326
Tricosane	163.670	208.073	183.803	61.754	125.604	72.502
Tetracosane	128.399	187.694	157.722	53.203	83.283	58.235
Pentacosane	288.071	381.820	346.361	77.533	171.208	119.732
Hexacosane	200.976	289.624	258.827	62.858	97.326	85.433
Heptacosane	471.684	651.559	614.460	131.524	nd	221.183
Octacosane	176.219	463.810	297.948	126.956	nd	108.809
Nonacosane	615.817	1357.492	975.299	302.006	353.886	400.960
Triacontane	59.667	474.457	202.798	162.161	266.817	80.440
Hentriacontane	478.797	834.909	765.772	276.573	380.245	443.270
Dotriacontane	43.127	71.163	73.579	45.425	61.937	56.879
Tritriacontane	nd	nd	nd	nd	145.737	nd
Tetratriacontane	nd	nd	nd	nd	nd	nd
Pentatriacontane	nd	nd	nd	nd	nd	nd
Hexatriacontane	nd	nd	nd	nd	nd	nd

Sediment Core NU-WAB-10											
Depth (cm)	0-1	1-2	2-3	3-4	4-5	5-6	6-7	7-8	8-9	9-10	10-12
Undecane	434.508	nd	nd	nd	37.910	nd	20.625	nd	nd	nd	nd
n-Dodecane	nd	nd	nd	nd	190.758	520.605	160.290	nd	59.002	443.278	6.094
Tridecane	182.419	143.450	nd	nd	nd	265.015	nd	nd	13.860	256.012	5.294
Tetradecane	213.540	178.522	3.475	nd	210.204	217.337	153.271	34.322	67.660	377.305	52.042
Pentadecane	117.878	87.586	4.265	42.618	11.666	79.492	15.773	48.314	6.124	100.172	17.616
Hexadecane	105.652	72.821	6.213	56.452	20.186	83.186	26.621	94.746	21.668	129.783	28.207
Heptadecane	157.747	160.808	8.788	94.304	18.861	77.661	55.982	169.397	10.322	109.359	34.347
Octadecane	29.108	24.952	6.023	20.969	7.544	27.747	9.817	31.269	8.048	33.136	10.165
Nonadecane	37.975	31.955	14.377	21.454	17.591	33.409	26.052	34.146	15.641	38.946	35.314
Eiscosane	40.307	38.313	20.262	27.476	23.156	35.759	39.247	39.572	26.755	39.943	49.454
Heneicosane	73.232	78.579	26.778	44.344	30.177	57.542	41.096	52.544	33.764	52.201	55.362
Docosane	93.584	87.523	73.531	nd	81.689	nd	98.991	nd	72.734	nd	114.809
Tricosane	130.720	136.184	121.957	113.338	131.492	139.077	128.741	121.583	116.836	140.152	168.889
Tetracosane	86.862	88.200	99.377	75.808	121.846	86.121	108.626	93.579	101.414	132.269	136.141
Pentacosane	185.087	183.000	252.113	165.330	289.206	181.969	223.859	180.362	224.756	258.808	302.539
Hexacosane	251.738	273.276	186.409	99.347	233.086	102.824	162.831	103.070	162.527	208.370	199.680
Heptacosane	549.678	677.092	486.082	231.577	613.880	254.092	373.701	225.620	402.756	337.711	521.002
Octacosane	215.179	263.998	193.652	95.347	334.272	83.557	156.211	83.608	180.043	175.579	182.984
Nonacosane	670.341	864.951	692.555	299.546	1273.228	304.051	537.570	275.751	649.385	385.240	762.370
Triacontane	149.467	232.611	94.782	97.133	310.110	66.069	83.554	66.453	85.893	142.040	91.905
Hentriacontane	619.545	885.375	475.137	357.793	977.411	321.156	419.411	319.514	566.772	401.048	644.725
Dotriacontane	114.007	206.130	53.311	92.900	90.630	48.183	39.732	49.382	52.879	81.976	47.613
Tritriacontane	338.965	nd	166.657	166.655	nd	128.117	nd	135.322	nd	168.871	nd
Tetratriacontane	112.271	nd	71.300	71.301	nd	nd	nd	nd	nd	nd	nd
Pentatriacontane	66.626	nd	45.987	45.991	nd	26.969	nd	nd	nd	40.281	nd
Hexatriacontane	92.488	nd	66.124	66.120	nd	nd	nd	nd	nd	nd	nd

Sediment Core NU-WAB-14										
Depth (cm)	2-3	3-4	4-5	5-6	6-7	7-8	8-9	9-10	10-12	12-13
Undecane	12.030	19.452	4.523	1.718	2.620	7.035	nd	nd	nd	51.220
n-Dodecane	169.932	133.805	9.019	36.421	41.844	75.487	3.918	nd	nd	276.788
Tridecane	57.155	45.890	22.168	39.955	17.450	46.300	11.503	8.620	5.155	177.770
Tetradecane	248.667	140.368	85.216	155.293	120.729	164.172	69.391	49.939	46.702	245.344
Pentadecane	29.265	17.534	22.043	24.366	24.995	30.287	26.939	25.496	16.754	36.477
Hexadecane	43.929	25.428	32.199	31.944	39.035	40.395	33.764	35.717	32.450	43.289
Heptadecane	nd	10.428	25.049	15.543	16.915	16.902	18.529	20.932	28.369	19.104
Octadecane	nd	5.444	8.739	6.507	7.128	6.312	5.214	6.053	nd	nd
Nonadecane	nd	9.310	17.733	13.905	14.674	14.139	13.526	26.070	nd	17.765
Eiscosane	25.109	15.354	28.092	19.657	21.746	17.529	15.091	25.879	22.278	21.402
Heneicosane	nd	13.497	28.060	19.214	20.232	15.993	18.071	38.632	25.023	21.924
Docosane	92.144	30.285	67.195	41.436	38.699	32.157	33.525	69.075	53.375	41.077
Tricosane	60.033	34.982	82.184	56.182	79.676	46.099	56.914	118.737	81.636	64.154
Tetracosane	209.577	41.492	85.455	56.279	51.132	40.118	45.240	125.243	94.441	65.963
Pentacosane	326.142	57.564	193.826	70.861	113.280	71.200	104.853	306.306	191.647	144.949
Hexacosane	589.041	48.594	162.302	48.544	69.184	44.728	64.198	215.272	154.487	98.216
Heptacosane	173.955	100.441	426.536	84.721	159.693	87.552	149.362	566.154	372.256	248.748
Octacosane	493.689	78.948	234.227	127.836	66.987	54.292	56.926	243.823	175.347	90.943
Nonacosane	146.222	211.624	877.759	297.722	245.506	153.164	195.742	1015.136	689.477	370.537
Triacontane	1071.482	53.888	158.854	156.568	51.239	53.986	38.212	132.001	114.856	42.961
Hentriacontane	1071.480	147.048	886.290	203.669	261.071	169.081	200.908	990.270	641.693	341.254
Dotriacontane	659.060	40.482	82.486	36.981	41.557	36.032	nd	73.707	56.274	nd
Tritriacontane	nd	nd	nd	nd	nd	nd	nd	nd	nd	nd
Tetratriacontane	nd	nd	nd	nd	nd	nd	nd	nd	nd	nd
Pentatriacontane	nd	nd	nd	nd	nd	nd	nd	nd	nd	nd
Hexatriacontane	nd	nd	nd	nd	nd	nd	nd	nd	nd	nd

Sediment Core NU-WAB-16				
Depth (cm)	2-3	3-4	4-5	5-6
Undecane	94.881	5.148	nd	3.575
n-Dodecane	21.266	8.428	nd	3.300
Tridecane	67.402	45.453	nd	10.390
Tetradecane	6.384	8.693	nd	7.303
Pentadecane	13.059	17.424	nd	11.990
Hexadecane	7.063	15.155	7.347	14.967
Heptadecane	6.337	8.199	5.314	6.424
Octadecane	10.114	19.071	11.251	20.311
Nonadecane	20.851	25.507	17.975	24.851
Eiscosane	23.877	27.875	23.228	29.029
Heneicosane	63.172	51.366	53.574	60.902
Docosane	100.768	82.470	95.385	93.182
Tricosane	117.200	65.644	94.424	104.647
Tetracosane	216.883	148.541	165.221	183.400
Pentacosane	219.029	115.170	181.972	190.449
Hexacosane	405.280	245.734	323.588	307.365
Heptacosane	315.384	118.627	268.984	217.202
Octacosane	849.184	328.205	682.057	472.961
Nonacosane	309.362	60.532	226.492	105.423
Triacontane	645.847	208.065	571.295	484.490
Hentriacontane	86.764	nd	92.866	79.479
Dotriacontane	nd	nd	nd	nd
Tritriacontane	nd	nd	nd	nd
Tetratriacontane	nd	nd	nd	nd
Pentatriacontane	nd	nd	nd	nd
Hexatriacontane	nd	nd	nd	nd

Sediment Core CI-08									
Depth (cm)	0-1	1-2	2-3	3-4	4-5	5-6	6-7	7-8	8-9
Undecane	161.666	nd	nd	nd	nd	nd	10.236	nd	nd
n-Dodecane	nd	nd	11.712	179.729	7.798	30.813	45.795	31.631	3.557
Tridecane	54.429	nd	7.485	102.865	21.685	17.062	47.109	17.358	6.074
Tetradecane	100.967	nd	39.680	249.043	98.473	35.674	92.798	39.707	44.147
Pentadecane	61.878	53.709	15.340	168.270	71.230	27.908	60.266	30.478	38.412
Hexadecane	60.912	43.003	21.693	183.694	103.243	27.643	78.602	30.551	62.355
Heptadecane	80.654	58.601	6.929	56.755	21.481	12.263	11.982	12.422	11.000
Octadecane	18.474	15.674	nd	17.131	nd	16.275	4.986	15.000	5.038
Nonadecane	20.923	19.534	nd	18.698	25.913	19.399	16.164	14.651	19.478
Eiscosane	21.900	19.567	15.042	24.510	38.899	26.619	32.500	20.079	22.369
Heneicosane	31.968	30.054	13.971	29.185	46.335	30.625	37.815	24.082	34.983
Docosane	59.203	53.043	52.743	nd	214.627	nd	146.835	43.250	102.636
Tricosane	52.655	49.815	38.323	57.807	221.847	47.348	147.300	41.450	123.313
Tetracosane	57.108	58.195	59.783	43.392	501.279	42.524	294.958	37.140	239.303
Pentacosane	69.073	104.136	101.933	97.375	738.243	nd	537.431	71.296	526.429
Hexacosane	140.188	187.463	95.278	61.165	874.844	123.671	864.110	47.553	654.484
Heptacosane	228.866	271.036	164.413	132.175	1044.241	185.781	nd	89.039	909.294
Octacosane	124.235	165.838	199.239	58.003	1245.625	132.553	1141.390	47.241	734.057
Nonacosane	260.130	266.526	460.461	163.637	1983.208	199.168	1651.603	109.350	1163.376
Triacontane	91.241	131.530	301.517	47.776	611.153	81.169	596.285	43.361	249.435
Hentriacontane	271.183	266.419	352.892	194.375	1151.883	212.455	820.292	129.911	778.061
Dotriacontane	54.015	53.530	50.171	45.420	150.322	49.902	127.578	36.827	100.199
Tritriacontane	89.140	70.384	53.671	76.552	182.807	90.247	127.493	nd	131.164
Tetratriacontane	21.984	15.914	nd	nd	56.628	nd	40.390	nd	46.572
Pentatriacontane	18.888	10.998	nd	nd	91.367	nd	52.061	nd	70.017
Hexatriacontane	nd	13.290	nd	nd	nd	nd	nd	nd	nd

Sediment Core CI-08						
Depth (cm)	9-10	10-12	12-14	14-16	16-18	18-20
Undecane	nd	11.698	nd	nd	nd	17.014
n-Dodecane	562.119	53.102	276.385	nd	282.841	59.170
Tridecane	356.613	46.026	149.764	4.658	242.130	44.306
Tetradecane	292.793	115.792	130.344	28.576	102.415	93.957
Pentadecane	162.125	66.131	57.504	47.438	60.790	60.098
Hexadecane	165.232	88.910	54.013	83.968	67.488	76.789
Heptadecane	104.030	15.796	34.105	13.532	53.043	10.038
Octadecane	41.717	5.009	13.982	nd	21.162	4.219
Nonadecane	38.423	17.026	15.094	17.253	13.249	12.444
Eiscosane	44.606	23.302	15.435	23.070	25.462	16.541
Heneicosane	53.726	27.602	22.052	33.528	26.261	23.240
Docosane	nd	89.771	39.104	86.097	45.739	61.044
Tricosane	93.559	98.585	43.205	119.680	46.460	83.252
Tetracosane	106.924	198.601	37.900	nd	47.025	132.311
Pentacosane	211.230	404.549	74.683	nd	107.991	268.796
Hexacosane	228.290	436.352	46.396	nd	107.455	221.709
Heptacosane	309.816	nd	90.054	520.572	148.806	359.446
Octacosane	199.031	470.421	43.420	423.040	82.733	245.569
Nonacosane	294.735	736.664	102.785	741.096	132.097	470.630
Triacontane	120.873	194.619	42.315	nd	53.524	130.164
Hentriacontane	295.829	509.488	125.554	480.551	134.439	355.176
Dotriacontane	68.513	70.277	36.221	55.786	33.813	46.740
Tritriacontane	120.567	86.502	60.167	nd	47.827	63.493
Tetratriacontane	nd	27.440	33.813	nd	nd	nd
Pentatriacontane	nd	36.160	nd	nd	nd	nd
Hexatriacontane	nd	nd	nd	nd	nd	nd

Sediment Core CI-24									
Depth (cm)	2-3	3-4	4-5	5-6	6-7	7-8	8-9	9-10	10-11.5
Undecane	nd	nd	17.796	nd	6.263	nd	nd	nd	11.786
n-Dodecane	4.233	nd	82.998	8.418	33.921	3.673	nd	5.620	73.256
Tridecane	8.682	5.901	100.630	17.726	41.674	8.004	nd	10.398	53.987
Tetradecane	40.894	33.326	153.505	88.786	125.709	53.202	31.745	51.796	113.086
Pentadecane	17.849	42.317	77.730	54.196	67.989	46.503	31.221	45.177	51.784
Hexadecane	28.931	79.603	105.379	75.619	91.478	72.691	58.999	66.438	63.087
Heptadecane	15.372	15.578	26.019	13.230	19.276	14.464	10.564	13.982	11.067
Octadecane	nd	4.562	7.334	4.824	4.070	4.945	3.845	4.445	3.889
Nonadecane	nd	15.329	27.121	19.753	16.220	13.357	11.179	11.690	9.847
Eiscosane	15.573	18.842	34.875	20.647	40.994	24.395	15.715	15.921	12.816
Heneicosane	16.234	28.624	47.672	33.719	32.706	25.225	24.219	21.357	17.964
Docosane	28.724	76.493	132.992	98.257	117.600	67.826	62.762	52.049	41.209
Tricosane	29.111	104.750	177.624	148.615	104.975	74.611	88.306	76.608	63.870
Tetracosane	27.686	138.704	260.138	215.396	161.417	81.147	105.014	nd	65.438
Pentacosane	nd	329.569	591.662	526.290	323.933	196.513	230.536	88.269	169.044
Hexacosane	nd	280.991	615.320	607.150	366.155	154.199	190.426	202.312	141.925
Heptacosane	nd	513.791	973.278	878.710	577.012	339.012	378.581	211.272	291.769
Octacosane	nd	291.340	641.196	524.483	505.620	186.213	275.417	364.455	184.286
Nonacosane	nd	702.463	1271.360	861.841	976.510	479.417	699.637	266.210	411.057
Triacontane	43.998	146.753	249.317	158.282	409.530	107.099	241.553	505.808	96.068
Hentriacontane	190.250	550.059	829.574	507.779	728.360	401.052	500.871	164.406	423.233
Dotriacontane	nd	60.237	79.902	60.885	119.878	48.460	62.206	286.724	70.745
Tritriacontane	nd	nd	119.576	74.206	122.189	nd	nd	44.7540	nd
Tetratriacontane	nd	nd	27.066	nd	40.997	nd	nd	nd	nd
Pentatriacontane	nd	nd	30.085	nd	78.941	nd	nd	nd	nd
Hexatriacontane	nd	nd	nd	nd	nd	nd	nd	nd	nd

Appendix 3

Concentrations of Mo, Mn (ppm), Fe, S, Al, TC, TIC, TOC ^{210}Pb, ^{137}Cs activities and Porosity in sediment cores of varying lengths collected from 7 stations across Wager Bay.

Sediment core PLK-NU-15											
Depth (cm)	Porosity	^{210}Pb activity Bq/kg	^{137}Cs activity Bq/kg	Mo (ppm)	Mn (ppm)	Fe (%)	S (%)	Al (%)	TC (%)	TIC (%)	TOC (%)
0-1	0.913	216.624	8.689	0.870	261.000	2.280	0.350	1.220	na	na	na
1-2	0.875	220.955	11.693	0.670	269.000	2.260	0.290	1.230	na	na	na
2-3	0.855	207.604	8.012	0.670	265.000	2.200	0.240	1.260	na	na	na
3-4	0.836	193.054	7.805	0.720	261.000	2.120	0.250	1.180	2.227	0.357	1.870
4-5	0.834	172.309	6.520	1.180	259.000	2.170	0.250	1.230	na	na	na
5-6	0.789	123.222	6.161	2.060	242.000	2.050	0.300	1.130	1.930	0.325	1.605
6-7	0.769	114.517	0.000	2.350	239.000	2.060	0.340	1.100	na	na	na
7-8	0.755	104.506	0.000	1.810	238.000	2.040	0.330	1.070	2.078	0.343	1.736
8-9	0.717	110.570	0.000	1.640	230.000	1.970	0.310	1.030	na	na	na
9-10	0.733	101.493	0.000	1.770	234.000	2.060	0.340	1.090	1.762	0.299	1.461
10-12	0.704	72.829	0.000	2.100	227.000	2.000	0.380	1.030	na	na	na
12-14	0.695	64.873	0.000	2.870	258.000	2.400	0.570	1.240	1.638	0.325	1.302
14-16	0.725	56.790	0.000	3.570	277.000	2.540	0.650	1.270	na	na	na
16-18	0.711	56.972	0.000	3.440	273.000	2.520	0.650	1.270	1.625	0.325	1.299

na – not analysed
nd – not detected

Sediment core NU-WAB-08											
Depth (cm)	Porosity	^{210}Pb activity Bq/kg	^{137}Cs activity Bq/kg	Mo (ppm)	Mn (ppm)	Fe (%)	S (%)	Al (%)	TC (%)	TIC (%)	TOC (%)
0-1	0.983	283.599	0.000	1.000	554.000	1.950	0.760	1.070	na	na	na
1-2	0.920	334.377	0.000	0.880	374.000	2.210	0.440	1.280	na	na	na
2-3	0.902	321.805	8.741	0.700	313.000	2.210	0.320	1.330	na	na	na
3-4	0.824	302.195	0.000	1.030	286.000	2.070	0.300	1.330	3.063	0.962	2.101
4-5	0.870	266.970	0.000	na	na	na	na	na	na	na	na
5-6	0.863	251.659	0.000	3.180	445.000	2.330	0.340	1.320	3.031	0.947	2.084
6-7	0.861	213.056	0.000	na	na	na	na	na	na	na	na
7-8	0.850	189.841	0.000	5.030	317.000	2.300	0.470	1.340	2.920	0.999	1.920
8-9	0.842	147.000	0.000	na	na	na	na	na	na	na	na
9-10	0.845	66.453	0.000	4.580	276.000	2.200	0.580	1.210	2.918	0.935	1.983
10-12	0.832	106.105	0.000	na	na	na	na	na	na	na	na
12-14	0.832	84.268	0.000	6.150	309.000	2.350	0.690	1.340	3.017	1.105	1.912
14-16	0.827	71.731	0.000	na	na	na	na	na	na	na	na
16-18	0.822	65.617	0.000	4.570	337.000	2.480	0.770	1.380	3.108	1.212	1.851
18-20	0.814	69.038	0.000	4.030	330.000	2.430	0.770	1.350	na	na	na
20-25	0.804	70.951	0.000	4.230	348.000	2.480	0.800	1.370	2.818	1.178	1.640
25-27	0.805	70.674	0.000	5.750	336.000	2.380	0.770	1.330	na	na	na

Sediment core NU-WAB-10											
Depth (cm)	Porosity	^{210}Pb activity Bq/kg	^{137}Cs activity Bq/kg	Mo (ppm)	Mn (ppm)	Fe (%)	S (%)	Al (%)	TC (%)	TIC (%)	TOC (%)
0-1	0.875	201.000	5.855	1.430	246.000	1.930	0.380	1.090	na	na	na
1-2	0.854	174.372	0.000	2.890	237.000	1.990	0.460	1.110	na	na	na
2-3	0.843	152.520	0.000	3.580	243.000	2.020	0.520	1.110	na	na	na
3-4	0.830	132.631	0.000	3.830	246.000	1.960	0.490	1.080	2.414	0.572	1.841
4-5	0.822	116.990	0.000	na	na	na	na	na	na	na	na
5-6	0.803	98.341	0.000	3.520	239.000	1.990	0.520	1.100	2.303	0.547	1.755
6-7	0.772	92.503	0.000	na	na	na	na	na	na	na	na
7-8	0.782	83.603	0.000	3.370	232.000	2.020	0.590	1.100	2.200	0.542	1.659
8-9	0.777	68.226	0.000	4.720	235.000	2.140	0.750	1.110	na	na	na
9-10	0.785	67.188	0.000	6.160	254.000	2.340	0.910	1.160	2.080	0.582	1.498
10-12	0.782	65.755	0.000	5.340	261.000	2.200	0.800	1.130	na	na	na
12-13	0.775	63.129	0.000	4.860	264.000	2.180	0.730	1.170	2.270	0.625	1.645

Sediment core NU-WAB-14			
Depth (cm)	Porosity	^{210}Pb activity Bq/kg	^{137}Cs activity Bq/kg
0-1	0.846	179.916	0.000
1-2	0.805	167.856	0.000
2-3	0.746	132.800	0.000
3-4	0.725	104.023	2.131
4-5	0.723	73.299	0.000
5-6	0.711	63.753	0.000
6-7	0.705	60.018	0.000
7-8	0.709	60.525	0.000
8-9	0.702	61.041	0.000
9-10	0.700	61.041	0.000
10-12	0.684	73.134	0.000
12-13	0.697	64.863	0.000

Sediment core NU-WAB-16			
Depth (cm)	Porosity	^{210}Pb activity Bq/kg	^{137}Cs activity Bq/kg
0-1	0.791	149.267	0.000
1-2	0.747	115.707	0.000
2-3	0.744	111.131	0.000
3-4	0.719	102.489	0.000
4-5	0.780	125.057	0.000
5-6	0.739	64.630	0.000

Sediment core CI-08											
Depth (cm)	Porosity	^{210}Pb activity Bq/kg	^{137}Cs activity Bq/kg	Mo (ppm)	Mn (ppm)	Fe ()	S ()	Al ()	TC ()	TIC ()	TOC ()
0-1	0.755	142.000	0.000	0.670	93.000	0.970	0.140	0.370	na	na	na
1-2	0.700	128.669	0.000	0.880	98.000	0.980	0.150	0.390	na	na	na
2-3	0.686	136.121	0.000	0.980	96.000	0.980	0.140	0.400	na	na	na
3-4	0.676	128.268	0.000	2.040	99.000	1.060	0.180	0.440	1.379	0.463	0.916
4-5	0.654	111.259	0.000	na	na	na	na	na	na	na	na
5-6	0.635	104.190	0.000	3.250	100.000	1.040	0.230	0.410	1.269	0.452	0.817
6-7	0.635	80.744	0.000	na	na	na	na	na	na	na	na
7-8	0.628	75.568	0.000	1.690	93.000	1.020	0.220	0.380	1.234	0.449	0.785
8-9	0.602	65.156	0.000	na	na	na	na	na	na	na	na
9-10	0.601	56.875	0.000	1.880	90.000	1.010	0.200	0.360	1.117	0.419	0.698
10-12	0.578	47.498	0.000	na	na	na	na	na	na	na	na
12-14	0.587	36.860	0.000	2.280	96.000	1.060	0.260	0.410	1.198	0.597	0.601
14-16	0.597	34.516	0.000	na	na	na	na	na	na	na	na
16-18	0.578	28.326	0.000	2.010	96.000	1.100	0.260	0.410	1.249	0.502	0.747
18-20	0.565	26.819	0.000	1.700	104.000	1.080	0.250	0.430	na	na	na
20-21.5	0.577	20.346	0.000	1.830	102.000	1.090	0.260	0.430	1.177	0.511	0.666

Sediment core CI-24			
Depth (cm)	Porosity	Pb-210 activity Bq/kg	Cs-137 activity Bq/kg
0-1.5	0.729	166.421	0.000
1.5-2	0.698	150.498	0.000
2-3	0.678	132.203	0.000
3-4	0.653	100.201	0.000
4-5	0.648	81.278	3.602
5-6	0.661	81.446	3.822
6-7	0.646	63.798	0.000
7-8	0.653	55.601	0.000
8-9	0.645	55.267	0.000
9-10	0.665	33.198	0.000
10-11.5	0.658	26.731	0.000